Theory of Modulation Response of Semiconductor Quantum Dot Lasers

Yuchang Wu

Dissertation submitted to the faculty of the
Virginia Polytechnic Institute and State University
in partial fulfillment of the requirements for the degree of

Doctor of Philosophy
In
Materials Science and Engineering

Levon V. Asryan, Chair
Louis J. Guido
Mariusz K. Orlowski
Gary R. Pickrell

May 13, 2013
Blacksburg, Virginia

Keywords: quantum dot lasers, semiconductor lasers

Theory of Modulation Response of Semiconductor Quantum Dot Lasers

Yuchang Wu

Abstract

In this dissertation, a theory of modulation response of a semiconductor quantum dot (QD) laser is developed. The effect of the following factors on the modulation bandwidth of a QD laser is studied and the following results are obtained:

1) Carrier capture delay from the optical confinement layer into QDs

Closed-form analytical expressions are obtained for the modulation bandwidth $\omega_{-3\,\mathrm{dB}}$ of a QD laser in the limiting cases of fast and slow capture into QDs. $\omega_{-3\,\mathrm{dB}}$ is highest in the case of instantaneous capture into QDs, when the cross-section of carrier capture into a QD $\sigma_n = \infty$. With reducing σ_n, $\omega_{-3\,\mathrm{dB}}$ decreases and becomes zero at a certain non-vanishing $\sigma_n^{\min}$. This $\sigma_n^{\min}$ presents the minimum tolerable capture cross-section for the lasing to occur at a given dc component j_0 of the injection current density. The higher is j_0, the smaller is $\sigma_n^{\min}$ and hence the direct modulation of the output power is possible at a slower capture. The use of multiple layers with QDs is shown to considerably improve the modulation response of the laser – the same $\omega_{-3\,\mathrm{dB}}$ is obtained in a multi-layer structure at a much lower j_0 than in a single-layer structure.

2) Internal optical loss in the optical confinement layer

The internal optical loss, which increases with free-carrier density in the waveguide region, considerably reduces the modulation bandwidth $\omega_{-3\,\mathrm{dB}}$ of a QD laser. With internal loss cross-section σ_{int} increasing and approaching its maximum tolerable value, the modulation bandwidth decreases and becomes zero. There exists the optimum cavity length, at which $\omega_{-3\,\mathrm{dB}}$ is highest; the larger is σ_{int}, the longer is the optimum cavity.

3) Excited states in QDs

Direct and indirect (excited-state-mediated) mechanisms of capture of carriers from the waveguide region into the lasing ground state in QDs are considered, and the modulation response of a laser is calculated. It is shown that, when only indirect capture is involved, the excited-to-ground-state relaxation delay strongly limits the ground-state modulation bandwidth of the laser — at the longest tolerable relaxation time, the bandwidth becomes zero. When direct capture is also involved, the effect of excited-to-ground-state relaxation is less significant and the modulation bandwidth is considerably higher.

Acknowledgments

I would like to give my sincere thanks to the following people for their encouragement and support throughout my Ph.D. course:

- My advisor, Dr. Levon Asryan, for bringing me to Virginia Tech as well as for his guidance and advice throughout my Ph.D. course. His profound knowledge and attitude toward research and teaching gave me both inspiration and encouragement to my research. What I learned from him is of great benefit to me.
- Dr. Louis Guido for giving me very insightful guidance on my Ph.D. study and spending his valuable time on detailed discussions and comments about my research.
- Dr. Mariusz Orlowski and Dr. Gary Pickrell for taking time to be on my committee and for the courses taught to me. Their courses really helped me to extend my knowledge in the field of electronic materials and devices.
- Dr. Dae-Seob Han and Dr. Li Jiang, my former colleagues, for their helpful discussions and encouragements.

I would like to thank all the members of the MSE Department and my friends I have come to know in Blacksburg, who added a lot of joy to my life.

I would like to thank my church friends who sacrificed so much of their time and effort to make my life better. Especially I would like to thank Pastor Chris Hutchinson, Dr. William Reynolds Jr., Mrs. Mariko Reynolds, Mrs. Sue Rodi, and Mrs. Jamie Walker.

I would like to acknowledge the U.S. Army Research Office (Grant No. W911-NF-08-1-0462) and China Scholarship Council for funding of this work.

My most sincere thank you goes to my parents, whose love, support, and encouragement never decay but increase with time and distance. They set me an excellent example of being parents, honest and upright persons.

Last but not least, I give special thank you to my wife, Yanjun Ma, to whom I owe so much, for her love, patience, understanding, and encouragements.

Table of Contents

List of Figures

List of Tables

Chapter 1

Introduction

1.1. Lasing in semiconductors

A semiconductor laser uses a p-n junction to achieve lasing and, for this reason, it is also called a laser diode or diode laser. Being pumped by electric current, a semiconductor laser is also called an injection laser. Diode lasers are widely used in our daily life, e.g., in laser printers, bar-code readers, and laser pointers. They play an important role in high-speed optical communication systems. Since diode lasers can be directly modulated by a varying electric current, they are used in optical fiber communication as transmitters that convert electrical signals to optical.

The foundation of semiconductor laser operation is the stimulated emission during which an incident photon stimulates the emission of another photon via recombination of an electron-hole pair. Fig. 1.1 shows schematically the interactions of light with matter. When a photon is incident on a semiconductor, it can be absorbed by an electron in the valence band, and the electron will be excited to the conduction band leaving a positively charged hole in the valence band. As a result, an electron-hole pair is created [Fig. 1.1 (a)]. Without any external influence, radiative recombination of electron-hole pairs can occur. This process is called spontaneous emission [Fig. 1.1(c)], and photons are emitted in random directions with different phases. When stimulated by an incident photon, the electron-hole pair can recombine creating one more photon, which will have the same wavelength, phase and direction of propagation as the incident photon [Fig. 1.1 (c)]. This process is called stimulated emission and the photons are coherent. In a semiconductor under thermal equilibrium, the electron distribution follows the Fermi-Dirac statistics and the higher energy level is less populated than the lower energy level. As a result, the photon absorption process dominates and no coherent light will be emitted. To achieve lasing, the stimulated emission of photons should overcome the photon absorption process. Pumping is, therefore, needed to make the upper energy level more populated than the lower one, i.e., to create the population inversion – so that the optical gain and amplification of electro–

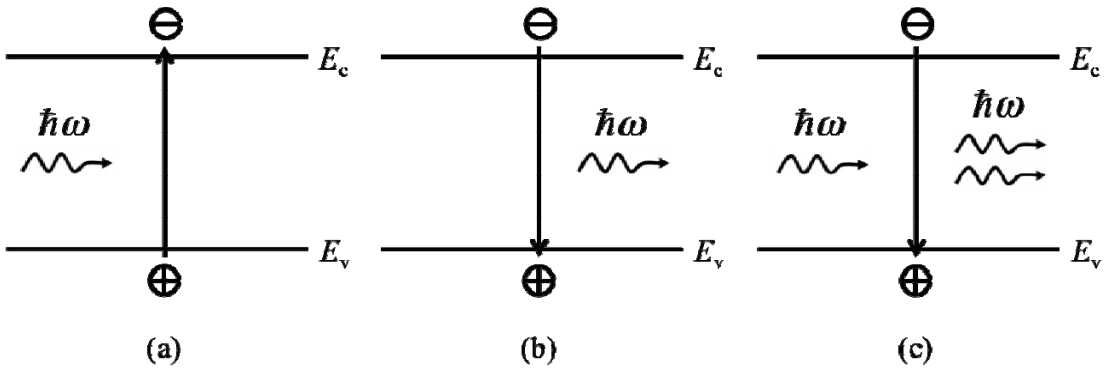

Fig. 1.1. Schematic illustration of (a) excitation of an electron from the valence band to the conduction band by absorbing a photon, (b) spontaneous emission, and (c) stimulated emission by an incident photon.

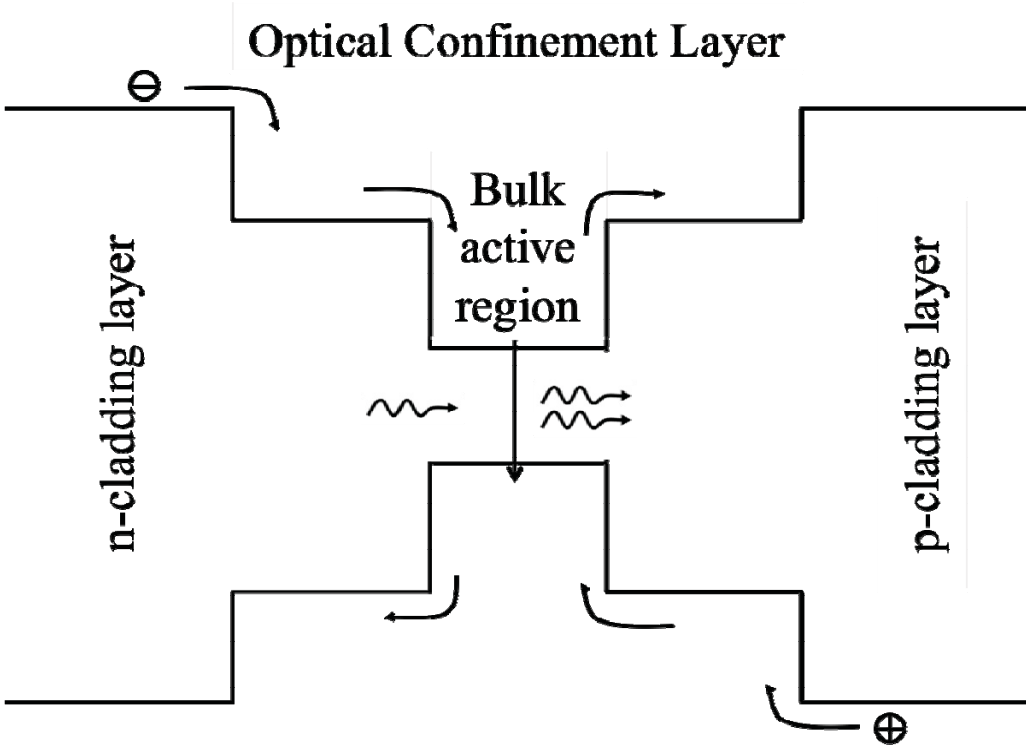

Fig. 1.2. Energy band diagram of a separate confinement double heterostructure laser.

magnetic radiation can be established. The term laser stands for "light amplification by stimulated emission of radiation".

Fig. 1.2 shows a typical separate confinement double heterostructure semiconductor laser. A layer of a narrow band gap semiconductor material is sandwiched between semiconductor layers with a wider band gap. The structure is electrically pumped – electrons and holes are injected into the conduction band and valence band, respectively. The electron-hole pairs recombine via spontaneous and stimulated recombination in the active layer. The emitted photons are confined within the waveguide layer (optical confinement layer – OCL) due to its larger refractive index compared to the cladding layers. Besides the population inversion, the optical feedback is also needed for lasing. In a Fabry-Perot cavity, this is provided by the cleaved cavity facets. Photons leave the cavity from the facet(s) as the optical output of the laser.

1.2. Bulk semiconductor lasers

1.2.1. Homojunction lasers

Early studies of using semiconductors for lasing were published in the late 1950s and early 1960s [1-3]. In 1962, Hall *et al.* [4] realized the first electrically operated semiconductor laser based on a GaAs p-n junction at 77 K. In the same year, several other groups also obtained semiconductor lasing in the infrared and visible light range [5, 6]. However, these structures were based on p-n junctions formed using the same semiconductor material and they suffered from high threshold current densities and poor lasing efficiencies. As a result, they were only able to operate at cryogenic temperatures.

1.2.2. Double heterostructure lasers

In 1963, an ingenious concept of double-heterostructure (DHS) laser was suggested by Alferov and Kazarinov [7] and Kroemer [8]. By 1970, Alferov [9], Hayashi [10], and Panish [11] had demonstrated double heterostructure lasers continuously operating at room temperature with a significantly lower threshold current density compared with that in homojunction lasers. In a separate-confinement double-heterostructure laser, as shown in Fig. 1.2, injected carriers (i.e., electrons and holes) are confined in the active layer due to the fact that the narrow band gap active layer is sandwiched by larger band gap layers. Besides, because of a higher refractive

index of the OCL compared to that of the cladding layers, a waveguide is formed, which effectively confines the emitted photons within the OCL. Due to separate confinement of carriers and photons, the lasing threshold is reduced and room temperature continuous wave (cw) operation becomes possible.

1.3. Low-dimensional semiconductor lasers

The early heterostructure lasers used bulk material as the active region wherein the carriers were free to move in all three directions and the performance of the laser was limited. To have a better performance, further confinement of carriers is needed. If the thickness of the narrow band gap active region is shrunk to be comparable to the carrier de Broglie wavelength, the carrier will be quantum-mechanically confined and its energy spectrum will become discrete. Depending on the number of degrees of freedom of the carrier — 2, 1, and 0, there can be quantum well (QW), quantum wire (QWR), and quantum dot (QD) lasers, respectively.

The motivation for using QWs, QWRs, or QDs as the active region is to achieve a much better (compared to bulk) laser performance. For instance, the emitted photon wavelength can be tuned by merely changing the thickness of the active layer whereas a bulk laser has to change the composition of the active layer to change the energy band gap, which determines the wavelength [12]. The advantages of a semiconductor laser with reduced dimensionality of the active region stem from the character of the density of states (the number of states per unit volume per unit energy interval) there [12, 13]. As can be seen in Fig. 1.3, while the density of states increases with energy in a bulk material, it is a delta-function in a QD. With reducing dimensionality, the threshold current density j_{th} (injection current density at which the gain is equal to the loss and, hence, the lasing starts) decreases.

The temperature dependence of the threshold current in bulk lasers is due to thermal spreading of carriers over a wide range of energy states. In QW lasers, where the density of state is a step-function [Fig. 1.3(b)], such thermal spreading is smaller [14]. In case of QWR lasers, there is a further suppression of the temperature effect because the density of states is a decreasing function of energy [Fig. 1.3(c)]. In QD lasers, the thermal spreading of carriers should ideally vanish because the density of state is a delta-function [Fig. 1.3(d)] and there are no available states for carriers to thermally spread. Hence the temperature dependence of the

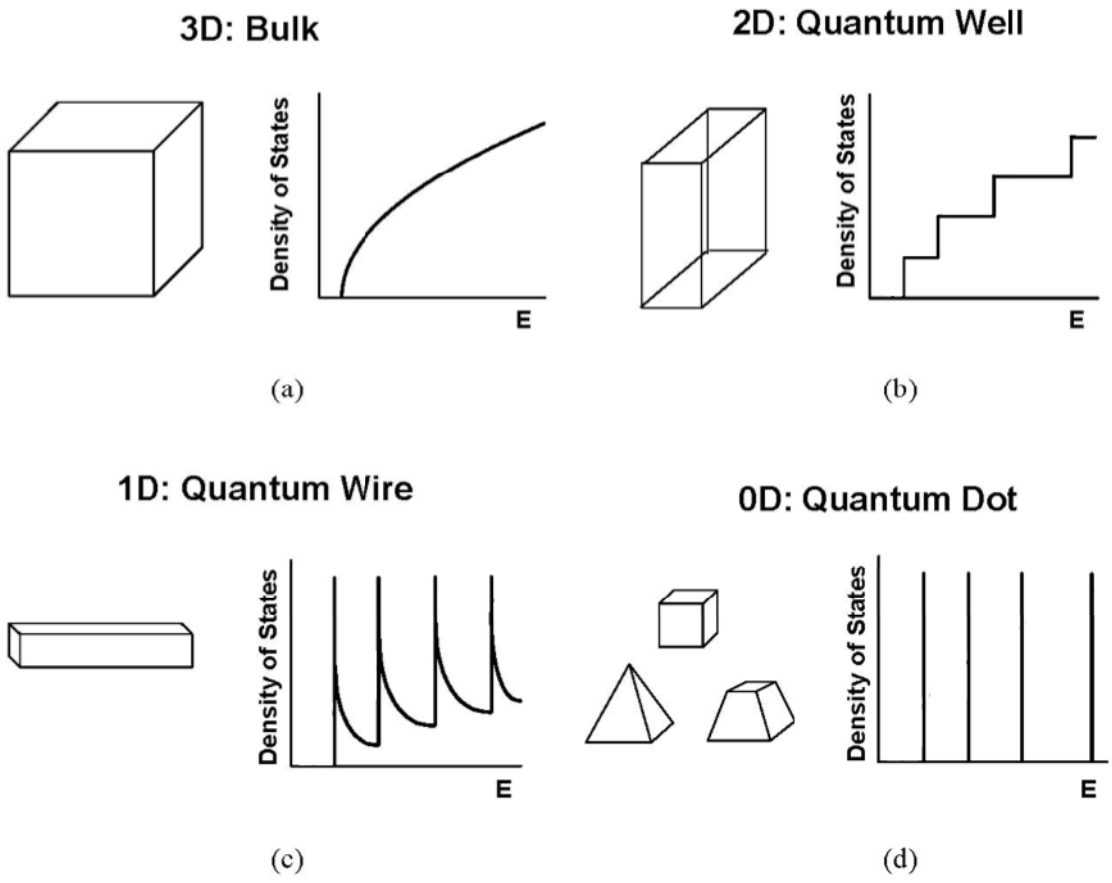

Fig. 1.3. Density of states in materials with different dimensionalities: (a) three-dimensional (bulk), (b) two-dimensional (quantum well), (c) one-dimensional (quantum wire), and (d) zero-dimensional (quantum dot).

threshold current will totally disappear in an ideal QD laser.

1.3.1. Quantum well lasers

Due to the ease of fabrication, QW lasers were first studied and fabricated. Now, they almost totally replaced bulk semiconductor lasers [15]. In 1974, Dingle *et al*. [16] observed the manifestations of quantum confinement in AlGaAs-GaAs-AlGaAs semiconductor heterostructures with an ultrathin GaAs layer. Later in the patent [12], they predicted the advantages of using QWs as the laser active region. The first QW lasing was obtained by Van Der Ziel *et al.* in 1975 [17]. The full potential of QW lasers could, however, be only realized after the developments in the crystal growth techniques, such as molecular beam epitaxy (MBE),

so that the growth of a good quality nanometer-range thin active layers became possible. As a result, the lowest threshold current density of 50 A/cm^2 was reported in the 1990s [18, 19].

1.3.2. Quantum wire and quantum dot lasers

The successful use of QW lasers stimulated a shift of interests to further reducing the dimensionality of the active region. This led to the concepts of QWR and QD heterostructure lasers. The use of QWRs and QDs for lasing was first proposed by Arakawa and Sakaki in 1982 [13]. Due to a stronger quantum confinement of carriers, a much weaker temperature-sensitivity of the threshold current density was predicted. For an ideal QD laser, it was predicted that the threshold current should be temperature insensitive. At that time, it was difficult to fabricate such structures. To confirm the concept and simulate a QWR laser, a bulk DHS laser was placed in a strong magnetic field, confining the carriers in the plane perpendicular to the field. An improvement in the temperature stability was indeed observed in the presence of the magnetic field.

There has been much effort devoted to the fabrication of QD lasers. Initially, etching was used and the laser performance was limited by high density of defects and nonuniformity in QD size and shape. A real breakthrough in QD lasers was the use of self-organization growth technique, which made it possible to grow high quality relatively uniform QD ensembles with reduced density of defects. The self-organized Stranski-Krastanow (SK) growth mode was most successful in growing uniform, dense, and defect-free QDs. It should be noted that a two-dimensional (2-D) wetting layer (WL) is inherently present in self-organized SK grown QD structures [20-23]. Fig. 1.4 shows typical plan-view and cross-sectional TEM images of a self-organized QD structure, and Fig. 1.5 shows a pyramidal-shape self-organized single QD.

The first optically pumped QD lasing was demonstrated in 1994 using an MBE grown InGaAs-GaAs structure [24]. In the same year, the first electrically pumped lasing of a self-organized InGaAs QD laser was also reported [25, 26]. Since then much effort has been made to improve the QD laser static characteristics, such as to reduce the threshold current density, increase the temperature stability, increase the power, and to cover a wide range of emitting wavelengths.

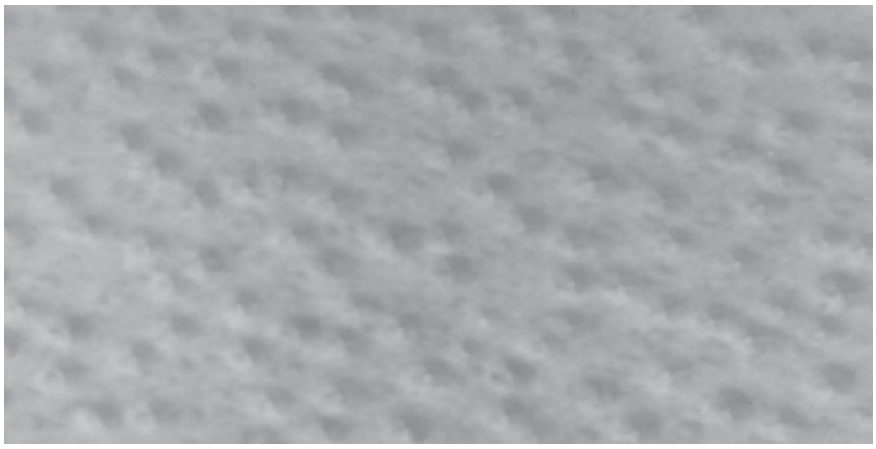

(a)

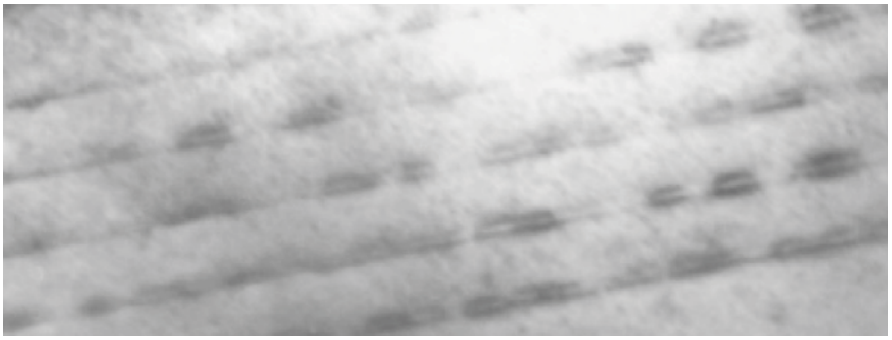

(b)

Fig. 1.4. Plan-view (a) and cross-sectional (b) TEM images of a QD structure. (Reprinted with permission from Fig. 2 of [27], Copyright (2003) by Elsevier.)

By now, much has been achieved in the development of QD lasers. In [28], a threshold current density j_{th} below 10 A/cm^2 was predicted at room temperature in a properly optimized QD laser. A record-low value of 10.4 A/cm^2 threshold current density for any kind of injection lasers was reported in [29]. In a carefully designed QD laser, a temperature insensitive threshold current was obtained in the temperature range of 5 – 70°C [30]. The highest cw power from a QD laser reached 16 W per chip at room temperature [31]. Operation of QD lasers in the visible spectral range and at longer wavelengths have also been demonstrated.

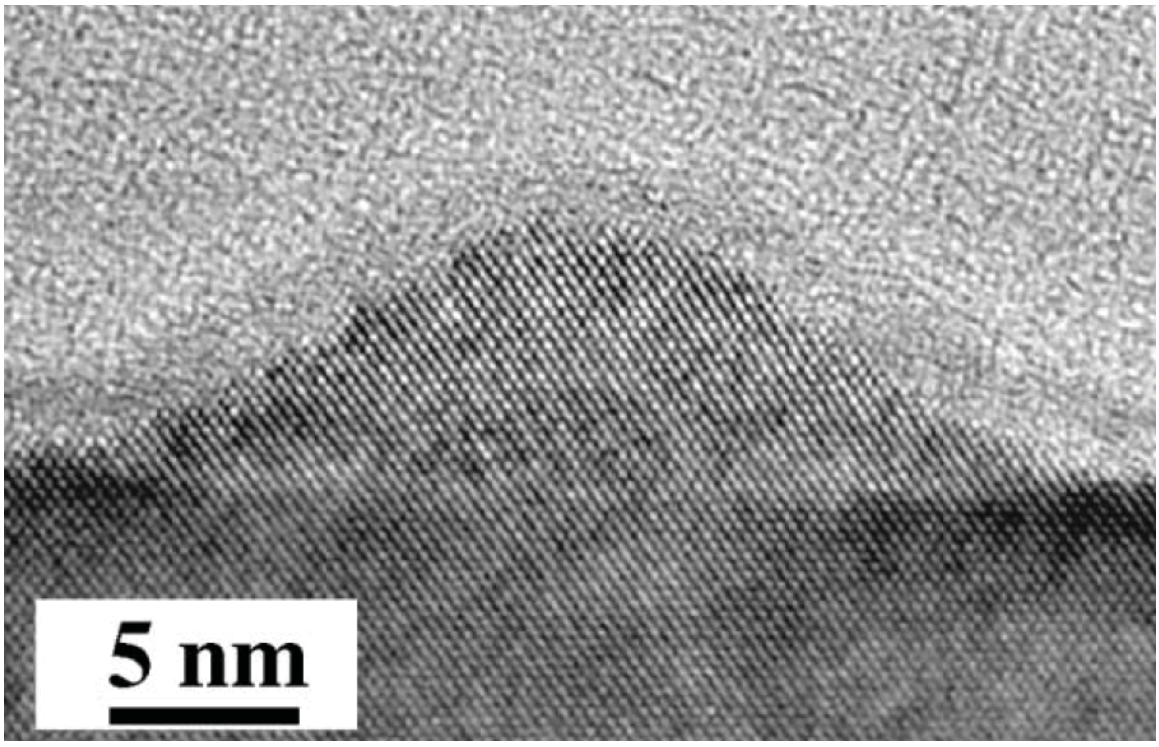

Fig. 1.5. High resolution TEM image of a single pyramidal self-organized InGaAs QD grown in Stranski–Krastonov mode using MBE. (Reprinted with permission from Fig. 2 of [32], Copyright (2001) by Elsevier.)

1.4. Modulation response of semiconductor QD lasers

Due to the compact size and the capability of direct modulation of the optical output by simply alternating the electric current, semiconductor lasers are widely used in high-speed communication systems. With the success in the improvement of QD laser static characteristics, the research has also been focused on the dynamic properties of QD lasers. Fig. 1.6 shows a simple optical fiber communication system, in which the transmitter is an injection laser that converts electrical signals to optical. As an input signal to the laser, the directly-modulating bias current causes a corresponding change in the laser optical output power and thus the information is transmitted. In such a lightwave system, the highest frequency (i.e., the modulation bandwidth), at which the modulation is still efficient, determines the amount of information that will be transmitted per unit time. For a non-return-to-zero binary format digital system, the maximum transmitted data rate (bit rate) is approximately twice the small-signal harmonic

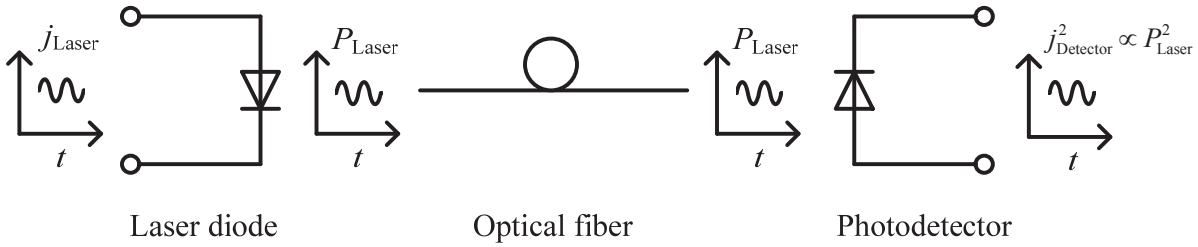

Fig. 1.6. Schematic diagram of a simple optical fiber communication system.

modulation bandwidth [33]. Hence, understanding the response of a semiconductor laser to a small time-harmonic modulating pump current is important for successful applications of semiconductor lasers in high-speed communication systems.

For optical data transmission using a typical single-mode silica fiber, 1.3 μm wavelength is used for short distance communications due to the minimum dispersion in the fiber. 1.55 μm is commonly used in long-haul systems due to the minimum attenuation in the fiber. Considerable amount of work has been done on the lasers emitting in this long-wavelength range. The material systems of choice for these applications are InGaAsP/InP, InGaAs/AlGaAs, InGaAs/GaAs, InAs/GaAs [34]. The first room-temperature 1.3 μm QD lasing was realized under pulse-current injection [35], and then the cw operation was also demonstrated [36]. Room-temperature cw 1.5 μm lasing was also realized using either GaAs [37] or InP [38] as the substrate.

Soon after the proposal of the concept of QD lasers [13], their dynamic properties were investigated using a simple set of two rate-equations [39-41]. In [42], the upper limit for the modulation bandwidth of a QD laser was calculated and it was found that the highest possible bandwidth in a single-QD-layer GaInAsP structure at 10% QD-size fluctuation is about 60 GHz. The experimental bandwidth in practical QD lasers is considerably lower. The highest state-of-the-art modulation bandwidth $\omega_{-3\text{ dB}}$ (– 3 dB bandwidth is used for modulation bandwidth in diode lasers) is only 7.5 GHz in a single-QD-layer laser [43]. Even in a 3-QD-layer laser, the highest reported value of $\omega_{-3\text{ dB}}$ (25 GHz – see [44]) is lower than that in a 4-quantum-well laser (40 GHz – see [45]).

Hence, the potential of QD lasers for high-speed direct modulation of the output optical power by injection current should be clarified.

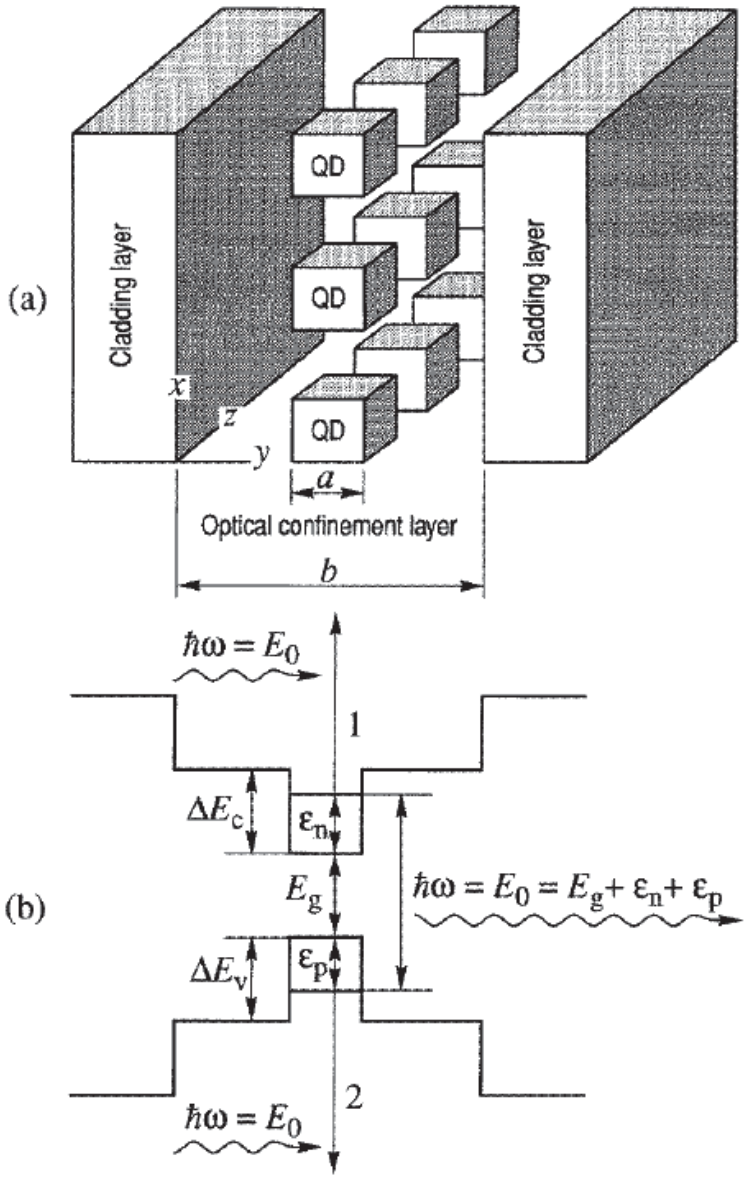

Fig. 1.7. Schematic illustration (a) and energy band diagram (b) of a QD laser structure. The QD lasing is produced by the electron-hole stimulated recombination in QDs. (Reprinted with permission from Fig. 1 of [28]. Copyright (1996) by the IOP.)

Several factors can limit the modulation bandwidth in QD lasers. The most important factors are discussed in this subsection.

In an ideal QD laser, all the QDs should be identical, and the density of state should be a delta-function [Fig. 1.3(d)]， whence the advantages of QD lasers follow. However, actual QDs

vary in size and shape – the QD size fluctuations are inherent in self-assembled grown QD ensembles [46]. The size fluctuation leads to a variation in the energies of electron and hole levels, which results in inhomogeneous gain spectrum broadening and reduction of the modal gain [28]. Particularly, there exists a maximum inhomogeneous broadening [28], beyond which the lasing is not attainable and thus the modulation bandwidth is reduced to zero. Therefore, by increasing the uniformity of QDs, the modulation bandwidth can be enhanced (Fig. 3 in [42]).

Ideally, carriers should be instantaneously transported to the active region and instantaneously captured by QDs, as was discussed in [42, 47] to estimate the highest possible modulation bandwidth. However, in an actual QD laser, carriers need time to transport through the bulk OCL (Fig. 1.7) to reach the active region. It was found in [48] that the carrier transport delay can reduce the modulation bandwidth in a QW laser. A similar situation should happen in QD lasers.

In actual lasers, there is also the carrier capture delay from the OCL into QDs. The carrier capture into a quantum confined active region was discussed in [28, 49, 50], and it was shown that the capture time cannot be properly defined for a single QD; the capture time can only be defined for the QD ensemble as a whole. The capture cross-section, which is the only parameter that adequately describes the carrier capture into a single QD, was used in [28, 49, 50]. Since the carriers confined in QDs produce the stimulated emission, their supply by capture process has a strong effect on the QD laser dynamics. The delay in carrier capture from the OCL into QDs can significantly reduce the laser modulation bandwidth. The study of this effect is one of the objectives of this dissertation.

The internal optical loss can also strongly limit the modulation bandwidth of a semiconductor laser. In [51-53], the effect of internal loss on the steady-state characteristics of a QD laser was studied assuming that the internal loss coefficient is linearly proportional to the free carrier density in the OCL. It was found that the internal loss places considerable restrictions on the conditions for lasing. Particularly, the use of a short-cavity structure for obtaining high modulation bandwidth [42] will be limited by the internal loss. In this dissertation, the effect of free-carrier-density-dependent internal optical loss in the OCL on the modulation bandwidth of a QD laser is studied.

In an ideal QD laser, there should be only one electron level in the conduction band and one hole level in the valence band in QDs. In actual QD lasers, there are excited-states in QDs

[54-58]. A non-zero relaxation time from the excited- to ground-state will affect the characteristics of a QD laser. If the carrier capture into the QD ground-state is excited-stated-mediated only, the output power saturation occurs. The longest relaxation time was shown to exist, at which the optical power becomes zero [59]. The carrier relaxation from the excited- to ground-state should also strongly affect the modulation response of a QD laser. This effect is explored in this dissertation.

1.5. Objectives, structure, and main results of the dissertation

The main objective of this research is a comprehensive theoretical study of the effect of different factors on the modulation bandwidth of a QD laser. The structure of the dissertation, the topics of the research, and the main results are presented below.

1) Effect of carrier capture delay from the OCL into QDs on the modulation bandwidth of a QD laser (Chapter 2)

A comprehensive theoretical model, which includes the effect of capture delay is developed [A1–A4][*)]. It is shown that the carrier capture delay can strongly limit the modulation bandwidth $\omega_{-3\,\mathrm{dB}}$ of a QD laser. Closed-form analytical expressions are obtained for the bandwidth in the limiting case of fast and slow capture. $\omega_{-3\,\mathrm{dB}}$ is highest in the case of instantaneous capture into QDs, when the cross-section of carrier capture into a QD $\sigma_\mathrm{n} = \infty$. With reducing σ_n, $\omega_{-3\,\mathrm{dB}}$ decreases and becomes zero at a certain non-vanishing $\sigma_\mathrm{n}^{\min}$. This $\sigma_\mathrm{n}^{\min}$ presents the minimum tolerable capture cross-section for the lasing to occur at a given dc component j_0 of the injection current density. The higher is j_0, the smaller is $\sigma_\mathrm{n}^{\min}$ and hence the direct modulation of the output power is possible at a slower capture. The use of multiple layers with QDs is shown to considerably improve the modulation response of the laser – the same $\omega_{-3\,\mathrm{dB}}$ is obtained in a multi-layer structure at a much lower j_0 than in a single-layer structure. At a plausible value of $\sigma_\mathrm{n} = 10^{-11}$ cm^2, $\omega_{-3\,\mathrm{dB}}$ as high as 19 GHz is attainable in a 5-QD-layer structure.

[*)] "A" in the reference number indicates the publications of the author of this dissertation.

2) Effect of internal optical loss in the OCL on the modulation bandwidth of a QD laser (Chapter 3)

The internal optical loss, which increases with free-carrier density in the waveguide region, is included in the rate equations model. The dependence of the modulation bandwidth on the internal loss is calculated [A4, A5]. The internal loss considerably reduces the modulation bandwidth $\omega_{-3\,\mathrm{dB}}$ of a QD laser. At a certain optimum value j_0^{opt} of the dc component of the injection current density, the maximum bandwidth $\omega_{-3\,\mathrm{dB}}^{\mathrm{max}}$ is attained and the modulation response function becomes as flat as possible. At this optimum current, the dependence of the modulation response function on the normalized modulation frequency $\omega/\omega_{-3\mathrm{dB}}^{\mathrm{max}}$ is found in a universal form. With internal loss cross-section σ_{int} increasing and approaching its maximum tolerable value, $\omega_{-3\,\mathrm{dB}}^{\mathrm{max}}$ decreases and becomes zero. As with j_0^{opt}, there also exists the optimum cavity length, at which $\omega_{-3\,\mathrm{dB}}$ is highest; the larger is σ_{int}, the longer is the optimum cavity.

3) Effect of excited-states in QDs on the modulation bandwidth of a QD laser (Chapter 4)

We consider direct and indirect (excited-state-mediated) capture of carriers from the waveguide region into the lasing ground state in QDs and calculate the modulation response of a QD laser [A6]. We show that, when only indirect capture is involved, the excited-to-ground-state relaxation delay strongly limits the ground-state modulation bandwidth of the laser — at the longest tolerable relaxation time, the bandwidth becomes zero. When direct capture is also involved, the effect of excited-to-ground-state relaxation is less significant and the modulation bandwidth is considerably higher.

List of publications of the author of this dissertation

[A1] L. V. Asryan, Y. Wu, and R. A. Suris, "Carrier capture delay and modulation bandwidth in an edge-emitting quantum dot laser," ***Appl. Phys. Lett.***, vol. 98, no. 13, Art. no. 131108, Mar. 2011.

[A2] L. V. Asryan, Y. Wu, and R. A. Suris, "Capture delay and modulation bandwidth in a quantum dot laser," ***Proc. SPIE***, vol. 7947, pp. 794708-1--794708-8, Jan. 2011.

[A3] L. V. Asryan, Y. Wu, and R. A. Suris, "Carrier capture delay and modulation bandwidth in an edge-emitting quantum dot laser," ***Proc. "Nanostructures: Physics and Technology"***, pp. 19-20, June 2011.

[A4] L. V. Asryan, Y. Wu, and R. A. Suris, "Modulation bandwidth of a quantum dot laser: The upper limit and limiting factors," ***Proc. 15th International Conf. "Laser Optics 2012"***, June 25-29, 2012, St. Petersburg, Russia. Paper no. WeR3-22.

[A5] Y. Wu, R. A. Suris, and L. V. Asryan, "Effect of internal optical loss on the modulation bandwidth of a quantum dot laser," ***Appl. Phys. Lett.***, vol. 100, no. 13, Art. no. 131106, Mar. 2012.

[A6] Y. Wu, R. A. Suris, and L. V. Asryan, "Effect of excited states on the ground-state modulation bandwidth in quantum dot lasers," ***Appl. Phys. Lett.***, vol. 102, no. 19, Art. no. 191102, May 2013.

Presentations at the conferences

Y. Wu, R. A. Suris, and L. V. Asryan, "Effect of excited states in quantum dots on the modulation bandwidth of a quantum dot laser," ***SPIE Photonics West,*** San Francisco, CA, Feb. 4, 2013.

Presentations at the seminars at the Department of Materials Science and Engineering at Virginia Polytechnic Institute and State University

1) Y. Wu, "Theoretical study of direct modulation of the optical output of quantum dot lasers by electric current," Dec. 3, 2010.
2) Y. Wu, "Effect of carrier capture delay on the modulation bandwidth of quantum dot lasers," Sept. 2, 2011.

References

[1] N. G. Basov, B. M. Vul and Y. M. Popov, "Quantum-mechanical semiconductor generators and amplifiers of electromagnetic oscillations," *Sov. Phys. JETP*, vol. 10, pp. 416, 1960.

[2] W. S. Boyle and D. G. Tomas, "Optical maser," U.S. Patent 3 059 117, Oct. 16, 1962.

[3] N. G. Basov, O. N. Krokhin and Y. M. Popov, "Production of negative-temperature states in p-n junctions of degenerate semiconductors," *Sov. Phys. JETP*, vol. 13, pp. 1320-1321, 1961.

[4] R. N. Hall, G. E. Fenner, J. D. Kingsley, T. J. Soltys and R. O. Carlson, "Coherent Light Emission From GaAs Junctions," *Phys. Rev. Lett.*, vol. 9, no. 9, pp. 366-368, Nov. 1962.

[5] J. N. Holonyak and S. F. Bevacqua, "Coherent (visible) light emission from $Ga(As_{1-x}P_x)$ junctions," *Appl. Phys. Lett.*, vol. 1, no. 4, pp. 82-83, Dec. 1962.

[6] M. I. Nathan, W. P. Dumke, G. Burns, J. F. H. Dill and G. Lasher, "Stimulated emission of radiation from GaAs p-n junctions," *Appl. Phys. Lett.*, vol. 1, no. 3, pp. 62-64, Nov. 1962.

[7] Zh. I. Alferov and R. F. Kazarinov, "Semiconductor laser with electric pumping," USSR Patent 181737, Mar. 30, 1963.

[8] H. Kroemer, "Solid state radiation emitters," U.S. Patent 3 309 553, Aug. 16, 1963.

[9] Zh. I. Alferov, V. M. Andreev, D. Z. Garbuzov, Yu. V. Zhilyaev, E. P. Morozov, E. L. Portnoi and V. G. Trofim, "Investigation of influence of AlAs-GaAs heterostructure parameters on laser threshold current and realization of continuous emission at room temperature," *Fiz. Tekh. Poluprovodn.*, vol. 4, no. 9, pp. 1826-1829, 1970.

[10] I. Hayashi, M. B. Panish, P. W. Foy and S. Sumski, "Junction lasers which operate continuously at room temperature," *Appl. Phys. Lett.*, vol. 17, no. 3, pp. 109-111, Aug. 1970.

[11] M. B. Panish, I. Hayashi and S. Sumski, "Double-heterostructure injection lasers with room-temperature thresholds as low as 2300 A/cm^2," *Appl. Phys. Lett.*, vol. 16, no. 8, pp. 326-327, Apr. 1970.

[12] R. Dingle and C. H. Henry, "Quantum effects in heterostructure lasers," U.S. Patent 3 982 207, Sept. 21, 1976.

[13] Y. Arakawa and H. Sakaki, "Multidimensional quantum well laser and temperature dependence of its threshold current," *Appl. Phys. Lett.*, vol. 40, no. 11, pp. 939-941, 1982.

[14] K. Hess, B. A. Vojak, N. Holonyak and R. Chin, "Temperature dependence of threshold current for a quantum well heterostructure laser," *Solid State Electron.*, vol. 23, no. 6, pp. 585-589, 1980.

[15] P. S. Zory, Quantum well lasers, Academic Press, 1993, p. 504.

[16] R. Dingle, W. Wiegmann and C. H. Henry, "Quantum states of confined carriers in very thin $Al_xGa_{1-x}As$-GaAs-$Al_xGa_{1-x}As$ heterostructures," *Phys. Rev. Lett.*, vol. 33, no. 14, pp. 827-830, Sept. 1974.

[17] J. P. van der Ziel, R. Dingle, R. C. Miller, W. Wiegmann and W. A. Nordland, "Laser oscillation from quantum states in very thin GaAs−$Al_{0.2}Ga_{0.8}As$ multilayer structures," *Appl. Phys. Lett.*, vol. 26, no. 8, pp. 463, 1975.

[18] N. Chand, E. E. Becker, J. P. van der Ziel, S. N. G. Chu and N. K. Dutta, "Excellent uniformity and very low (< 50 A/cm^2) Threshold current density strained InGaAs quantum well diode lasers on GaAs substrate," *Appl. Phys. Lett.*, vol. 58, no. 16, pp. 1704-1706, Apr. 1991.

[19] G. W. Turner, H. K. Choi and M. J. Manfra, "Ultralow-threshold (50 A/cm^2) strained single-quantum-well GaInAsSb/AlGeAsSb lasers emitting at 2.05 μm," *Appl. Phys. Lett.*, vol. 72, no. 8, pp. 876-878, Feb. 1998.

[20] R. Leon, Y. Kim, C. Jagadish, M. Gal, J. Zou and D. J. H. Cockayne, "Effects of interdiffusion on the luminescence of InGaAs/GaAs quantum dots," *Appl. Phys. Lett.*, vol. 69, no. 13, pp. 1888-1890, Sept. 1996.

[21] K. Nishi, R. Mirin, D. Leonard, G. MedeirosRibeiro, P. M. Petroff and A. C. Gossard, "Structural and optical characterization of InAs/InGaAs self-assembled quantum dots grown on (311)B GaAs," *J. Appl. Phys.*, vol. 80, no. 6, pp. 3466-3470, Sept. 1996.

[22] A. Patane, A. Polimeni, P. C. Main, M. Henini and L. Eaves, "High-temperature light emission from InAs quantum dots," *Appl. Phys. Lett.*, vol. 75, no. 6, pp. 814-816, Aug. 1999.

[23] J. S. Kim and I. H. Bae, "Optical properties of wetting layer in InAs quantum dots at different growth temperatures," *J Korean Phys Soc*, vol. 42, pp. S483-S486, Feb. 2003.

[24] N. N. Ledentsov, V. M. Ustinov, A. Yu. Egorov, A. E. Zhukov, M. V. Maksimov, I. G. Tabatadze and P. S. Kop'ev, "Optical properties of heterostructures with InGaAs-GaAs quantum clusters," *Semiconductors*, vol. 28, no. 8, pp. 832-834, Aug. 1994.

[25] A. Yu. Egorov, A. E. Zhukov, P. S. Kop'ev, N. N. Ledentsov, M. V. Maksimov and V. M. Ustinov, "Effect of deposition conditions on the formation of (In,Ga)As quantum clusters in a GaAs matrix," *Semiconductors*, vol. 28, no. 8, pp. 809-811, Aug. 1994.

[26] N. Kirstädter, N. N. Ledentsov, M. Grundmann, D. Bimberg, V. M. Ustinov, S. S. Ruvimov, M. V. Maximov, P. S. Kop'ev, Zh. I. Alferov, U. Richter, P. Werner, U. Gösele and J. Heydenreich, "Low threshold, large T_0 injection laser emission from (InGa)As quantum dots," *Electron. Lett.*, vol. 30, no. 17, pp. 1416-1417, Aug. 1994.

[27] J. S. Kim, J. H. Lee, S. U. Hong, W. S. Han, H. S. Kwack and D. K. Oh, "Influence of InGaAs overgrowth layer on structural and optical properties of InAs quantum dots," *J. Crystal Growth*, vol. 255, no. 1-2, pp. 57-62, Jul 2003.

[28] L. V. Asryan and R. A. Suris, "Inhomogeneous line broadening and the threshold current density of a semiconductor quantum dot laser," *Semicond. Sci. Technol.*, vol. 11, no. 4, pp. 554-567, Apr. 1996.

[29] D. G. Deppe, K. Shavritranuruk, G. Ozgur, H. Chen and S. Freisem, "Quantum dot laser diode with low threshold and low internal loss," *Electron. Lett.*, vol. 45, no. 1, pp. 54-55, Jan. 2009.

[30] Z. Mi, P. Bhattacharya and S. Fathpour, "High-speed 1.3 μm tunnel injection quantum-dot lasers," *Appl. Phys. Lett.*, vol. 86, no. 15, Apr. 2005.

[31] P. Crump, S. Patterson, S. Elim, S. Zhang, M. Bougher, J. Patterson, S. Das, W. Dong, M. Grimshaw, J. Wang, D. Wise, M. DeFranza, J. Bell, J. Farmer, M. DeVito, R. Martinsen, A. Kovsh, F. Toor and C. F. Gmachl, "Extending the wavelength range of single-emitter diode lasers for medical and sensing applications: 12xx-nm quantum dots, 2000-nm wells, > 5000-nm cascade lasers," vol. 6456, pp. 64560E-11, 2007.

[32] P. Bhattacharya, S. Krishna, J. Phillips, P. J. McCann and K. Namjou, "Carrier dynamics in self-organized quantum dots and their application to long-wavelength sources and detectors," *J. Crystal Growth*, vol. 227-228, pp. 27-35, Jul. 2001.

[33] D. Derickson, Fiber optic test and measurement, Prentice-Hall, 1998, p. 642.

[34] D. Bimberg, M. Grundmann and N. N. Ledentsov, Quantum dot heterostructures, John Wiley, 1999, p. 328.

[35] D. L. Huffaker, G. Park, Z. Zou, O. B. Shchekin and D. G. Deppe, "1.3 μm room-temperature GaAs-based quantum-dot laser," *Appl. Phys. Lett.*, vol. 73, no. 18, pp. 2564-2566, Nov. 1998.

[36] K. Mukai, Y. Nakata, K. Otsubo, M. Sugawara, N. Yokoyama and H. Ishikawa, "1.3-μm cw lasing of InGaAs-GaAs quantum dots at room temperature with a threshold current of 8 mA," *IEEE Photon. Technol. Lett.*, vol. 11, no. 10, pp. 1205-1207, Oct. 1999.

[37] N. N. Ledentsov, A. R. Kovsh, A. E. Zhukov, N. A. Maleev, S. S. Mikhrin, A. P. Vasil'ev, E. S. Sernenova, M. V. Maximov, Y. M. Shernyakov, N. Kryzhanovskaya, V. Ustinov and D. Bimberg, "High performance quantum dot lasers on GaAs substrates operating in 1.5 μm range," *Electron. Lett.*, vol. 39, no. 15, pp. 1126-1128, Jul. 2003.

[38] H. D. Kim, W. G. Jeong, J. H. Lee, J. S. Yim, D. Lee, R. Stevenson, P. D. Dapkus, J. W. Jang and S. H. Pyun, "Continuous-wave operation of 1.5 μm InGaAs/InGaAsP/InP quantum dot lasers at room temperature," *Appl. Phys. Lett.*, vol. 87, no. 8, Aug. 2005.

[39] Y. Arakawa and A. Yariv, "Quantum well lasers - gain, spectra, dynamics," *IEEE J. Quantum. Electron.*, vol. 22, no. 9, pp. 1887-1899, Sept. 1986.

[40] K. Y. Lau, N. Barchaim, I. Ury, C. Harder and A. Yariv, "Direct amplitude modulation of short-cavity GaAs lasers up to X-band frequencies," *Appl. Phys. Lett.*, vol. 43, no. 1, pp. 1-3, 1983.

[41] K. Uomi, N. Chinone, T. Ohtoshi and T. Kajimura, "High relaxation oscillation frequency (beyond 10 GHz) of GaAlAs multiquantum well lasers," *Jpn J Appl Phys 2*, vol. 24, no. 7, pp. L539-L541, Jul. 1985.

[42] L. V. Asryan and R. A. Suris, "Upper limit for the modulation bandwidth of a quantum dot laser," *Appl. Phys. Lett.*, vol. 96, no. 22, Art. no. 221112, May 2010.

[43] K. Kamath, J. Phillips, H. Jiang, J. Singh and P. Bhattacharya, "Small-signal modulation and differential gain of single-mode self-organized $In_{0.4}Ga_{0.6}As$/GaAs quantum dot lasers," *Appl. Phys. Lett.*, vol. 70, no. 22, pp. 2952-2953, Jun. 1997.

[44] S. Fathpour, Z. Mi and P. Bhattacharya, "High-speed quantum dot lasers," *J. Phys. D. Appl. Phys.*, vol. 38, no. 13, pp. 2103-2111, Jul. 2005.

[45] S. Weisser, E. C. Larkins, K. Czotscher, W. Benz, J. Daleiden, I. Esquivias, J. Fleissner, J. D. Ralston, B. Romero, R. E. Sah, A. Schonfelder and J. Rosenzweig, "Damping-limited

modulation bandwidths up to 40 GHz in undoped short-cavity $In_{0.35}Ga_{0.65}As$-GaAs multiple-quantum-well lasers," *IEEE Photon. Technol. Lett.*, vol. 8, no. 5, pp. 608-610, May 1996.

[46] D. Leonard, S. Fafard, K. Pond, Y. H. Zhang, J. L. Merz and P. M. Petroff, "Structural and Optical-Properties of Self-Assembled Ingaas Quantum Dots," *J Vac Sci Technol B*, vol. 12, no. 4, pp. 2516-2520, Jul./Aug. 1994.

[47] L. V. Asryan and R. A. Suris, "Theory of relaxation oscillations and modulation response of a quantum dot laser," *Proc. SPIE*, vol. 7610, pp. 76100R-1--76100R-7, Jan. 2010.

[48] R. Nagarajan, M. Ishikawa, T. Fukushima, R. S. Geels and J. E. Bowers, "High speed quantum-well lasers and carrier transport effects," *IEEE J. Quantum. Electron.*, vol. 28, no. 10, pp. 1990-2008, Oct. 1992.

[49] L. V. Asryan, S. Luryi and R. A. Suris, "Intrinsic nonlinearity of the light-current characteristic of semiconductor lasers with a quantum-confined active region," *Appl. Phys. Lett.*, vol. 81, no. 12, pp. 2154-2156, Sept. 2002.

[50] L. V. Asryan, S. Luryi and R. A. Suris, "Internal efficiency of semiconductor lasers with a quantum-confined active region," *IEEE J. Quantum. Electron.*, vol. 39, no. 3, pp. 404-418, Mar. 2003.

[51] L. V. Asryan and S. Luryi, "Two lasing thresholds in semiconductor lasers with a quantum-confined active region," *Appl. Phys. Lett.*, vol. 83, no. 26, pp. 5368-5370, Dec. 2003.

[52] L. V. Asryan and S. Luryi, "Effect of internal optical loss on threshold characteristics of semiconductor lasers with a quantum-confined active region," *IEEE J. Quantum. Electron.*, vol. 40, no. 7, pp. 833-843, Jul. 2004.

[53] L. Jiang and L. V. Asryan, "Internal-loss-limited maximum operating temperature and characteristic temperature of quantum dot laser," *Laser Phys. Lett.*, vol. 4, no. 4, pp. 265-269, Apr. 2007.

[54] O. Stier, M. Grundmann and D. Bimberg, "Electronic and optical properties of strained quantum dots modeled by 8-band k·p theory," *Phys. Rev. B*, vol. 59, no. 8, pp. 5688-5701, Feb. 1999.

[55] L. W. Wang, J. N. Kim and A. Zunger, "Electronic structures of [110]-faceted self-assembled pyramidal InAs/GaAs quantum dots," *Phys. Rev. B*, vol. 59, no. 8, pp. 5678-5687, Feb. 1999.

[56] L. F. Lester, A. Stintz, H. Li, T. C. Newell, E. A. Pease, B. A. Fuchs and K. J. Malloy, "Optical characteristics of 1.24-μm InAs quantum-dot laser diodes," *IEEE Photon. Technol. Lett.*, vol. 11, no. 8, pp. 931-933, Aug. 1999.

[57] M. V. Maximov, Y. M. Shernyakov, I. N. Kaiander, D. A. Bedarev, E. Y. Kondrat'eva, P. S. Kop'ev, A. R. Kovsh, N. A. Maleev, S. S. Mikhrin, A. F. Tsatsul'nikov, V. M. Ustinov, B. V. Volovik, A. E. Zhukov, Zh. J. Alferov, N. N. Ledentsov and D. Bimberg, "Single transverse mode operation of long wavelength (similar to 1.3 μm) InAsGaAs quantum dot laser," *Electron. Lett.*, vol. 35, no. 23, pp. 2038-2039, Nov. 1999.

[58] G. Park, O. B. Shchekin, S. Csutak, D. L. Huffaker and D. G. Deppe, "Room-temperature continuous-wave operation of a single-layered 1.3 μm quantum dot laser," *Appl. Phys. Lett.*, vol. 75, no. 21, pp. 3267-3269, Nov. 1999.

[59] L. Jiang and L. V. Asryan, "Excited-state-mediated capture of carriers into the ground state and the saturation of optical power in quantum-dot lasers," *IEEE Photon. Technol. Lett.*, vol. 18, no. 24, pp. 2611-2613, Dec. 2006.

Chapter 2

Effect of carrier capture delay from the bulk optical confinement layer into quantum dots on the modulation bandwidth of a quantum dot laser

Summary

A comprehensive theoretical rate equations model for the modulation response of a quantum dot (QD) laser, which accounts for the carrier capture delay into QDs, is developed [A1-A4]*). It is shown that the carrier capture delay can strongly limit the modulation bandwidth $\omega_{-3\ \mathrm{dB}}$ of a QD laser. Closed-form analytical expressions are obtained for the bandwidth in the limiting cases of fast and slow capture. $\omega_{-3\ \mathrm{dB}}$ is highest in the case of instantaneous capture into QDs, when the cross-section of carrier capture into a QD $\sigma_n = \infty$. With reducing σ_n, $\omega_{-3\ \mathrm{dB}}$ decreases and becomes zero at a certain non-vanishing value of $\sigma_n^{\min}$. This $\sigma_n^{\min}$ presents the minimum tolerable capture cross-section for the lasing to occur at a given dc component j_0 of the injection current density. The higher is j_0, the smaller is $\sigma_n^{\min}$ and hence the direct modulation of the output power is possible at a slower capture. The use of multiple layers with QDs is shown to considerably improve the modulation response of the laser – the same $\omega_{-3\ \mathrm{dB}}$ is obtained in a multi-layer structure at a much lower j_0 than in a single-layer structure. At a plausible value of $\sigma_n = 10^{-11}$ cm^2, $\omega_{-3\ \mathrm{dB}}$ as high as 19 GHz is attainable in a 5-QD-layer structure.

2.1. Introduction

High modulation bandwidth diode lasers present a critical component for optical fiber communication systems [1]. In [2], the highest modulation bandwidth attainable in QD lasers was estimated by assuming an idealized situation of instantaneous carrier capture from the optical confinement layer (OCL) into QDs. In actual quantum well (QW), quantum wire (QWR),

---

*) "A" in the reference number indicates the publications of the author of this dissertation.

and QD lasers, the quantum-confined active region is embedded in a bulk reservoir region (OCL). The carriers are first injected into this bulk reservoir region and then captured into the active region (Fig. 2.1). Noninstantaneous capture limits the laser operating characteristics – the threshold current is increased [3] and more temperature-unstable [4], and the output optical power is decreased [5, 6]. Due to capture delay into the active region, the bandwidth of direct modulation of the output power by injection current is also reduced.

2.2. Theoretical model

2.2.1. Main assumptions

In this chapter, the effect of noninstantaneous capture of carriers into QDs on the modulation bandwidth of an edge-emitting QD laser is studied [A1-A4]. To mainly focus on the effect of noninstantaneous carrier capture, the following assumptions and simplifications are made.

1) There is only one electron/hole energy level in the conduction/valence band. The effect of excited-states in QDs will be discussed in Chapter 4.
2) Heating effects in the device are not considered.
3) Spatial hole burning (SHB) effect is neglected so that the free carrier density in the OCL and the confined carrier level occupancy in a QD are independent of the longitudinal coordinate (z direction in Fig. 1.7 of Chapter 1).
4) The free carrier density in the OCL is uniform in the transverse direction (x direction in Fig. 1.7).
5) The fraction of spontaneous emission in the lasing mode is ignored.
6) The internal optical loss is not taken into consideration. The effect of free carrier density dependent internal optical loss in the OCL will be discussed in Chapter 3.
7) Auger recombination in the OCL and QDs is not included in our model.

2.2.2. Rate equations

Our model is based on the following set of three coupled rate equations for free carriers in the OCL, carriers confined in QDs, and photons:

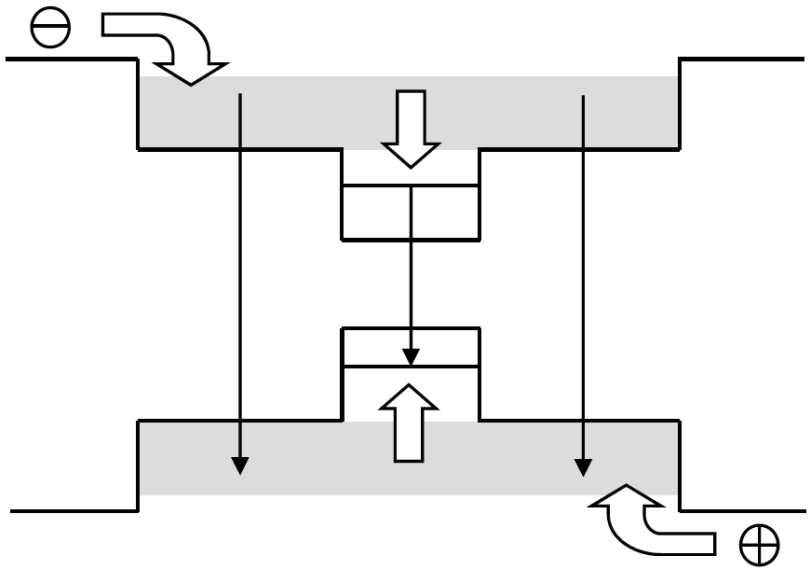

Fig. 2.1. Indirect carrier injection into QDs. (Reprinted with permission from Fig. 1 of ref. [A2], Copyright (2011) by SPIE.)

$$\frac{\partial n_{\mathrm{OCL}}}{\partial t} = \frac{j}{eb} - \sigma_{\mathrm{n}} \mathrm{v}_{\mathrm{n}} \frac{N_{\mathrm{s}}}{b}\left(1 - f_{\mathrm{n}}\right) n_{\mathrm{OCL}} + \sigma_{\mathrm{n}} \mathrm{v}_{\mathrm{n}} n_1 \frac{N_{\mathrm{s}}}{b} f_{\mathrm{n}} - B n_{\mathrm{OCL}}^2, \tag{2.1}$$

$$\frac{\partial}{\partial t}\left(2\frac{N_{\mathrm{S}}}{b} f_{\mathrm{n}}\right) = \sigma_{\mathrm{n}} \mathrm{v}_{\mathrm{n}} \frac{N_{\mathrm{s}}}{b}\left(1 - f_{\mathrm{n}}\right) n_{\mathrm{OCL}} - \sigma_{\mathrm{n}} \mathrm{v}_{\mathrm{n}} n_1 \frac{N_{\mathrm{s}}}{b} f_{\mathrm{n}} - \frac{N_{\mathrm{s}}}{b} \frac{f_{\mathrm{n}}^2}{\tau_{\mathrm{QD}}} - \mathrm{v}_{\mathrm{g}} g^{\max}\left(2 f_{\mathrm{n}} - 1\right) n_{\mathrm{ph}}, \tag{2.2}$$

$$\frac{\partial n_{\mathrm{ph}}}{\partial t} = \mathrm{v}_{\mathrm{g}} g^{\max}\left(2 f_{\mathrm{n}} - 1\right) n_{\mathrm{ph}} - \mathrm{v}_{\mathrm{g}} \beta n_{\mathrm{ph}}, \tag{2.3}$$

where n_{OCL} is the free carrier density in the OCL, j is the injection current density, b is the OCL thickness, σ_{n} is the cross-section of carrier capture into a QD, v_{n} is the carrier thermal velocity, N_{S} is the surface density of QDs, f_{n} is the occupancy of the energy-level of a carrier confined in a QD, B is the spontaneous radiative recombination constant for the OCL, τ_{QD} is the spontaneous radiative time in a QD, v_{g} is the group velocity of light, $g^{\max}$ is the maximum modal gain [3], and n_{ph} is the photon density (per unit volume of the OCL) in the lasing mode.

The mirror loss

$$\beta = \frac{1}{L} \ln \frac{1}{R}, \tag{2.4}$$

where L is the cavity length and R is the facet reflectivity.

The quantity n_1 in (2.1) and (2.2) characterizes the carrier thermal escape from a QD to the OCL and is given as

$$n_1 = N_c^{3D} \exp\left(-\frac{\Delta E_c - \varepsilon_n^{QD}}{T} \right), \tag{2.5}$$

where

$$N_c^{3D} = 2\left(\frac{m_c^{OCL} T}{2\pi\hbar^2} \right)^{\frac{3}{2}} \tag{2.6}$$

is the effective density of states in the OCL, m_c^{OCL} is the carrier effective mass in the OCL, ΔE_c is the band offset between the OCL and a QD, ε_n^{QD} is the quantized energy level in a QD and T is the temperature measured in units of energy.

The rates entering into the right-hand side of (2.1) – (2.3) are presented in Table 2.1.

In the strict sense, the time for the carrier capture into a single QD cannot be introduced properly. An adequate physical quantity, describing correctly the carrier capture into a single QD, is the capture cross-section σ_n. Using σ_n, two distinct characteristic times can be introduced – the capture time into an unoccupied QD ensemble [6] and the thermal escape time from an individual QD [3, 6],

$$\tau_{capt,0} = \frac{1}{\sigma_n v_n \frac{N_S}{b}}, \tag{2.7}$$

$$\tau_{esc} = \frac{1}{\sigma_n v_n n_1}. \tag{2.8}$$

The capture time into an unoccupied QD ensemble and the escape time from a QD are shown in Fig. 2.2 as a function of σ_n. In a specific structure considered in this Chapter, $\tau_{capt,0} = 1.63$ ps and $\tau_{esc} = 0.07$ ps at $\sigma_n = 10^{-11}$ cm^2.

Table 2.1. Rates entering into eqs. (2.1)–(2.3)

$\frac{j}{eb}$	Carrier injection into the OCL
$\sigma_{\mathrm{n}} \mathrm{v}_{\mathrm{n}} \frac{N_{\mathrm{S}}}{b}\left(1-f_{\mathrm{n}}\right) n_{\mathrm{OCL}}$	Capture from the OCL into QDs
$\sigma_{\mathrm{n}} \mathrm{v}_{\mathrm{n}} n_1 \frac{N_{\mathrm{S}}}{b}\left(1-f_{\mathrm{n}}\right)$	Thermal escape from QDs to the OCL
$B n_{\mathrm{OCL}}^2$	Spontaneous radiative recombination in the OCL
$\frac{N_{\mathrm{S}}}{b} \frac{f_{\mathrm{n}}^2}{\tau_{\mathrm{QD}}}$	Spontaneous radiative recombination in QDs
$\mathrm{v}_{\mathrm{g}} g^{\max}\left(2 f_{\mathrm{n}}-1\right) n_{\mathrm{ph}}$	Stimulated radiative recombination in QDs
$\mathrm{v}_{\mathrm{g}} \beta n_{\mathrm{ph}}$	Mirror loss of photons

The spontaneous radiative recombination is considered as the only mechanism of nonstimulated recombination in the OCL and QDs. The inclusion of the nonradiative Auger recombination will increase the threshold current density and the steady-state carrier density in the OCL, and, within the framework of the small-signal analysis, will decrease the differential nonstimulated recombination time, while not otherwise affecting our main derivations.

Our rate equation model does not include the wetting layer (WL), which is inherently present in self-assembled Stranski–Krastanow (SK) grown QD structures [7-10]. The WL can affect the carrier capture into QDs. In addition to the capture from the bulk OCL into QDs, carriers can also be first captured from the OCL into the two-dimensional WL and then from the WL into QDs.

At the steady-state, the carrier and photon densities are time-independent [i.e., $\partial\left(n_{\mathrm{OCL}}, f_{\mathrm{n}}, n_{\mathrm{ph}}\right) / \partial t=0$], and the steady-state rate equations are

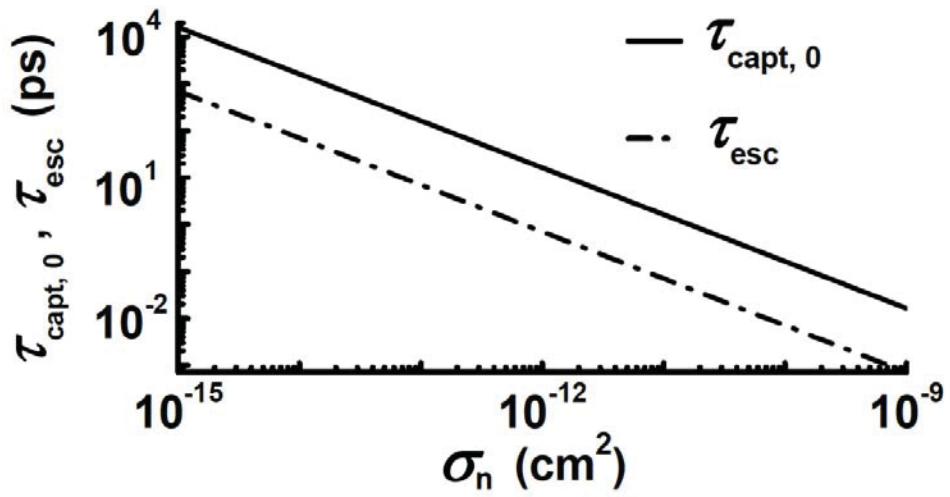

Fig. 2.2. Capture time from the OCL into an unoccupied (f_n = 0) QD-ensemble and thermal escape time from a QD vs. capture cross-section. The surface density of QDs $N_S = 6.11\times10^{10}$ cm^{-2}, the OCL thickness $b = 0.28$ μm, and the cavity length $L = 1.1$ mm (at this L and the as-cleaved facet reflectivity $R = 0.32$, the mirror loss $\beta = 10$ cm^{-1}). We assume 10% QD-size fluctuations, a single-layer structure, and an ideal overlap between the electron and hole wave functions in a QD. At these parameters, the maximum modal gain for this structure $g^{max} = 29.52$ cm^{-1}. (Reprinted with permission from Fig. 2 of ref. [A2], Copyright (2011) by SPIE.)

$$0 = \frac{j_0}{eb} - \sigma_n v_n \frac{N_s}{b}\left(1 - f_{n,0}\right) n_{OCL,0} + \sigma_n v_n n_1 \frac{N_s}{b} f_{n,0} - B n_{OCL,0}^2, \tag{2.9}$$

$$0 = \sigma_n v_n \frac{N_s}{b}\left(1 - f_{n,0}\right) n_{OCL,0} - \sigma_n v_n n_1 \frac{N_s}{b} f_{n,0} - \frac{N_s}{b}\frac{f_{n,0}^2}{\tau_{QD}} - v_g g^{max}\left(2 f_{n,0} - 1\right) n_{ph,0}, \tag{2.10}$$

$$0 = v_g g^{max}\left(2 f_{n,0} - 1\right) n_{ph,0} - v_g \beta n_{ph,0}. \tag{2.11}$$

The steady-state values (denoted by subscript "0") of the free carrier density in the OCL, level occupancy in a QD, and photon density are obtained from the above equations [5, 6]. They are given as follows:

$$f_{\mathrm{n},0} = \frac{1}{2}\left(1 + \frac{\beta}{g^{\max}}\right) = \frac{1}{2}\left(1 + \frac{1}{\mathrm{v}_\mathrm{g}\tau_{\mathrm{ph}} g^{\max}}\right), \tag{2.12}$$

$$n_{\mathrm{OCL},0}(j_0) = \frac{1}{2B}\left[\sqrt{\left(\frac{1-f_{\mathrm{n},0}}{\tau_{\mathrm{capt},0}}\right)^2 + 4B\left(\frac{N_\mathrm{S}}{b}\frac{f_{\mathrm{n},0}}{\tau_{\mathrm{esc}}} + \frac{j_0}{eb}\right)} - \frac{1-f_{\mathrm{n},0}}{\tau_{\mathrm{capt},0}}\right], \tag{2.13}$$

$$n_{\mathrm{ph},0}(j_0) = \tau_{\mathrm{ph}}\left[\frac{1-f_{\mathrm{n},0}}{\tau_{\mathrm{capt},0}} n_{\mathrm{OCL},0}(j_0) - \frac{N_\mathrm{S}}{b}\frac{f_{\mathrm{n},0}}{\tau_{\mathrm{esc}}} - \frac{N_\mathrm{S}}{b}\frac{f_{\mathrm{n},0}^2}{\tau_{\mathrm{QD}}}\right], \tag{2.14}$$

where the photon lifetime in the cavity is

$$\tau_{\mathrm{ph}} = \frac{1}{\mathrm{v}_\mathrm{g}\beta} = \frac{L}{\mathrm{v}_\mathrm{g}\ln\frac{1}{R}}. \tag{2.15}$$

As seen from (2.12), the steady-state confined-carrier level-occupancy $f_{\mathrm{n},0}$ in a QD is pinned at its threshold value and does not change with j_0 above the lasing threshold. In contrast to $f_{\mathrm{n},0}$, the steady-state free-carrier density $n_{\mathrm{OCL},0}$ in the OCL is not pinned – it rises with j_0 above the lasing threshold. It should be emphasized that it is the non-instantaneous capture of carriers from the OCL into QDs that causes this rise in $n_{\mathrm{OCL},0}$ above the lasing threshold [5, 6].

With (2.12), the steady-state light-current characteristic (the output optical power P_0 versus j_0) is written as

$$P_0(j_0) = \hbar\omega_0 \frac{n_{\mathrm{ph},0}(j_0)}{\tau_{\mathrm{ph}}} WLb = \hbar\omega_0 WLb\left[\frac{1-f_{\mathrm{n},0}}{\tau_{\mathrm{capt},0}} n_{\mathrm{OCL},0}(j_0) - \frac{N_\mathrm{S}}{b}\frac{f_{\mathrm{n},0}}{\tau_{\mathrm{esc}}} - \frac{N_\mathrm{S}}{b}\frac{f_{\mathrm{n},0}^2}{\tau_{\mathrm{QD}}}\right], \tag{2.16}$$

where $\hbar\omega_0$ is the photon energy and W is the lateral size of the device.

We apply the small-signal analysis [11-17] of rate equations (2.1) – (2.3) (see Appendix I), and consider the injection current density in (2.1) in the form of

$$j = j_0 + \left(\delta j_\mathrm{m}\right)\exp\left(i\omega t\right), \tag{2.17}$$

where j_0 is the dc component and the amplitude $\delta j_{\rm m}$ of the time-harmonic ac component is small ($\delta j_{\rm m} << j_0 - j_{\rm th}$, where $j_{\rm th}$ is the threshold current density). Correspondingly, we look for $n_{\rm OCL}$, $f_{\rm n}$, and $n_{\rm ph}$ in (2.1) – (2.3) in the form of

$$n_{\rm OCL} = n_{\rm OCL,0} + (\delta n_{\rm OCL\text{-}m})\exp(i\omega t), \tag{2.18}$$

$$f_{\rm n} = f_{\rm n,0} + (\delta f_{\rm n\text{-}m})\exp(i\omega t), \tag{2.19}$$

$$n_{\rm ph} = n_{\rm ph,0} + (\delta n_{\rm ph\text{-}m})\exp(i\omega t), \tag{2.20}$$

We obtain from (2.1)–(2.3) a set of algebraic equations in the frequency-dependent small amplitudes $\delta n_{\rm OCL–m}$, $\delta f_{\rm n–m}$, and $\delta n_{\rm ph–m}$, the solution of which yields the modulation response function

$$H(\omega) = \left|\frac{\delta n_{\rm ph\text{-}m}(\omega)}{\delta n_{\rm ph\text{-}m}(0)}\right|^2 = \frac{A_0^2}{(A_0 - A_2\omega^2)^2 + (\omega^3 - A_1\omega)^2}. \tag{2.21}$$

The coefficients A_0 , A_1, and A_2 are functions of the laser structure parameters and dc component of injection current density j_0. They are given as follows:

$$A_0 = \frac{b}{N_{\rm S}} {\rm v_g} g^{\max} \frac{n_{\rm ph,0}}{\tau_{\rm ph}} \left[\sigma_{\rm n} {\rm v_n} \frac{N_{\rm S}}{b}(1 - f_{\rm n,0}) + 2Bn_{\rm OCL,0} \right], \tag{2.22}$$

$$\begin{aligned} A_1 = {} & \sigma_{\rm n} {\rm v_n}(n_{\rm OCL,0} + n_1)Bn_{\rm OCL,0} + \left(\frac{f_{\rm n,0}}{\tau_{\rm QD}} + \frac{b}{N_{\rm S}} {\rm v_g} g^{\max} n_{\rm ph} \right) \left[\sigma_{\rm n} {\rm v_n} \frac{N_{\rm S}}{b}(1 - f_{\rm n,0}) + 2Bn_{\rm OCL,0} \right] \\ & + \frac{b}{N_{\rm S}} {\rm v_g} g^{\max} \frac{n_{\rm ph}}{\tau_{\rm ph}}, \end{aligned} \tag{2.23}$$

$$A_2 = \frac{1}{2}\sigma_{\rm n} {\rm v_n}(n_{\rm OCL,0} + n_1) + \sigma_{\rm n} {\rm v_n} \frac{N_{\rm S}}{b}(1 - f_{\rm n,0}) + \frac{f_{\rm n,0}}{\tau_{\rm QD}} + \frac{b}{N_{\rm S}} {\rm v_g} g^{\max} n_{\rm ph,0} + 2Bn_{\rm OCL,0}. \tag{2.24}$$

The photodetection generates an electric current linearly proportional to the optical power (i.e., proportional to the photon density). Since the electric power is measured, which is quadratic in electric current, the photon density is squared in the modulation response function as is shown in (2.21) (see Fig. 1.6 in Chapter 1) [18].

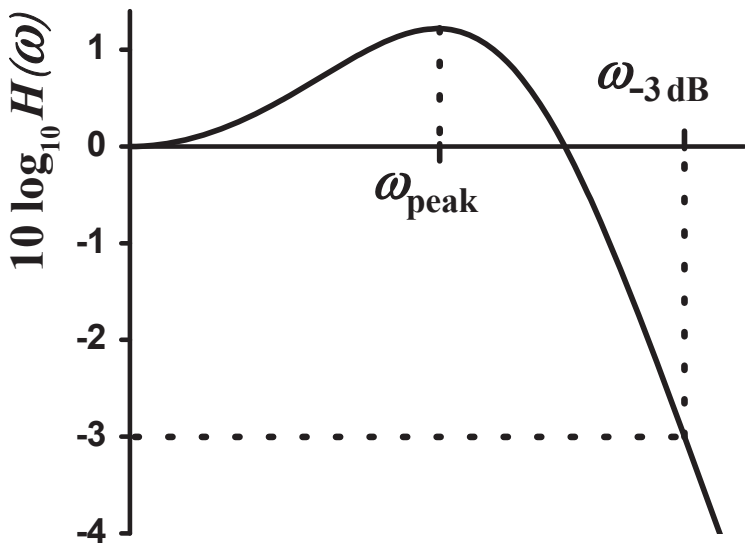

Fig. 2.3. Modulation response function vs. modulation frequency ω. The –3 dB bandwidth is indicated in the figure: $10\log_{10} H(\omega_{-3\mathrm{dB}}) = -3$.

At a fixed value of $j_0 > j_{\mathrm{th}}$, with increasing the modulation frequency ω from zero, the modulation response function increases, approaches its peak at a certain value of ω_{peak} and then decreases (see Fig. 2.3). The expression for ω_{peak} obtained by taking the derivative of the denominator of (2.19) with respect to ω and setting it to zero is

$$\omega_{\mathrm{peak}} = \sqrt{\frac{-\left(A_2^2 - 2A_1\right) + \sqrt{\left(A_2^2 - 2A_1\right)^2 - 3\left(A_1^2 - 2A_0A_2\right)}}{3}}. \tag{2.25}$$

ω_{peak} exists (it must be real and positive) only for a certain range of j_0. At a certain value of j_0, when

$$A_1^2 - 2A_0A_2 = 0, \tag{2.26}$$

ω_{peak} becomes equal to zero. Eq. (2.26) is a quadratic equation in j_0.

The modulation bandwidth is defined as the -3 dB bandwidth, i.e., the frequency at which $H(\omega)$ has fallen to half its dc ($\omega = 0$) value (as indicated in Fig. 2.3),

$$10\log_{10} H\left(\omega_{-3\text{ dB}}\right) = -3. \tag{2.27}$$

Using (2.21), a cubic equation for the square of the modulation bandwidth $\omega_{-3\text{ dB}}$ is obtained,

$$\omega_{-3\text{ dB}}^6 + \left(A_2^2 - 2A_1\right)\omega_{-3\text{ dB}}^4 + \left(A_1^2 - 2A_0A_2\right)\omega_{-3\text{ dB}}^2 - \left(r-1\right)A_0^2 = 0, \tag{2.28}$$

where the numerical parameter $r = 10^{0.3} \approx 1.995$ originates from the definition of the –3 dB bandwidth.

2.3. Discussion

For illustration of our results, room-temperature operation of a GaInAsP heterostructure lasing near 1.55 μm [3] is considered here. We assume 10% QD-size fluctuations, the surface density of QDs in a single-layer $N_S = 6.11\times10^{10}$ cm^{-2}, and an ideal overlap between the electron and hole wave functions in a QD. At these parameters, the maximum modal gain in a single-QD-layer structure $g^{\max} = 29.52$ cm^{-1}. The OCL thickness $b = 0.28$ μm and the cavity length $L =$ 1.1 mm (at this L and the as-cleaved facet reflectivity $R = 0.32$, the mirror loss $\beta = 10$ cm^{-1}).

The modulation bandwidth depends strongly on the capture cross-section σ_n. At a fixed j_0, with making slower the capture into QDs (reducing σ_n), $\omega_{-3\text{ dB}}$ decreases and finally becomes zero (Figs. 2.4. and 2.5.).

As seen from Fig. 2.5., $\omega_{-3\text{ dB}} = 0$ at a certain non-vanishing value $\sigma_n^{\min}$. This is due to the fact that, at a given j_0, no lasing is attainable in the structure if $\sigma_n < \sigma_n^{\min}$. Indeed, while j_0 is fixed, the threshold current density increases with decreasing σ_n (the curve corresponding to the left axis in the figure),

$$j_{\text{th}} = \frac{eN_S}{\tau_{QD}} f_{n,0}^2 + ebB\left(n_1 \frac{f_{n,0}}{1-f_{n,0}} + \frac{1}{\sigma_n v_n \tau_{QD}} \frac{f_{n,0}^2}{1-f_{n,0}}\right)^2, \tag{2.29}$$

where $f_{n,0}$ is given by (2.10). In order for the lasing to occur, j_0 should be higher than j_{th}. At a certain $\sigma_n^{\min}$, j_{th} becomes equal to j_0 (Fig. 2.5.). At $\sigma_n \le \sigma_n^{\min}$, $j_{\text{th}} \ge j_0$, which means that there can be no lasing and hence no direct modulation in the structure (the shaded region in Fig. 2.5.).

The minimum tolerable capture cross-section for the lasing to occur at j_0 is found from the condition $j_{\text{th}} = j_0$ and is given by

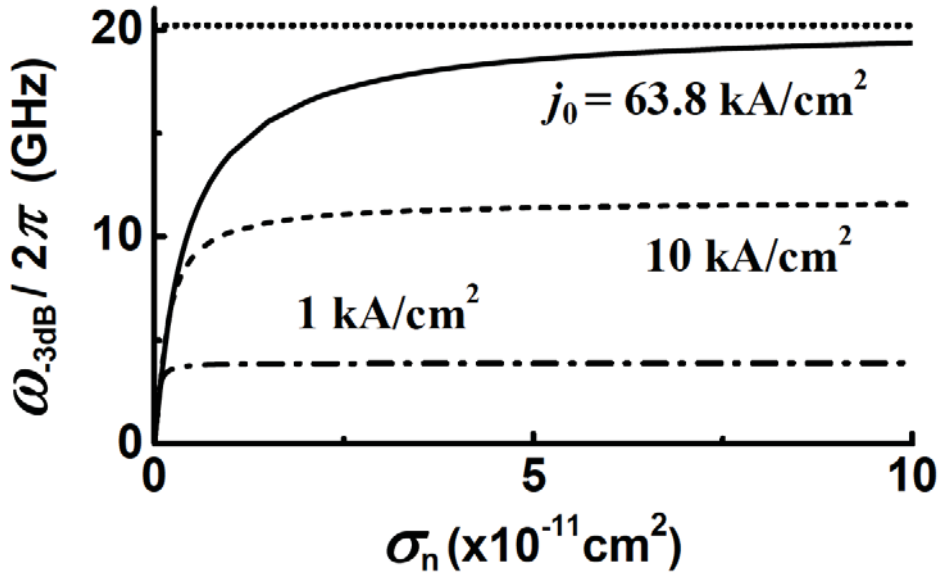

Fig. 2.4. Modulation bandwidth vs. capture cross-section into a QD at different values of the dc component j_0 of the injection current density in a single-layer structure. The horizontal dashed lines show $\omega_{-3\,\mathrm{dB}}$ for the case of instantaneous capture (eq. (9) of Ref. [2]). 63.8 kA/cm^2 is the optimum value of j_0 maximizing $\omega_{-3\,\mathrm{dB}}$ for the case of instantaneous capture and, correspondingly, the top horizontal line shows $\omega_{-3\,\mathrm{dB}}^{\max}$ for that case [eq. (2.31)]. T = 300 K and L = 1.1 mm. (Reprinted with permission from Fig. 3 of ref. [A2], Copyright (2011) by SPIE.)

$$\sigma_{\mathrm{n}}^{\min}(j_0) = \frac{1}{\mathrm{v}_{\mathrm{n}}\tau_{\mathrm{QD}}}\frac{f_{\mathrm{n},0}^2}{1-f_{\mathrm{n},0}}\sqrt{ebB}\,\frac{\sqrt{j_0 - \dfrac{eN_{\mathrm{S}}}{\tau_{\mathrm{QD}}}f_{\mathrm{n},0}^2} + \sqrt{j_{\mathrm{th}}^{\mathrm{eq}} - \dfrac{eN_{\mathrm{S}}}{\tau_{\mathrm{QD}}}f_{\mathrm{n},0}^2}}{j_0 - j_{\mathrm{th}}^{\mathrm{eq}}}, \tag{2.30}$$

where $j_{\mathrm{th}}^{\mathrm{eq}}$ is the threshold current density for the case of instantaneous capture into QDs [$j_{\mathrm{th}}^{\mathrm{eq}}$ is obtained using $\sigma_{\mathrm{n}} = \infty$ in (2.29)],

$$j_{\mathrm{th}}^{\mathrm{eq}} = \frac{eN_{\mathrm{S}}}{\tau_{\mathrm{QD}}}f_{\mathrm{n},0}^2 + ebB\left(n_1\frac{f_{\mathrm{n},0}}{1-f_{\mathrm{n},0}}\right)^2. \tag{2.31}$$

The expression for $\sigma_{\mathrm{n}}^{\min}$ can also be obtained using (2.12) from the condition $n_{\mathrm{ph},0}\left(\sigma_{\mathrm{n}}^{\min}\right) = 0$.

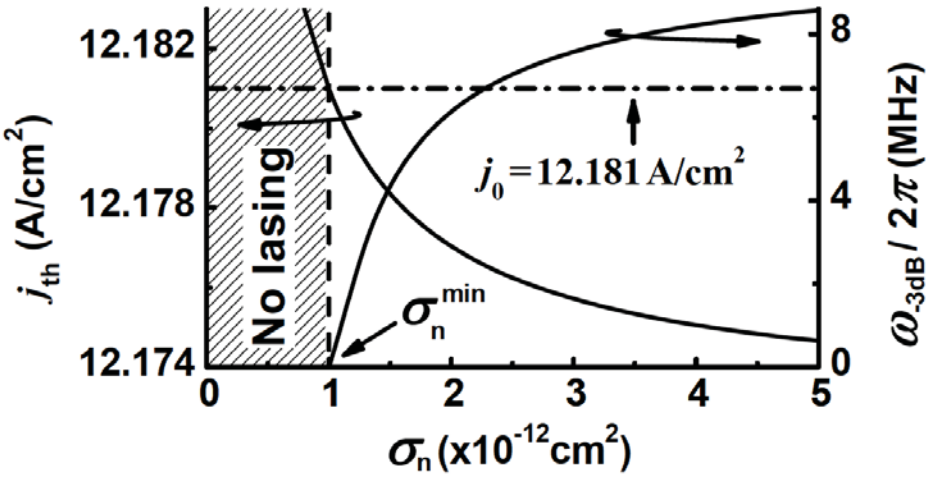

Fig. 2.5. Modulation bandwidth (at a very low dc component of the injection current density) and threshold current density vs. capture cross-section into a QD in a single-layer structure. No lasing is attainable in the structure if $\sigma_n < \sigma_n^{min}(j_0)$, where $\sigma_n^{min}(j_0)$ is given by (2.22). (Reprinted with permission from Fig. 4 of ref. [A2], Copyright (2011) by SPIE.)

The dependence of σ_n^{min} on j_0 is shown in Fig. 2.6. As seen from the figure and (2.25), when j_0 decreases and approaches j_{th}^{eq}, σ_n^{min} increases infinitely, i.e., no lasing is attainable at $j_0 \le j_{th}^{eq}$ even if the carrier capture into QDs is instantaneous. With increasing j_0, σ_n^{min} becomes smaller, i.e., the lasing can occur and hence the direct modulation of the output power is possible at a slower capture.

At $\sigma_n = \sigma_n^{min}(j_0)$, $j_0 = j_{th}$, $n_{ph,0} = 0$ [see (2.12)], and $A_0\left[\sigma_n^{min}(j_0)\right] = 0$ [see (2.22)]. Hence eq. (2.28) reduces to the following equation:

$$\omega_{-3\,dB}^6 + \left(A_2^2 - 2A_1\right)\omega_{-3\,dB}^4 + \left(A_1^2 - 2A_0A_2\right)\omega_{-3\,dB}^2 = 0, \tag{2.32}$$

whose solution $\omega_{-3\,dB} = 0$ is the physical solution since no direct modulation is possible at the lasing threshold when $n_{ph,0} = 0$. Hence

$$\omega_{-3\,dB}\left[\sigma_n^{min}(j_0)\right] = 0. \tag{2.33}$$

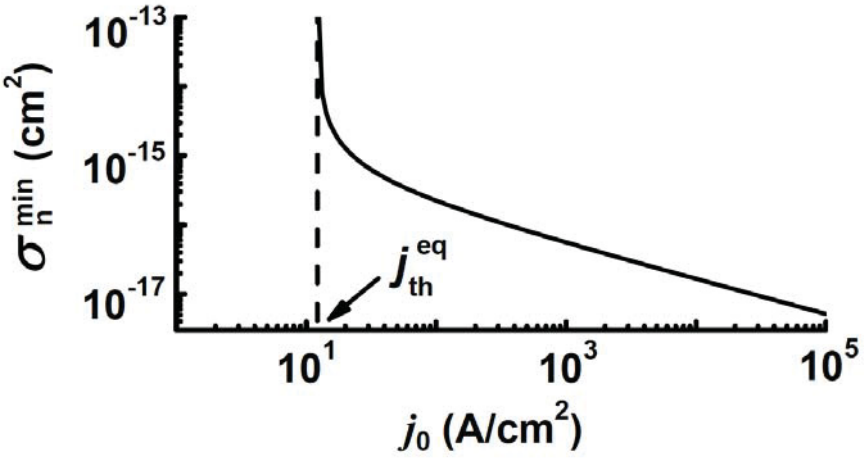

(a)

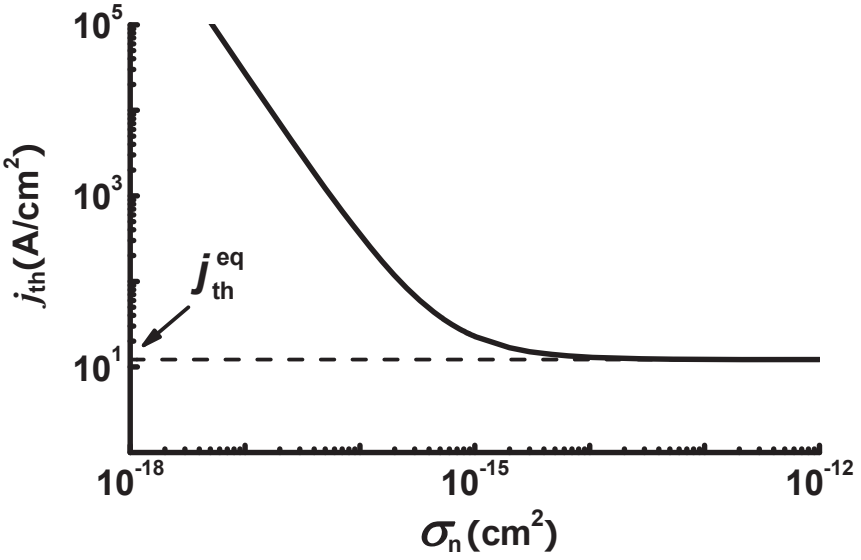

(b)

Fig. 2.6. Minimum tolerable cross-section of carrier capture into a QD vs. dc component j_0 of the injection current density (a), and threshold current density vs. capture cross-section (b). j_{th}^{eq} is the threshold current density for the case of instantaneous capture into a QD, i.e., the lowest threshold current density – for $j_0 < j_{th}^{eq}$, the lasing cannot occur even if the capture is instantaneous. (Fig. 2.6(a) is reprinted with permission from Fig. 5 of ref. [A2], .)

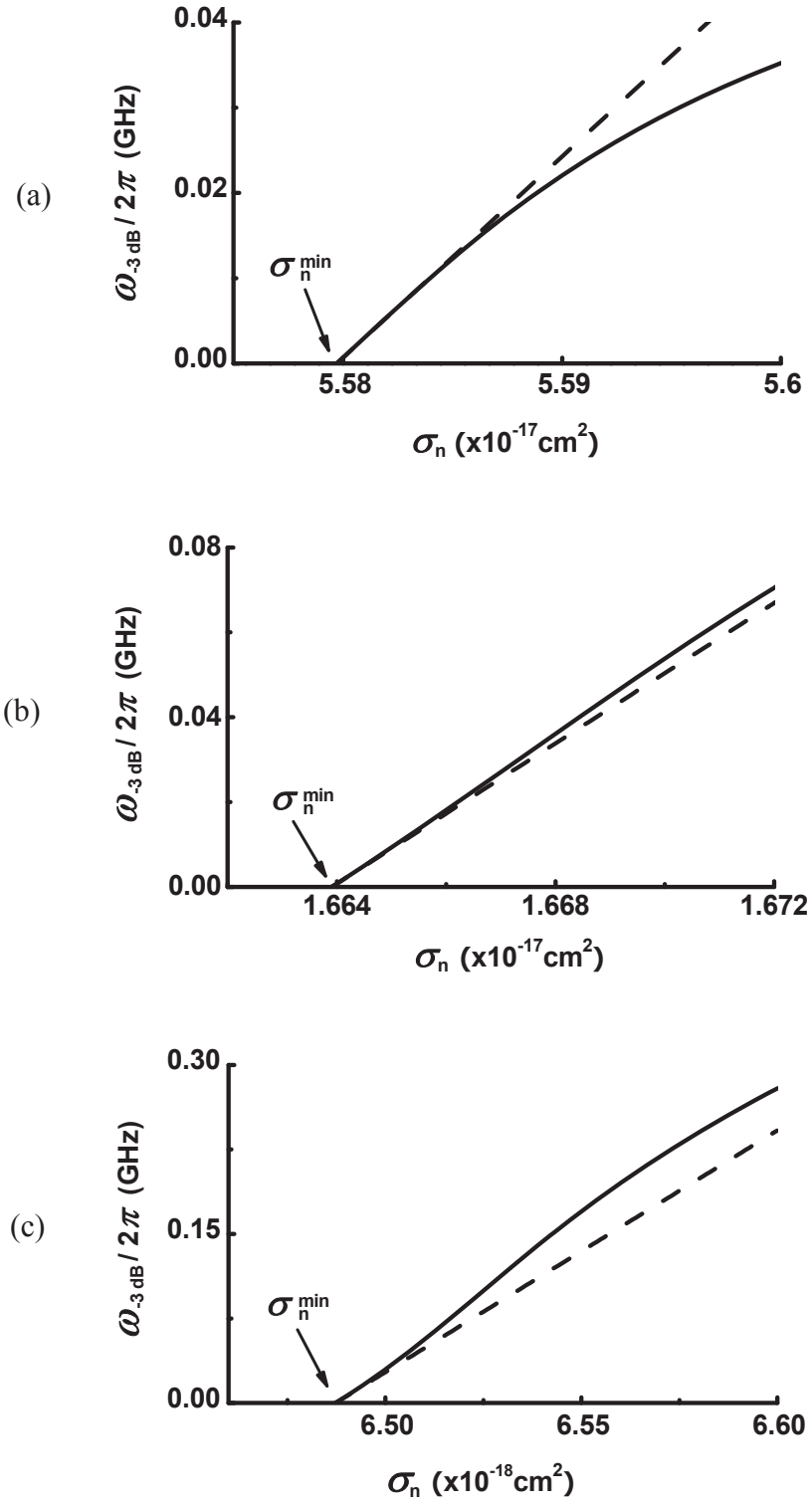

Fig. 2.7. $\omega_{-3\,dB}/2\pi$ vs. σ_n in the vicinity of $\sigma_n^{min}(j_0)$ for different values of the dc component j_0 of the injection current density. The solid curves are the numerical solutions of eq. (2.28) and the dashed lines are given by eq. (2.37). j_0 = 1, 10, and 63.8 kA/cm^2 in (a), (b), and (c), respectively.

Let us consider the situation when $\sigma_{\rm n}$ is slightly larger than $\sigma_{\rm n}^{\rm min}(j_0)$, i.e., $n_{\rm ph,\,0}$ is very small. Correspondingly, A_0 [which is proportional to $n_{\rm ph,\,0}$ – see (2.22)] will be very small and so will be $\omega_{-3\ {\rm dB}}$. The cubic equation (2.28) in $\omega_{-3\ {\rm dB}}^2$ will reduce to the linear equation in $\omega_{-3\ {\rm dB}}^2$

$$\left(A_1^2 - 2A_0A_2\right)\omega_{-3\ {\rm dB}}^2 - (r-1)A_0^2 = 0, \tag{2.34}$$

whose solution gives the following expression for $\omega_{-3\ {\rm dB}}$ when $\sigma_{\rm n}$ is slightly larger than $\sigma_{\rm n}^{\rm min}(j_0)$:

$$\omega_{-3\ {\rm dB}} \approx \sqrt{r-1}\,\frac{{\rm v_g}g^{\rm max}\left[\sigma_{\rm n}^{\rm min}{\rm v_n}\dfrac{N_{\rm S}}{b}(1-f_{\rm n,\,0}) + 2Bn_{\rm OCL,\,0}^{\rm th}\right]\left(-\left.\dfrac{\partial j_{\rm th}}{\partial\sigma_{\rm n}}\right|_{\sigma_{\rm n}=\sigma_{\rm n}^{\rm min}}\right)\dfrac{\eta_{\rm int}^{\rm th}}{eN_{\rm S}}\left(\sigma_{\rm n}-\sigma_{\rm n}^{\rm min}\right)}{\sigma_{\rm n}^{\rm min}{\rm v_n}\left(n_{\rm OCL,\,0}^{\rm th}+n_1\right)Bn_{\rm OCL,\,0}^{\rm th} + \dfrac{f_{\rm n,\,0}}{\tau_{\rm QD}}\left[\sigma_{\rm n}^{\rm min}{\rm v_n}\dfrac{N_{\rm S}}{b}(1-f_{\rm n,\,0}) + 2Bn_{\rm OCL,\,0}^{\rm th}\right]}, \tag{2.35}$$

where $n_{\rm OCL,\,0}^{\rm th}$, $\eta_{\rm int}^{\rm th}$, and $\left.\dfrac{\partial j_{\rm th}}{\partial\sigma_{\rm n}}\right|_{\sigma_{\rm n}=\sigma_{\rm n}^{\rm min}}$ are the threshold values of the corresponding quantities taken at $\sigma_{\rm n}=\sigma_{\rm n}^{\rm min}$ [$\sigma_{\rm n}^{\rm min}$ is given by (2.30)]. The internal differential quantum efficiency at the lasing threshold is given by [6]

$$\eta_{\rm int}^{\rm th} = \frac{1}{1+2\left.\dfrac{Bn_{\rm OCL,\,0}^{\rm th}}{\sigma_{\rm n}{\rm v_n}\dfrac{N_{\rm S}}{b}(1-f_{\rm n,\,0})}\right|_{\sigma_{\rm n}=\sigma_{\rm n}^{\rm min}}}. \tag{2.36}$$

At high j_0 (when $\sigma_{\rm n}^{\rm min}\to 0$), the asymptotic expression for $\omega_{-3\ {\rm dB}}$ for $\sigma_{\rm n}$ in the vicinity of $\sigma_{\rm n}^{\rm min}$ [$(\sigma_{\rm n}-\sigma_{\rm n}^{\rm min})/\sigma_{\rm n}^{\rm min} << 1$] is

$$\omega_{-3\ {\rm dB}} \approx 2\sqrt{r-1}\ {\rm v_g}g^{\rm max}\frac{f_{\rm n,\,0}(1-f_{\rm n,\,0})}{2-f_{\rm n,\,0}}\frac{\sigma_{\rm n}-\sigma_{\rm n}^{\rm min}}{\sigma_{\rm n}^{\rm min}}. \tag{2.37}$$

Hence, $\omega_{-3\ {\rm dB}}$ is a linear function of $\left(\sigma_{\rm n}-\sigma_{\rm n}^{\rm min}\right)$ in the vicinity of $\sigma_{\rm n}^{\rm min}$ and becomes zero at $\sigma_{\rm n}^{\rm min}$. The dependence of $\omega_{-3\ {\rm dB}}$ on $\sigma_{\rm n}$ in the vicinity of $\sigma_{\rm n}^{\rm min}$ for different values of j_0 is shown in Fig. 2.7.

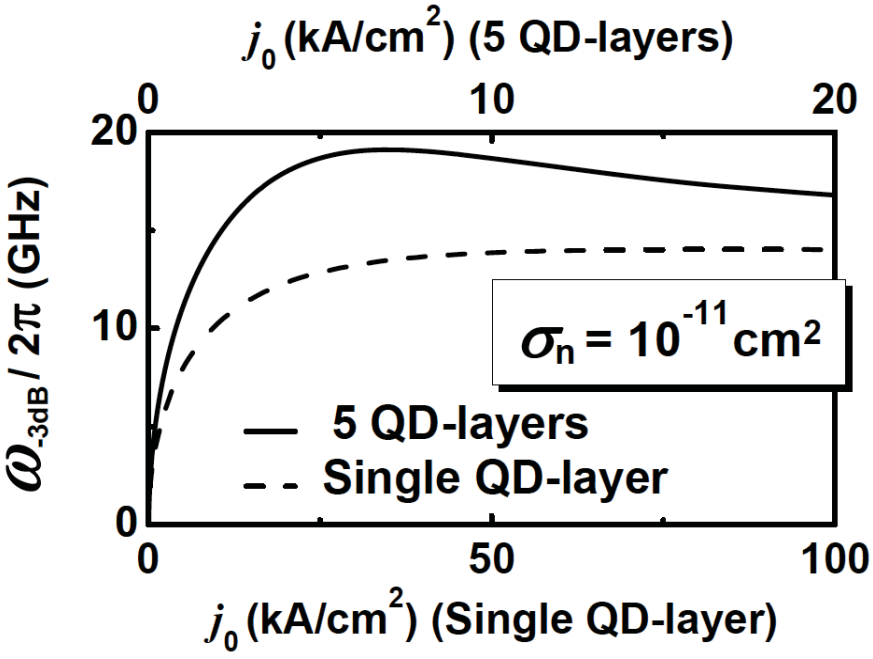

Fig. 2.8. Modulation bandwidth vs. dc component of the injection current density in single- and 5-QD-layer-structures. A plausible value of the capture cross-section $\sigma_n = 10^{-11}$ cm^2 is used [19, 20]. (Reprinted with permission from Fig. 6 of ref. [A2], Copyright (2011) by SPIE.)

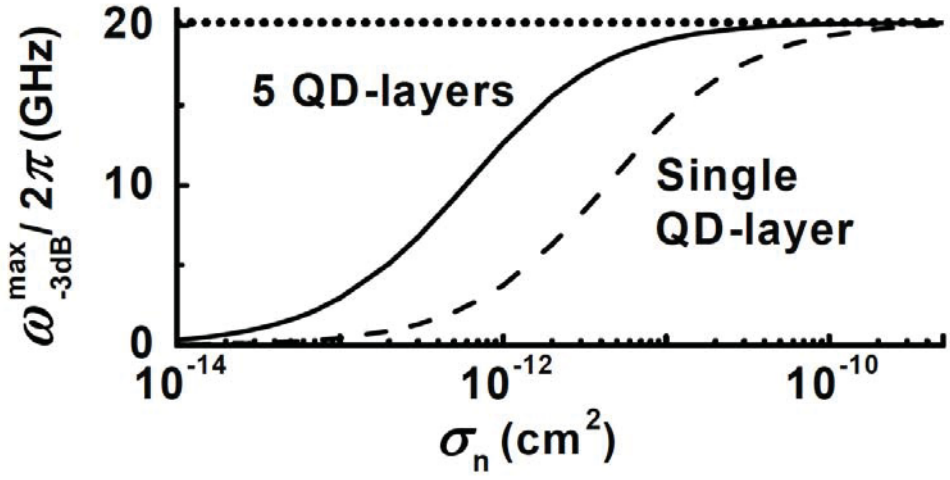

Fig. 2.9. Maximum modulation bandwidth vs. capture cross-section into a QD. The horizontal dashed line shows $\omega^{max}_{-3\ dB}$ for the case of instantaneous capture into QDs [eq. (2.40)]. (Reprinted with permission from Fig. 7 of ref. [A2], Copyright (2011) by SPIE.)

As a function of the dc component j_0 of the injection current density, $\omega_{-3\,\mathrm{dB}}$ has a maximum (Fig. 2.8). The dynamic performances of two laser structures are compared in the figure. All the structure parameters are the same except for the number of QD layers – one is a single-QD-layer structure and the other is a 5-QD-layer structure. In a single-QD-layer structure (the dashed curve), the optimum value j_{opt} of j_0, at which $\omega_{-3\,\mathrm{dB}}^{\max}$ is attained, is very high, i.e., $\omega_{-3\,\mathrm{dB}}^{\max}$ is unattainable. As seen from the figure, there are the following two advantages in a multi-QD-layer structure (the solid curve) as compared to a single-layer structure: (i) $\omega_{-3\,\mathrm{dB}}$ is considerably higher at the same j_0 and (ii) j_{opt} is considerably reduced, which means that $\omega_{-3\,\mathrm{dB}}^{\max}$ is practically attainable.

At large σ_{n}, when $\tau_{\mathrm{capt},0}/\tau_{\mathrm{ph}} \ll 1$ [$\tau_{\mathrm{capt},0}$ and τ_{ph} are given by (2.7) and (2.15), respectively], both $\omega_{-3\,\mathrm{dB}}$ at a given j_0 (Fig. 2.4) and $\omega_{-3\,\mathrm{dB}}^{\max}$ (Fig. 2.9) asymptotically approach their saturation values (the horizontal dotted lines) corresponding to the case of instantaneous capture into QDs,

$$\omega_{-3\ \mathrm{dB}}\Big|_{\sigma_{\mathrm{n}}=\infty} - \omega_{-3\ \mathrm{dB}} \propto \frac{\tau_{\mathrm{capt},\,0}}{\tau_{\mathrm{ph}}} \propto \frac{1}{\sigma_{\mathrm{n}}}, \tag{2.38}$$

$$\begin{aligned} \omega_{-3\ \mathrm{dB}}^{\max}\Big|_{\sigma_{\mathrm{n}}=\infty} - \omega_{-3\ \mathrm{dB}}^{\max} &\approx \frac{1}{\sigma_{\mathrm{n}} \mathrm{V}_{\mathrm{n}} \dfrac{N_{\mathrm{S}}}{b}} \frac{\sqrt{r}}{2\left(1-f_{\mathrm{n},\,0}\right)^2} \frac{1}{\tau_{\mathrm{ph}}^2} \\ &= \frac{\sqrt{2}}{\tau_{\mathrm{ph}}} \frac{1}{2} \sqrt{\frac{r}{2}} \frac{1}{\left(1-f_{\mathrm{n},\,0}\right)^2} \frac{\tau_{\mathrm{capt},\,0}}{\tau_{\mathrm{ph}}}, \end{aligned} \tag{2.39}$$

where $\omega_{-3\,\mathrm{dB}}\Big|_{\sigma_{\mathrm{n}}=\infty}$ is given by eq. (9) of [2] and $\omega_{-3\ \mathrm{dB}}^{\max}\Big|_{\sigma_{\mathrm{n}}=\infty}$ is

$$\omega_{-3\,\mathrm{dB}}^{\max}\Big|_{\sigma_{\mathrm{n}}=\infty} \approx \frac{\sqrt{2}}{\tau_{\mathrm{ph}}}. \tag{2.40}$$

As seen from Fig. 2.9. and (2.40), while the saturation value of $\omega_{-3\,\mathrm{dB}}^{\max}$ at $\sigma_{\mathrm{n}} \to \infty$ and at a fixed L does not depend on the number of QD-layers, $\omega_{-3\,\mathrm{dB}}^{\max}$ at a given finite σ_{n} is higher in a multi-layer structure as compared to a single-layer structure.

2.4. Conclusion

The small-signal analysis was applied to a set of rate equations for free carriers in the OCL, carriers confined in QDs, and photons. The modulation response function $H(\omega)$ and a cubic equation for $\omega^2_{-3\ \mathrm{dB}}$ of the modulation bandwidth were obtained. The time delay in carrier capture from the OCL into QDs strongly limits the modulation bandwidth of a QD laser. $\omega_{-3\ \mathrm{dB}}$ is highest in the case of instantaneous capture into QDs, when the cross-section of carrier capture into a QD $\sigma_\mathrm{n} = \infty$. Asymptotic expressions for $\omega_{-3\ \mathrm{dB}}$ for the case of large and small σ_n were derived. With reducing σ_n, $\omega_{-3\ \mathrm{dB}}$ decreases and becomes zero at a certain non-vanishing $\sigma_\mathrm{n}^{\min}$. This $\sigma_\mathrm{n}^{\min}$ presents the minimum tolerable σ_n for the lasing to occur at a given dc component j_0 of the injection current density.

The use of multiple layers with QDs has been shown to significantly improve the modulation response of the laser – $\omega_{-3\ \mathrm{dB}}$ is considerably higher in a multilayer structure as compared to a single-layer structure at the same j_0. At a plausible cross-section $\sigma_\mathrm{n} = 10^{-11}\ \mathrm{cm}^2$ [19, 20], $\omega_{-3\ \mathrm{dB}}$ as high as 19 GHz can be obtained in a 5-QD-layer structure with the cavity length $L = 1.1$ mm at a practical value of $j_0 = 7\ \mathrm{kA/cm}^2$. This analysis provides a basis for optimizing the QD laser design for high-speed operation.

Appendix I

Relaxation oscillations and modulation response in a QD laser: Small-signal analysis

The rate equations for free carriers in the OCL, carriers confined in QDs, and photons are given by (2.1) – (2.3).

Let us linearize eqs. (2.1) – (2.3), i.e., consider the injection current density in the form

$$j = j_0 + j_{\mathrm{m}}(t), \tag{A1}$$

and, correspondingly, the solutions of (2.1) – (2.3) in the form

$$f_{\mathrm{n}} = f_{\mathrm{n},0} + \varphi(t), \tag{A2}$$

$$n_{\mathrm{OCL}} = n_{\mathrm{OCL},0} + \nu(t), \tag{A3}$$

$$n_{\mathrm{ph}} = n_{\mathrm{ph},0} + s(t), \tag{A4}$$

where $j_{\mathrm{m}}(t)$, $\varphi(t)$, $\nu(t)$, and $s(t)$ are small quantities compared to j_0, $n_{\mathrm{OCL},0}$, $f_{\mathrm{n},0}$, and $n_{\mathrm{ph},0}$, respectively, i.e.,

$$j_{\mathrm{m}}(t) << j_0, \tag{A5}$$

$$\varphi(t) << f_{\mathrm{n},0}, \tag{A6}$$

$$\nu(t) << n_{\mathrm{OCL},0}, \tag{A7}$$

$$s(t) << n_{\mathrm{ph},0}, \tag{A8}$$

where j_0 is the dc component of the injection current density, and $f_{\mathrm{n},0}$, $n_{\mathrm{OCL},0}$, and $n_{\mathrm{ph},0}$ are the solutions of the rate equations at the steady-state, i.e., at $j = j_0$, which are given by (2.12), (2.13), and (2.14), respectively. To ensure lasing, the following condition should hold for $j_{\mathrm{m}}(t)$:

$$j_{\mathrm{m}} << j_0 - j_{\mathrm{th}}, \tag{A9}$$

where j_{th} is the threshold current density given by (2.29).

Using (A1) – (A4) in (2.1) – (2.3) and dropping the quadratic terms in the small quantities $\varphi(t)$, $\nu(t)$, and $s(t)$, we obtain the following set of linearized differential equations:

$$\frac{\partial \varphi\,(t)}{\partial t} = -\left[\frac{1}{2}\sigma_{\mathrm{n}}\mathrm{v}_{\mathrm{n}}(n_{\mathrm{OCL},0}+n_1)+\frac{f_{\mathrm{n},0}}{\tau_{\mathrm{QD}}}+\frac{b}{N_{\mathrm{S}}}\mathrm{v}_{\mathrm{g}}g^{\max}n_{\mathrm{ph},0}\right]\varphi(t)+\frac{1}{2}\sigma_{\mathrm{n}}\mathrm{v}_{\mathrm{n}}(1-f_{\mathrm{n},0})\,\nu(t) - \frac{1}{2}\frac{b}{N_{\mathrm{S}}}\frac{1}{\tau_{\mathrm{ph}}}s(t), \tag{A10}$$

$$\frac{\partial \nu(t)}{\partial t} = \sigma_{\mathrm{n}}\mathrm{v}_{\mathrm{n}}(n_{\mathrm{OCL},0}+n_1)\frac{N_{\mathrm{S}}}{b}\varphi(t)-\left[\sigma_{\mathrm{n}}\mathrm{v}_{\mathrm{n}}\frac{N_{\mathrm{S}}}{b}(1-f_{\mathrm{n},0})+2Bn_{\mathrm{OCL},0}\right]\nu(t)+\frac{j_{\mathrm{m}}(t)}{eb}, \tag{A11}$$

$$\frac{\partial s(t)}{\partial t} = 2\mathrm{v}_{\mathrm{g}}g^{\max}n_{\mathrm{ph},0}\varphi(t), \tag{A12}$$

where the photon lifetime in the cavity τ_{ph} is given by (2.15).

For relaxation oscillations, we put

$$j_{\mathrm{m}} = 0 \tag{A13}$$

and look for the solutions of the set of linear first-order differential equations (A10) – (A12) in the form

$$\varphi(t) = (\delta f_{\mathrm{n\text{-}m}})\,e^{-ht}, \tag{A14}$$

$$\nu(t) = (\delta n_{\mathrm{OCL\text{-}m}})\,e^{-ht}, \tag{A15}$$

$$s(t) = (\delta n_{\mathrm{ph\text{-}m}})\,e^{-ht}. \tag{A16}$$

Using (A13) – (A16) in (A10) – (A12), we obtain

$$\begin{bmatrix} A_{11}(h) & A_{12} & A_{13} \\ A_{21} & A_{22}(h) & 0 \\ A_{31} & 0 & A_{33}(h) \end{bmatrix}\begin{pmatrix} \delta f_{\mathrm{n\text{-}m}} \\ \delta n_{\mathrm{OCL\text{-}m}} \\ \delta n_{\mathrm{ph\text{-}m}} \end{pmatrix} = 0, \tag{A17}$$

where

$$A_{11}(h) = -h+\frac{1}{2}\sigma_{\mathrm{n}}\mathrm{v}_{\mathrm{n}}(n_{\mathrm{OCL},0}+n_1)+\frac{f_{\mathrm{n},0}}{\tau_{\mathrm{QD}}}+\frac{b}{N_{\mathrm{S}}}\mathrm{v}_{\mathrm{g}}g^{\max}n_{\mathrm{ph},0}\,, \tag{A18}$$

$$A_{12} = -\frac{1}{2}\sigma_{\mathrm{n}}\mathrm{v}_{\mathrm{n}}(1-f_{\mathrm{n},0}), \tag{A19}$$

$$A_{13} = \frac{1}{2}\frac{b}{N_{\mathrm{S}}}\frac{1}{\tau_{\mathrm{ph}}}, \tag{A20}$$

$$A_{21} = -\sigma_{\mathrm{n}} \mathrm{v}_{\mathrm{n}} (n_{\mathrm{OCL},0} + n_1) \frac{N_{\mathrm{S}}}{b}, \tag{A21}$$

$$A_{22}(h) = -h + \sigma_{\mathrm{n}} \mathrm{v}_{\mathrm{n}} \frac{N_{\mathrm{S}}}{b} (1 - f_{\mathrm{n},0}) + 2Bn_{\mathrm{OCL},0}, \tag{A22}$$

$$A_{31} = -2\mathrm{v}_{\mathrm{g}} g^{\max} n_{\mathrm{ph},0}, \tag{A23}$$

$$A_{33}(h) = -h. \tag{A24}$$

A set (A17) of linear equations is homogeneous. The condition for the existence of non-zero solutions of (A17) is

$$\begin{vmatrix} A_{11} & A_{12} & A_{13} \\ A_{21} & A_{22} & 0 \\ A_{31} & 0 & A_{33} \end{vmatrix} = A_{11}A_{22}A_{33} - A_{12}A_{21}A_{33} - A_{13}A_{22}A_{31} = 0. \tag{A25}$$

Eq. (A25) is a cubic equation in h,

$$-h^3 + A_2 h^2 - A_1 h + A_0 = 0, \tag{A26}$$

where the coefficients A_0, A_1, and A_2 are given by (2.22), (2.23), and (2.24), respectively.

For the modulation response, the ac component j_{m} of the injection current density is not zero. We consider a time-harmonic j_{m},

$$j_{\mathrm{m}} = (\delta j_{\mathrm{m}}) e^{i\omega t}. \tag{A27}$$

We correspondingly look for the solutions of the set of linearized differential equations (A10) – (A12) in the form

$$\varphi(\omega) = (\delta f_{\mathrm{n\text{-}m}}) e^{i\omega t}, \tag{A28}$$

$$\nu(\omega) = (\delta n_{\mathrm{OCL\text{-}m}}) e^{i\omega t}, \tag{A29}$$

$$s(\omega) = (\delta n_{\mathrm{ph\text{-}m}}) e^{i\omega t}. \tag{A30}$$

Using (A27) – (A30) in (A10) – (A12), we obtain

$$\begin{pmatrix} C_{11} & C_{12} & C_{13} \\ C_{21} & C_{22} & 0 \\ C_{31} & 0 & C_{33} \end{pmatrix} \begin{pmatrix} \delta f_{\mathrm{n\text{-}m}} \\ \delta n_{\mathrm{OCL\text{-}m}} \\ \delta n_{\mathrm{ph\text{-}m}} \end{pmatrix} = \begin{pmatrix} 0 \\ \delta j_{\mathrm{m}} / eb \\ 0 \end{pmatrix}. \tag{A31}$$

The coefficients C_{nm} in (A31) are related to the coefficients A_{nm} in (A17) as follows:

$$C_{\mathrm{nm}} = A_{\mathrm{nm}}\big|_{h=-i\omega}, \tag{A32}$$

where A_{nm} are given by (A18) – (A24).

The solutions of the set (A31) are

$$\delta f_{\mathrm{n\text{-}m}}(\omega) = \frac{\begin{vmatrix} 0 & C_{12} & C_{13} \\ \delta j_{\mathrm{m}}/eb & C_{22} & 0 \\ 0 & 0 & C_{33} \end{vmatrix}}{\Delta}, \tag{A33}$$

$$\delta n_{\mathrm{OCL\text{-}m}}(\omega) = \frac{\begin{vmatrix} C_{11} & 0 & C_{13} \\ C_{21} & \delta j_{\mathrm{m}}/eb & 0 \\ C_{31} & 0 & C_{33} \end{vmatrix}}{\Delta}, \tag{A34}$$

$$\delta n_{\mathrm{ph\text{-}m}}(\omega) = \frac{\begin{vmatrix} C_{11} & C_{12} & 0 \\ C_{21} & C_{22} & \delta j_{\mathrm{m}}/eb \\ C_{31} & C_{32} & 0 \end{vmatrix}}{\Delta}, \tag{A35}$$

where

$$\begin{aligned} \Delta = \begin{vmatrix} C_{11} & C_{12} & C_{13} \\ C_{21} & C_{22} & 0 \\ C_{31} & 0 & C_{33} \end{vmatrix} &= C_{11}C_{22}C_{33} - C_{12}C_{21}C_{33} - C_{13}C_{22}C_{31} \\ &= \left(A_{11}A_{22}A_{33} - A_{12}A_{21}A_{33} - A_{13}A_{22}A_{31}\right)\big|_{h=-i\omega} \\ &= -i\omega^3 - A_2\omega^2 + i\,A_1\omega + A_0. \end{aligned} \tag{A36}$$

With eq. (A35) for $\delta n_{\mathrm{ph\text{-}m}}(\omega)$, we obtain eq. (2.21) for the modulation response function.

References [*)]

[A1] L. V. Asryan, Y. Wu, and R. A. Suris, "Carrier capture delay and modulation bandwidth in an edge-emitting quantum dot laser", *Appl. Phys. Lett*., vol. 98, no. 13, Art. no. 131108, Mar. 2011.

[A2] L. V. Asryan, Y. Wu, and R. A. Suris, "Capture delay and modulation bandwidth in a quantum dot laser," *Proc. SPIE*, vol. 7947, pp. 794708-1--794708-8, Jan. 2011.

[A3] L. V. Asryan, Y. Wu, and R. A. Suris, "Carrier capture delay and modulation bandwidth in an edge-emitting quantum dot laser", *Proc. 19th International Symposium "Nanostructures: Physics and Technology"*, June 20-25, 2011, Ekaterinburg, Russia. pp. 19-20.

[A4] L. V. Asryan, Y. Wu, and R. A. Suris, "Modulation bandwidth of a quantum dot laser: The upper limit and limiting factors," *Proc. 15th International Conf. "Laser Optics 2012"*, June 25-29, 2012, St. Petersburg, Russia. Paper no. WeR3-22.

[1] D. Derickson, Fiber optic test and measurement, Prentice-Hall, 1998, p. 642.

[2] L. V. Asryan and R. A. Suris, "Upper limit for the modulation bandwidth of a quantum dot laser," *Appl. Phys. Lett.*, vol. 96, no. 22, Art. no. 221112, May 2010.

[3] L. V. Asryan and R. A. Suris, "Inhomogeneous line broadening and the threshold current density of a semiconductor quantum dot laser," *Semicond. Sci. Technol.*, vol. 11, no. 4, pp. 554-567, Apr. 1996.

[4] L. V. Asryan and R. A. Suris, "Temperature dependence of the threshold current density of a quantum dot laser," *IEEE J. Quantum. Electron.*, vol. 34, no. 5, pp. 841-850, May 1998.

[5] L. V. Asryan, S. Luryi and R. A. Suris, "Intrinsic nonlinearity of the light-current characteristic of semiconductor lasers with a quantum-confined active region," *Appl. Phys. Lett.*, vol. 81, no. 12, pp. 2154-2156, Sept. 2002.

[*)] "A" in the reference number indicates the publications of the author of this dissertation.

[6] L. V. Asryan, S. Luryi and R. A. Suris, "Internal efficiency of semiconductor lasers with a quantum-confined active region," *IEEE J. Quantum. Electron.*, vol. 39, no. 3, pp. 404-418, Mar. 2003.

[7] R. Leon, Y. Kim, C. Jagadish, M. Gal, J. Zou and D. J. H. Cockayne, "Effects of interdiffusion on the luminescence of InGaAs/GaAs quantum dots," *Appl. Phys. Lett.*, vol. 69, no. 13, pp. 1888-1890, Sept. 1996.

[8] K. Nishi, R. Mirin, D. Leonard, G. MedeirosRibeiro, P. M. Petroff and A. C. Gossard, "Structural and optical characterization of InAs/InGaAs self-assembled quantum dots grown on (311)B GaAs," *J. Appl. Phys.*, vol. 80, no. 6, pp. 3466-3470, Sept. 1996.

[9] A. Patane, A. Polimeni, P. C. Main, M. Henini and L. Eaves, "High-temperature light emission from InAs quantum dots," *Appl. Phys. Lett.*, vol. 75, no. 6, pp. 814-816, Aug. 1999.

[10] J. S. Kim and I. H. Bae, "Optical properties of wetting layer in InAs quantum dots at different growth temperatures," *J Korean Phys Soc*, vol. 42, pp. S483-S486, Feb. 2003.

[11] T. Ikegami and Y. Suematsu, "Resonance-like characteristics of the direct modulation of a junction laser," *Proceedings of the IEEE*, vol. 55, no. 1, pp. 122-123, Jan. 1967.

[12] T. L. Paoli and J. E. Ripper, "Direct modulation of semiconductor lasers," *Proceedings of the IEEE*, vol. 58, no. 10, pp. 1457-1465, 1970.

[13] M. J. Adams, "Rate equations and transient phenomena in semiconductor lasers," *Opto-Electronics*, vol. 5, no. 2, pp. 201-215, 1973.

[14] R. F. Kazarinov and R. A. Suris, "Heterodyne reception of light by an injection laser," *Sov. Phys. JETP*, vol. 39, no. 3, pp. 522-527, Sept. 1974.

[15] C. B. Su and V. A. Lanzisera, "Ultra high-speed modulation of 1.3 μm InGaAsP diode lasers," *IEEE J. Quantum. Electron.*, vol. 22, no. 9, pp. 1568-1578, Sept. 1986.

[16] R. Olshansky, P. Hill, V. Lanzisera and W. Powazinik, "Frequency response of 1.3 μm InGaAsP high speed semiconductor lasers," *IEEE J. Quantum. Electron.*, vol. 23, no. 9, pp. 1410-1418, Sept. 1987.

[17] R. Nagarajan, M. Ishikawa, T. Fukushima, R. S. Geels and J. E. Bowers, "High speed quantum-well lasers and carrier transport effects," *IEEE J. Quantum. Electron.*, vol. 28, no. 10, pp. 1990-2008, Oct. 1992.

[18] L. A. Coldren and S. W. Corzine, Diode lasers and photonic integrated circuits, Wiley, 1995, p. 594.

[19] O. Engström, M. Kaniewska, Y. Fu, J. Piscator and M. Malmkvist, "Electron capture cross sections of InAs/GaAs quantum dots," *Appl. Phys. Lett.*, vol. 85, no. 14, pp. 2908-2910, Oct. 2004.

[20] S. K. Zhang, H. J. Zhu, F. Lu, Z. M. Jiang and X. Wang, "Erratum: Coulomb charging effect in self-assembled Ge quantum dots studied by admittance spectroscopy [Phys. Rev. Lett. 80, 3340 (1998)]," *Phys. Rev. Lett.*, vol. 82, no. 12, pp. 2622-2622, Mar. 1999.

Chapter 3

Effect of internal optical loss in the optical confinement layer on the modulation bandwidth of a quantum dot laser

Summary

The internal optical loss, which increases with free-carrier density in the optical confinement layer (OCL), is included in the rate equations model. The modulation bandwidth is calculated as a function of the dc component of the injection current density [A1, A2]*). At a certain optimum value j_0^{opt} of the dc component of the injection current density, the maximum bandwidth $\omega_{-3\,\text{dB}}^{\max}$ is attained and the modulation response function becomes as flat as possible. At this optimum current, the dependence of the modulation response function on the normalized modulation frequency $\omega/\omega_{-3\,\text{dB}}^{\max}$ is found in a universal form. The dependence of the modulation bandwidth on the internal loss cross-section is calculated. The internal loss considerably reduces the modulation bandwidth $\omega_{-3\,\text{dB}}$ of a QD laser. With internal loss cross-section σ_{int} increasing and approaching its maximum tolerable value, $\omega_{-3\,\text{dB}}^{\max}$ decreases and becomes zero. As with j_0^{opt}, there also exists the optimum cavity length, at which $\omega_{-3\,\text{dB}}$ is highest; the larger is σ_{int}, the longer is the optimum cavity.

3.1. Introduction

The optical output in edge-emitting semiconductor lasers is provided by photons leaving the cavity through its mirrors. In addition to this useful output loss, there is also parasitic loss of photons, which occurs within the laser cavity and, for this reason, is termed internal optical loss. There can be several mechanisms for internal loss [1-6], such as free-carrier absorption,

*) "A" in the reference number indicates the publications of the author of this dissertation.

intervalence band absorption, and scattering at rough surfaces. While there have been studies of the effect of internal loss on the threshold and power characteristics of semiconductor lasers with a quantum-confined active region and, particularly, quantum dot (QD) lasers [7-10], no consideration of the dynamic properties of QD lasers in the presence of internal loss has been given so far. In this chapter, we study the modulation response of a QD laser taking into account the carrier-density-dependent internal loss in the OCL [A1, A2].

3.2. Discussion

To mainly focus on the effect of internal loss, we do not consider here some other factors, among them the carrier capture delay from the OCL into QDs [11], which also affect the modulation bandwidth of a laser. Then we have the following set of two rate equations [12]

$$\frac{\partial n}{\partial t} = \frac{j}{eb} - Bn_{\mathrm{OCL}}^2 - \frac{N_{\mathrm{S}}}{b}\frac{f_{\mathrm{n}}^2}{\tau_{\mathrm{QD}}} - \mathrm{v}_{\mathrm{g}} g^{\max}\left(2f_{\mathrm{n}} - 1\right) n_{\mathrm{ph}}, \tag{3.1}$$

$$\frac{\partial n_{\mathrm{ph}}}{\partial t} = \mathrm{v}_{\mathrm{g}} g^{\max}\left(2f_{\mathrm{n}} - 1\right) n_{\mathrm{ph}} - \mathrm{v}_{\mathrm{g}}\left(\beta + \alpha_{\mathrm{int}}\right) n_{\mathrm{ph}}, \tag{3.2}$$

where

$$n = 2\frac{N_{\mathrm{S}}}{b} f_{\mathrm{n}} + n_{\mathrm{OCL}}, \tag{3.3}$$

is the total carrier density (per unit volume of the OCL), and

$$\alpha_{\mathrm{int}} = \alpha_0 + \sigma_{\mathrm{int}} n_{\mathrm{OCL}}, \tag{3.4}$$

is the internal loss coefficient [7-10]. All internal loss mechanisms can be grouped into two categories, one dependent on the free carrier density in the OCL and the other independent. The constant component α_0 accounts for scattering at rough surfaces and free-carrier absorption in the cladding layers, and the component $\sigma_{\mathrm{int}} n_{\mathrm{OCL}}$ describes free-carrier and intervalence band absorption in the OCL with σ_{int} being the effective cross-section for these absorption loss processes. The other parameters are introduced in Chapter 2.

At the steady-state [i.e., $\partial(n, n_{\mathrm{ph}})/\partial t = 0$], the rate equations (3.1) and (3.2) become

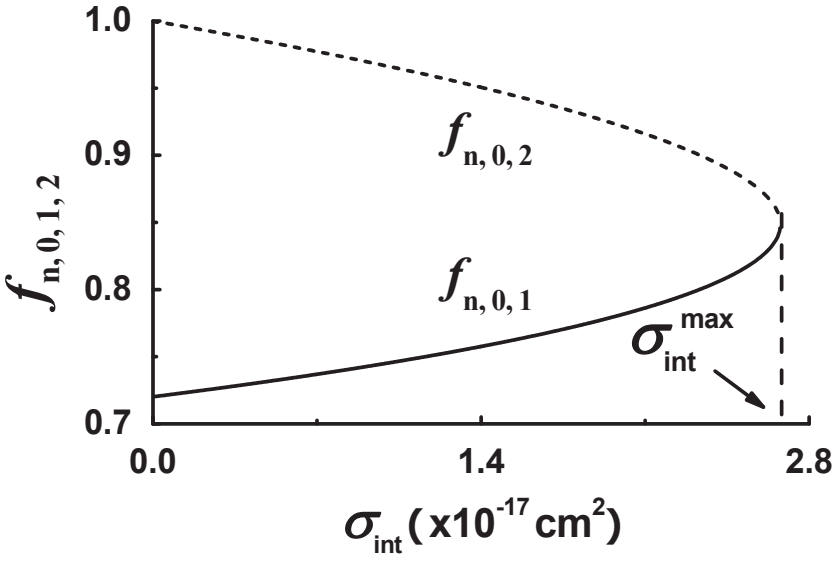

(a)

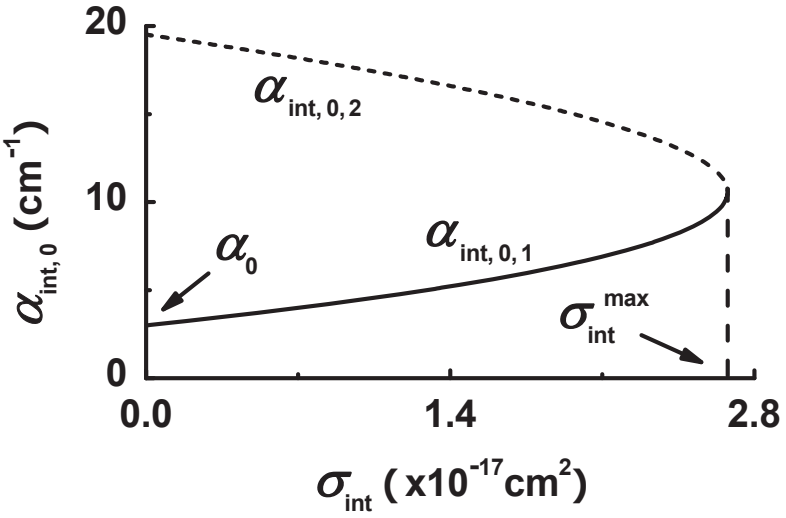

(b)

Fig. 3.1. (a) QD level occupancy and (b) internal loss $\alpha_{int,\,0}$ vs. effective cross-section σ_{int} for carrier-density-dependent absorption loss processes. The solid curves correspond to the conventional branch. The dashed curves are totally due to the carrier-density-dependent internal loss. The vertical dashed lines indicate the maximum tolerable σ_{int}^{max}. For our calculations, room-temperature operation of a GaInAsP structure of Ref. [13] with a single layer of QDs lasing near 1.55 μm is considered; 10% QD-size fluctuations are assumed; g^{max} = 29.52 cm^{-1}, α_0 = 3 cm^{-1}, and L = 1.139 mm. At these parameters, $\sigma_{int}^{max} = 2.677 \times 10^{-17}\,\mathrm{cm}^2$.

$$0 = \frac{j_0}{eb} - Bn_{\mathrm{OCL},0}^2 - \frac{N_\mathrm{S}}{b}\frac{f_{\mathrm{n},0}^2}{\tau_\mathrm{QD}} - \mathrm{v_g}g^{\max}\left(2f_{\mathrm{n},0}-1\right)n_{\mathrm{ph},0}, \tag{3.5}$$

$$0 = \mathrm{v_g}g^{\max}\left(2f_{\mathrm{n},0}-1\right)n_{\mathrm{ph},0} - \mathrm{v_g}\left(\beta+\alpha_{\mathrm{int},0}\right)n_{\mathrm{ph},0}. \tag{3.6}$$

We denote the steady-state quantities by the subscript "0" (except for α_0 and ω_0). Equations (3.1), (3.2), (3.5), and (3.6) hold true no matter whether the carrier exchange between the OCL and QDs is fast or slow. In the case of instantaneous exchange, which is assumed in this Chapter, the free carrier density in the OCL n_{OCL}, and the confined carrier density in QDs $2\frac{N_\mathrm{S}}{b}f_\mathrm{n}$ can be related by

$$n_{\mathrm{OCL},0} = n_1\frac{f_{\mathrm{n},0}}{1-f_{\mathrm{n},0}}. \tag{3.7}$$

In order to have non-zero solution for $n_{\mathrm{ph}0}$, we have from (3.6),

$$g^{\max}\left(2f_{\mathrm{n},0}-1\right) = \beta+\alpha_{\mathrm{int}}, \tag{3.8}$$

which is the lasing condition – equality of the gain to the total loss.

The photon lifetime in the cavity is

$$\tau_{\mathrm{ph},0} = \frac{1}{\mathrm{v_g}g^{\max}\left(2f_{\mathrm{n},0}-1\right)} = \frac{1}{\mathrm{v_g}\left(\beta+\alpha_{\mathrm{int},0}\right)}. \tag{3.9}$$

Due to the internal loss $\alpha_{\mathrm{int},0}$, $\tau_{\mathrm{ph},0}$ depends on the free-carrier density $n_{\mathrm{OCL},0}$ in the OCL.

With (3.4) and (3.7), a quadratic equation in $f_{\mathrm{n},0}$ is obtained from (3.8)

$$g^{\max}\left(2f_{\mathrm{n},0}-1\right) = \beta+\alpha_0+\sigma_{\mathrm{int}}n_1\frac{f_{\mathrm{n},0}}{1-f_{\mathrm{n},0}}. \tag{3.10}$$

Both roots of (3.10) are real and positive and have physical meaning [7, 8]. These roots are

$$f_{\mathrm{n}0,1,2} = \frac{1}{4}\left(3+\frac{\beta+\alpha_0-\sigma_{\mathrm{int}}n_1}{g^{\max}}\right) \mp \sqrt{\frac{1}{16}\left(3+\frac{\beta+\alpha_0-\sigma_{\mathrm{int}}n_1}{g^{\max}}\right)^2 - \frac{1}{2}\left(1+\frac{\beta+\alpha_0}{g^{\max}}\right)}. \tag{3.11}$$

Both $f_{\mathrm{n}0,1,2}$ are pinned (i.e., independent of j_0) at their threshold values and therefore, the steady-state free carrier density in the OCL is also pinned [see (3.7)]. Due to the free-carrier-density-

dependent internal loss, the confined-carrier level occupancy in a QD is itself a function of σ_{int} [Fig. 3.1(a)]. Due to the existence of two roots of (3.10) given by (3.11), the dependence of the internal loss α_{int0} on σ_{int} has two branches [see (3.4) and (3.7)]. As can be seen in Fig. 3.1, with increasing σ_{int}, these two branches approach each other and merge together at the maximum tolerable value σ_{int}^{max} of σ_{int}. No lasing is attainable for $\sigma_{int} > \sigma_{int}^{max}$.

According to [8], when one of the laser structure parameters (α_0, σ_{int}, L, N_S, or δ) is at its critical tolerable value, the following equation [eq. (17) of [8]] holds:

$$f_{n0,1} = f_{n0,2} = \sqrt{\frac{1}{2}\left(1 + \frac{\beta + \alpha_0}{g^{max}}\right)} = 1 - \sqrt{\frac{\sigma_{int} n_1}{2g^{max}}}, \tag{3.12}$$

from which the following expression for σ_{int}^{max} is obtained:

$$\sigma_{int}^{max} = \frac{\left(\sqrt{2g^{max}} - \sqrt{\beta + \alpha_0 + g^{max}}\right)^2}{n_1}. \tag{3.13}$$

It is easily seen from (3.11) that when $\alpha_0 = 0$ and $\sigma_{int} = 0$,

$$f_{n0,1} = \frac{1}{2}\left(1 + \frac{\beta}{g^{max}}\right), \tag{3.14}$$

$$f_{n0,2} = 1, \tag{3.15}$$

i.e., $f_{n0,1}$ corresponds to the conventional branch (denoted by "1" in subscript), while $f_{n0,2}$ is totally due to the carrier-density-dependent internal loss. If $\alpha_0 \neq 0$ and $\sigma_{int} \neq 0$,

$$\frac{1}{2}\left(1 + \frac{\beta}{g^{max}}\right) < f_{n0,1} < f_{n0,2} < 1. \tag{3.16}$$

From (3.5), the expressions for the threshold current density j_{th} and the photon density n_{ph0} are derived,

$$j_{th1,2} = ebBn_{OCL0,1,2}^2 + eN_S \frac{f_{n0,1,2}^2}{\tau_{QD}}, \tag{3.17}$$

$$n_{ph0,1,2} = \tau_{ph0,1,2} \frac{j_0 - j_{th1,2}}{eb}. \tag{3.18}$$

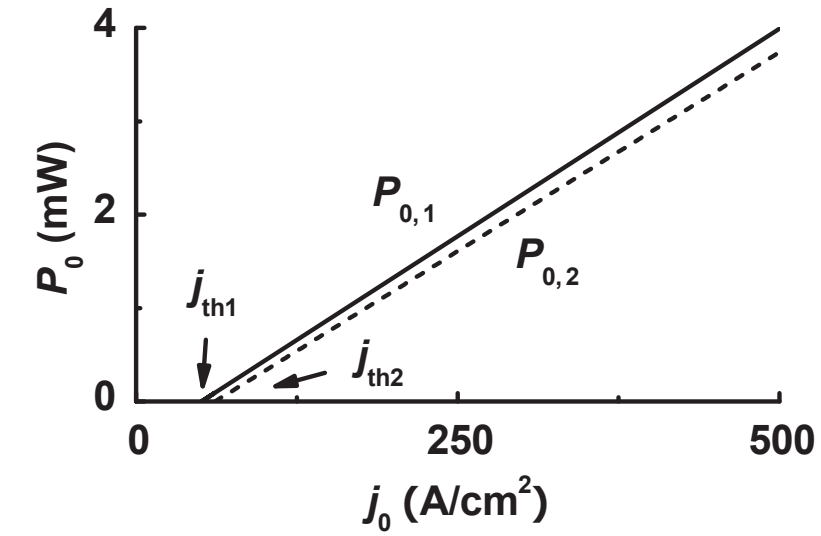

(a)

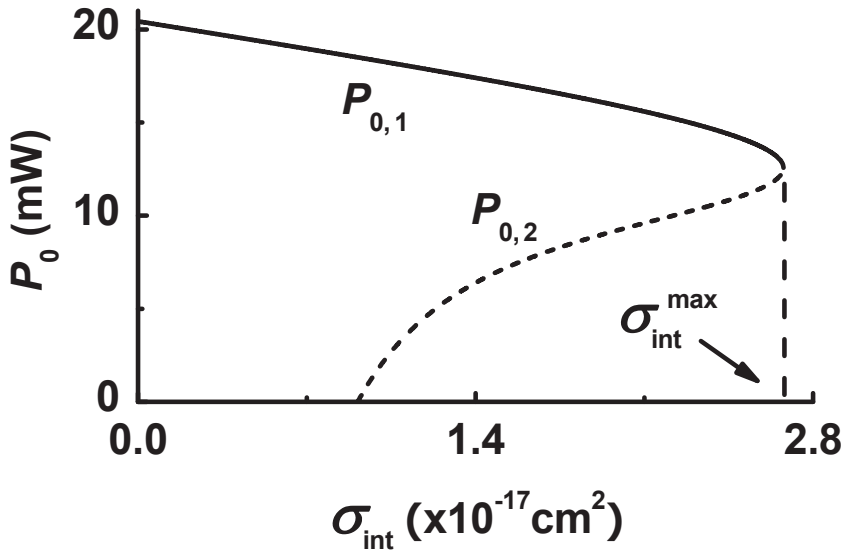

(b)

Fig. 3.2. (a) Two branches of the steady-state light-current characteristic (LCC) at $\sigma_{int} = 2.67\times10^{-17}$cm^2. The linearity of the LCCs originates from the assumption of instantaneous carrier exchange between the OCL and QDs. The two branches are not parallel to each other – they have difference slopes [see (3.19)]. (b) Two branches of the emitted optical power vs. σ_{int} at a fixed value of $j_0 = 1.5$ kA/cm^2. These two branches merge together at σ_{int}, beyond which the lasing is not attainable. The solid curve shows the conventional branch. The dashed curve is totally due to the carrier-density-dependent internal loss. In both figures, $\alpha_0 = 3$ cm^{-1} and $L = 1.139$ mm.

In the absence of carrier-density-dependent internal loss (i.e., $\sigma_{\text{int}} = 0$), $f_{\text{n0, 2}} = 1$, $n_{\text{OCL0, 2}} = \infty$, and $j_{\text{th2}} = \infty$ [see (3.7) and (3.17)], which means that the lasing of the second branch is not possible. However, due to a non-zero σ_{int}, the second lasing branch appears. Hence, the steady-state light current characteristic (LCC) has two braches

$$P_{0,\,1,\,2} = \hbar\omega \mathrm{v}_{\mathrm{g}} \beta S b n_{\text{ph0, 1, 2}} = \hbar\omega \frac{\tau_{\text{ph0, 1, 2}}}{\tau_{\text{mirror}}} S \frac{j_0 - j_{\text{th1, 2}}}{e}, \tag{3.19}$$

where

$$\tau_{\text{mirror}} = \frac{1}{\mathrm{v}_{\mathrm{g}} \beta}. \tag{3.20}$$

Both branches of the LCC are linear [see Fig. 3.2(a)] but they are not parallel to each other. This linearity originates from instantaneous carrier exchange between the OCL and QDs, due to which the level occupancy in QDs and the carrier density in the OCL are pinned above the lasing threshold. Fig. 3.2(b) shows the optical power in two branches vs. σ_{int} at a fixed dc injection current density. At $\sigma_{\text{int}} = \sigma_{\text{int}}^{\max}$, these two branches merge together; beyond this $\sigma_{\text{int}}^{\max}$, the lasing is not attainable.

To consider a direct modulation of the laser output by alternating current (ac), we use the small-signal analysis [14-20]. In this work, we restrict our consideration to the case of lasing in the conventional branch only (the subscripts of the corresponding quantities contain "1"). Using (3.7) in (3.1) and (3.2), we obtain for small variations δf_{n} and δn_{ph} of the level occupancy and photon density caused by a small ac component δj of the injection current density the following equations:

$$\left[2\frac{N_{\mathrm{S}}}{b} + \frac{n_1}{\left(1 - f_{\text{n,0}}\right)^2}\right] \frac{\partial}{\partial t}\left(\delta f_{\text{n}}\right) = \frac{1}{eb}\delta j - 2\left\{\left[\frac{N_{\mathrm{S}}}{b}\frac{f_{\text{n,0}}}{\tau_{\text{QD}}} + Bn_1^2 \frac{f_{\text{n,0}}}{\left(1 - f_{\text{n,0}}\right)^3}\right] + \mathrm{v}_{\mathrm{g}} g^{\max} n_{\text{ph,0}}\right\}\delta f_{\text{n}} - \frac{\delta n_{\text{ph}}}{\tau_{\text{ph,0}}}, \tag{3.21}$$

$$\frac{\partial}{\partial t}\left(\delta n_{\text{ph}}\right) = \mathrm{v}_{\mathrm{g}}\left[2g^{\max} - \sigma_{\text{int}} \frac{n_1}{\left(1 - f_{\text{n,0}}\right)^2}\right] n_{\text{ph,0}} \delta f_{\text{n}}. \tag{3.22}$$

Eq. (3.22) can be written as

$$\frac{\partial}{\partial t}\left(\delta n_{\mathrm{ph}}\right)=\mathrm{v}_{\mathrm{g}}\left(\frac{\partial g}{\partial f_{\mathrm{n}}}-\frac{\partial \alpha_{\mathrm{int}}}{\partial f_{\mathrm{n}}}\right) n_{\mathrm{ph},0}\,\delta f_{\mathrm{n}}, \tag{3.23}$$

or,

$$\frac{\partial}{\partial t}\left(\delta n_{\mathrm{ph}}\right)=\left[\mathrm{v}_{\mathrm{g}}\frac{\partial g}{\partial f_{\mathrm{n}}}-\frac{\partial}{\partial f_{\mathrm{n}}}\left(\frac{1}{\tau_{\mathrm{ph}}}\right)\right] n_{\mathrm{ph},0}\,\delta f_{\mathrm{n}}, \tag{3.24}$$

where

$$g = g^{\max}\,(2f_{\mathrm{n}} - 1), \tag{3.25}$$

is the modal gain. The set of equations (3.21) and (3.22) in δf and δn_{ph} can be easily solved.

As seen from (3.4), α_{int} will vary with time through such variation in the free-carrier density n_{OCL} caused by the alternating current (ac) current. Hence, as seen from (3.2) and (3.4), the temporal variation of the photon loss rate [the second term in the right-hand side of (3.2)] will be due to such variation of not only the photon density n_{ph} but n_{OCL} as well.

Considering a small time-harmonic ac injection current density in (3.21),

$$\delta j = (\delta j_{\mathrm{m}})\,e^{i\omega t}, \tag{3.26}$$

we will correspondingly look for the solutions of (3.21) in (3.22) in the form

$$\delta f_{\mathrm{n}} = (\delta f_{\mathrm{n-m}})\,e^{i\omega t}, \tag{3.27}$$

$$\delta n_{\mathrm{ph}} = (\delta n_{\mathrm{ph-m}})\,e^{i\omega t}. \tag{3.28}$$

We will obtain a set of algebraic equations for $\delta f_{\mathrm{n-m}}(\omega)$ and $\delta n_{\mathrm{ph-m}}(\omega)$. Solving this set, we then derive the following equation for the modulation response function:

$$H\left(\omega\right)=\left|\frac{\delta n_{\mathrm{ph}-m}(\omega)}{\delta n_{\mathrm{ph}-m}(0)}\right|^2=\frac{\omega_0^4}{\left(\omega^2-\omega_0^2\right)^2+4\Gamma_{\mathrm{dec}}^2\omega^2}. \tag{3.29}$$

While the shape of $H(\omega)$ depends strongly on the internal loss (Fig. 3.3), as a function of the frequency ω of direct modulation and parameters Γ_{dec} and ω_0, expression (3.29) is the same as for the case of no internal loss [12].

The decay rate of relaxation oscillations is given by

$$\Gamma_{\text{dec}} = \frac{1}{2}\left(\frac{1}{\tau_{\text{non-stim}}^{\text{dif}}} + \text{v}_\text{g} G^{\text{dif}} n_{\text{ph0, 1}} \right), \tag{3.30}$$

where

$$\begin{aligned} \frac{1}{\tau_{\text{non-stim}}^{\text{dif}}} &= \frac{\partial R_{\text{non-stim, 0}}}{\partial n_0} = \frac{\partial}{\partial n_0}\left(B n_{\text{OCL, 0}}^2 + \frac{N_S}{b}\frac{f_{\text{n0, 1}}^2}{\tau_{\text{QD}}} \right) \\ &= \frac{2\dfrac{N_\text{S}}{b}\dfrac{f_{\text{n0, 1}}}{\tau_{\text{QD}}} + 2Bn_1^2 \dfrac{f_{\text{n0, 1}}}{\left(1 - f_{\text{n0, 1}}\right)^3}}{2\dfrac{N_\text{S}}{b} + \dfrac{n_1}{\left(1 - f_{\text{n0, 1}}\right)^2}} \end{aligned} \tag{3.31}$$

is the reciprocal of the effective differential non-stimulated recombination time and

$$G^{\text{dif}} = \frac{\partial g}{\partial n_0} = \frac{2g^{\max}}{2\dfrac{N_\text{S}}{b} + \dfrac{n_1}{\left(1 - f_{\text{n0, 1}}\right)^2}} \tag{3.32}$$

is the effective differential gain.

In terms of the quantities $\tau_{\text{non–stim}}^{\text{dif}}$, G^{dif}, and $n_{\text{ph0, 1}}$, expression (3.30) is also the same as for the case of no internal loss [12]. Each of these quantities is, however, affected by the internal loss.

For ω_0 entering into (3.29), we have

$$\begin{aligned} \omega_0 &= \sqrt{\text{v}_\text{g} G^{\text{dif}} \frac{n_{\text{ph0,1}}}{\tau_{\text{ph0,1}}}} \sqrt{1 - \frac{\partial \alpha_{\text{int 0}}}{\partial g_0}} \\ &= \sqrt{\text{v}_\text{g} G^{\text{dif}} \frac{n_{\text{ph0,1}}}{\tau_{\text{ph0,1}}}} \sqrt{1 - \frac{\sigma_{\text{int}} n_1}{2g^{\max}\left(1 - f_{\text{n0,1}}\right)^2}}. \end{aligned} \tag{3.33}$$

For the modulation bandwidth, which is defined as the –3 dB bandwidth [$10\log_{10} H(\omega_{-3\text{ dB}}) = -3$, see Fig. 3.3], we derived

$$\begin{aligned} \omega_{-3\text{ dB}} &= \sqrt{\sqrt{\omega_{\text{peak}}^4 + (r-1)\omega_0^4} + \omega_{\text{peak}}^2} \\ &= \sqrt{\sqrt{\left(\omega_0^2 - 2\Gamma_{\text{dec}}^2\right)^2 + (r-1)\omega_0^4} + \left(\omega_0^2 - 2\Gamma_{\text{dec}}^2\right)}, \end{aligned} \tag{3.34}$$

where $r = 10^{0.3} \approx 1.995$,

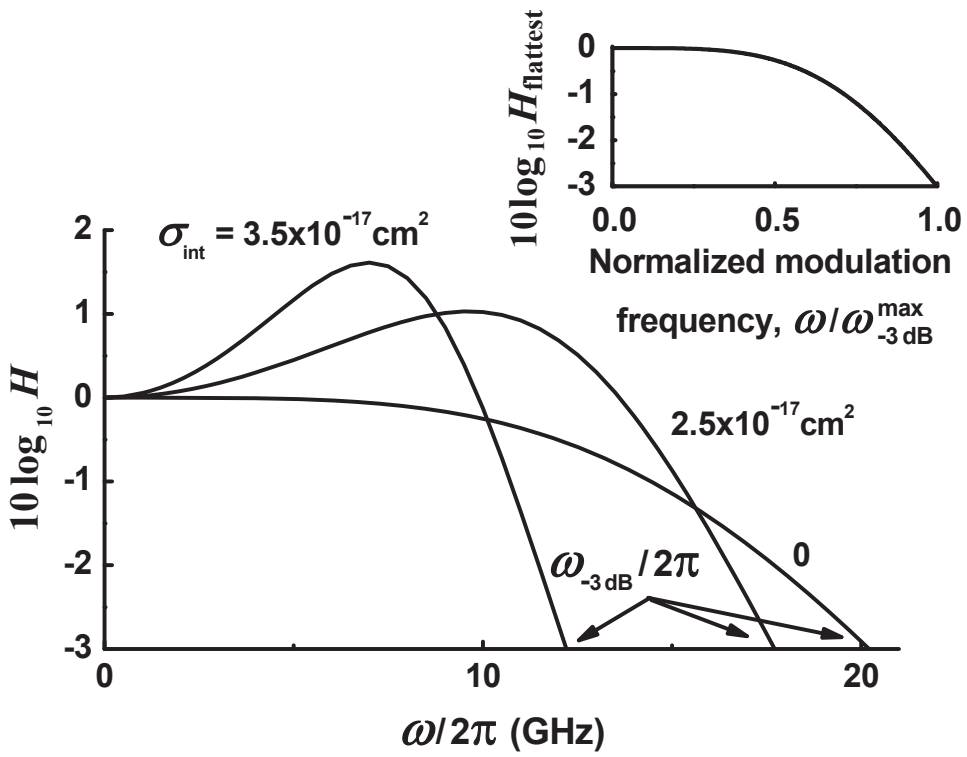

Fig. 3.3. Modulation response function at different values of the internal loss cross-section σ_{int}. For all the three curves, the dc component of the injection current density $j_0 = 64$ kA/cm^2; for the case of no internal loss, this value of j_0 is equal to j_0^{opt} and that is why the response function is flattest. The inset shows the flattest response function given by (3.41) vs. normalized modulation frequency $\omega/\omega_{-3\,\text{dB}}^{\text{max}}$; using this universal dependence and eq. (3.37) for $\omega_{-3\,\text{dB}}^{\text{max}}$, the flattest response function at a non-zero σ_{int} can be easily plotted. (Reprinted with permission from Fig. 1 of [A1]. Copyright (2012) by AIP.)

$$\omega_{\text{peak}} = \sqrt{\omega_0^2 - 2\Gamma_{\text{dec}}^2} = \sqrt{\Omega_{\text{osc}}^2 - \Gamma_{\text{dec}}^2}, \tag{3.35}$$

and

$$\Omega_{\text{osc}} = \sqrt{\omega_0^2 - \Gamma_{\text{dec}}^2} \tag{3.36}$$

is the frequency of relaxation oscillations.

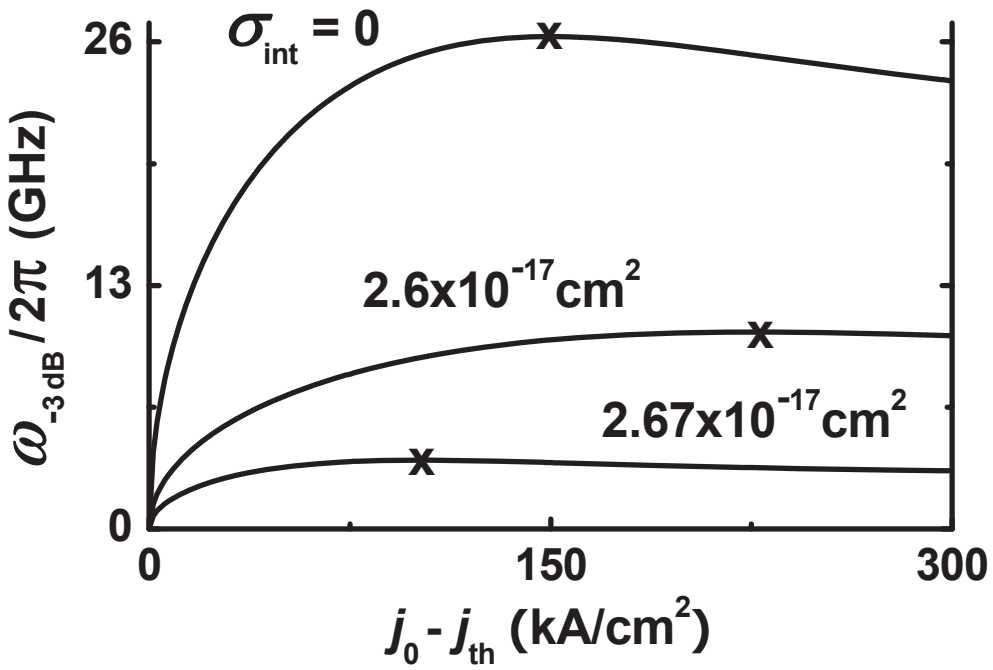

Fig. 3.4. Modulation bandwidth $\omega_{-3\,\mathrm{dB}}/2\pi$ vs. excess of the dc component of the injection current density over the threshold current density at different values of σ_{int}. $\alpha_0 = 3$ cm^{-1} and $L =$ 1.139 mm. The "x" symbol marks the maximum point (j_0^{opt}, $\omega_{-3\,\mathrm{dB}}^{\mathrm{max}}$) on each curve. (Reprinted with permission from Fig. 2 of [A1]. Copyright (2012) by AIP.)

The steady-state photon density $n_{\mathrm{ph0,\,1}}$, entering into (3.30) and (3.33), is a function of the dc component j_0 of the injection current density [see (3.18)]. Consequently, all the quantities Γ_{dec}, Ω_{osc}, ω_0, ω_{peak}, $\omega_{-3\,\mathrm{dB}}$, and the response function $H(\omega)$ depend on j_0 as well.

When $H(\omega)$ has a peak [which occurs only for a certain range of values of the dc component j_0 of the injection current density, namely, when ω_{peak} given by (3.35) is real and positive], (3.35) presents the frequency of the peak. Eq. (3.34) for $\omega_{-3\,\mathrm{dB}}$ holds also for those j_0 at which there is no peak in $H(\omega)$ – in that case too, ω_{peak} is formally given by (3.35) but the difference $\omega_0^2 - 2\Gamma_{\mathrm{dec}}^2$ in (3.35) is negative.

With increasing j_0 above the threshold current density j_{th}, the modulation bandwidth increases from zero, approaches its maximum value $\omega_{-3\,\mathrm{dB}}^{\mathrm{max}}$ (marked by the symbol "x" in

Fig. 3.4) at a certain optimum dc current density j_0^{opt}, then decreases and will asymptotically approach its saturation value $\omega_{-3\,\text{dB}}^{\text{sat}}$. At $j_0 = j_0^{\text{opt}}$, when the maximum bandwidth $\omega_{-3\,\text{dB}}^{\text{max}}$ is attained, the peak of the response function occurs at $\omega_{\text{peak}} = 0$ and the response function becomes as flat as possible (Fig. 3.3).

Analyzing (3.34) for $\omega_{-3\,\text{dB}}$ as a function of j_0, we obtained the following expression for $\omega_{-3\,\text{dB}}^{\text{max}}$:

$$\omega_{-3\,\text{dB}}^{\text{max}} \approx \frac{\sqrt{2}}{\tau_{\text{ph}0,1}}\left(1-\frac{\partial\alpha_{\text{int},0}}{\partial g_0}\right)=\frac{\sqrt{2}}{\tau_{\text{ph}0,1}}\left[1-\frac{\sigma_{\text{int}}n_1}{2g^{\text{max}}(1-f_{\text{n}0,1})^2}\right]. \tag{3.37}$$

Fig. 3.5 shows $\omega_{-3\,\text{dB}}^{\text{max}}/2\pi$ vs. σ_{int}. As seen from (3.37), Fig. 3.5 and also Fig. 3.4, $\omega_{-3\,\text{dB}}^{\text{max}}$ is highest for the case of no free-carrier-density-dependent internal loss ($\sigma_{\text{int}} = 0$). With σ_{int} increasing and approaching a certain maximum tolerable value $\sigma_{\text{int}}^{\text{max}}$ given by (3.13) [which can also be obtained by equalizing (3.37) to zero], $\omega_{-3\,\text{dB}}^{\text{max}}$ decreases and becomes zero. For $\sigma_{\text{int}} > \sigma_{\text{int}}^{\text{max}}$, the lasing is not attainable in the structure and, naturally, no direct modulation is possible.

The optimum dc current density j_0^{opt} at which $\omega_{\text{peak}} = 0$ is given by

$$j_0^{\text{opt}} = j_{\text{th}} + \frac{eb}{\text{v}_{\text{g}}G^{\text{dif}}\tau_{\text{ph}0,1}^2}\left[1-\frac{\partial\alpha_{\text{int},0}}{\partial g_0}-\frac{\tau_{\text{ph}0,1}}{\tau_{\text{non-stim}}^{\text{dif}}}+\sqrt{\left(1-\frac{\partial\alpha_{\text{int},0}}{\partial g_0}\right)\left(1-\frac{\partial\alpha_{\text{int},0}}{\partial g_0}-\frac{2\tau_{\text{ph}0,1}}{\tau_{\text{non-stim}}^{\text{dif}}}\right)}\right]. \tag{3.38}$$

The value of j_0^{opt} is very close to the value of the current density $j_0^{\text{opt-osc}}$ at which Ω_{osc} becomes maximum – see Appendix I for details.

The saturation value of $\omega_{-3\,\text{dB}}$ is

$$\begin{aligned}\omega_{-3\,\text{dB}}^{\text{sat}} &\approx \frac{\sqrt{r-1}}{\tau_{\text{ph}0,1}}\left(1-\frac{\partial\alpha_{\text{int},0}}{\partial g_0}\right)\\ &=\frac{\sqrt{r-1}}{\tau_{\text{ph}0,1}}\left[1-\frac{\sigma_{\text{int}}n_1}{2g^{\text{max}}(1-f_{\text{n}0,1})^2}\right].\end{aligned} \tag{3.39}$$

When one of the laser structure parameters is at its critical tolerable value (see [21] and [8] for the critical tolerable parameters α_0^{max}, $\sigma_{\text{int}}^{\text{max}}$, L^{min}, $N_{\text{S}}^{\text{min}}$, and δ^{max}), we have

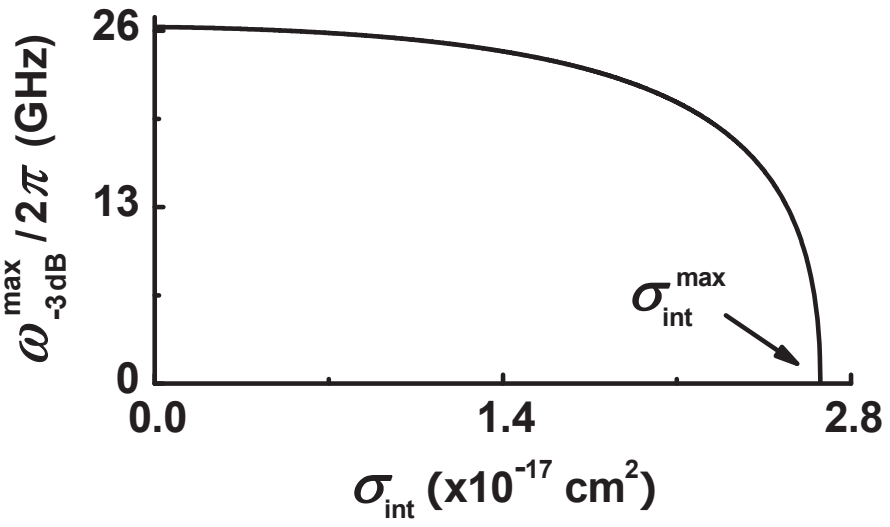

Fig. 3.5. Maximum modulation bandwidth $\omega_{-3\,\mathrm{dB}}^{\max}/2\pi$ vs. internal loss cross-section σ_{int}. α_0 = 3 cm^{-1} and L = 1.139 mm; $\sigma_{\mathrm{int}}^{\max} = 2.677\times10^{-17}\,\mathrm{cm}^2$. (Reprinted with permission from Fig. 3 of [A1]. Copyright (2012) by AIP.)

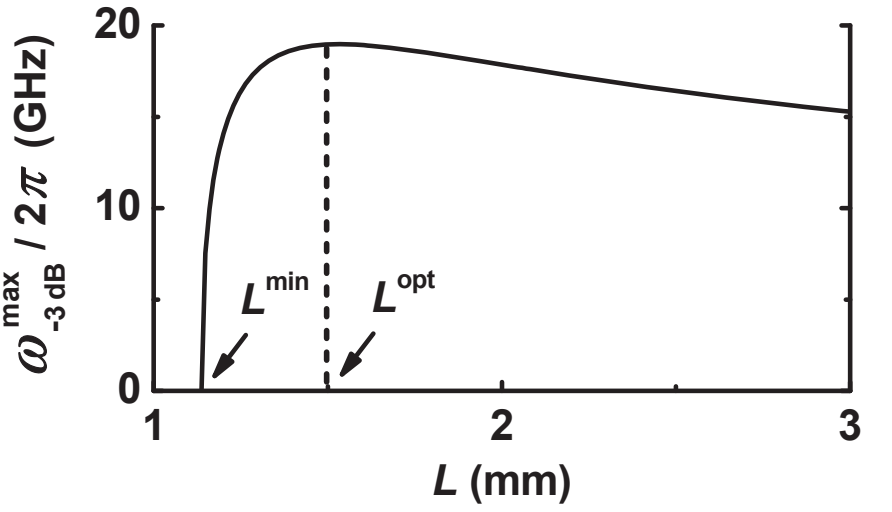

Fig. 3.6. Maximum modulation bandwidth $\omega_{-3\,\mathrm{dB}}^{\max}/2\pi$ vs. cavity length L. α_0 = 3 cm^{-1} and σ_{int} = 2.67 × 10^{-17} cm^2; L^{opt} = 1.5 mm. (Reprinted with permission from Fig. 4 of [A1]. Copyright (2012) by AIP.)

$$1-\frac{\partial\alpha_{\text{int},0}}{\partial g_0}=1-\frac{\sigma_{\text{int}}n_1}{2g^{\max}(1-f_{\text{n}0,1})^2}=0. \tag{3.40}$$

As seen from (3.37) and (3.39), both $\omega_{-3\text{ dB}}^{\max}$ and $\omega_{-3\text{ dB}}^{\text{sat}}$ will be reduced to zero.

While $\omega_{-3\,\text{dB}}^{\max}$ depends strongly on σ_{int}, the flattest response function (the response function at $j_0 = j_0^{\text{opt}}$) is universal in terms of the normalized modulation frequency $\omega/\omega_{-3\,\text{dB}}^{\max}$ (the inset in Fig. 3.3),

$$H_{\text{flattest}}\left(\frac{\omega}{\omega_{-3\text{ dB}}^{\max}}\right)=\frac{1}{1+\left(\dfrac{\omega}{\omega_{-3\text{ dB}}^{\max}}\right)^4}. \tag{3.41}$$

As seen from Fig. 3.6, as a function of the cavity length, $\omega_{-3\,\text{dB}}^{\max}$ has a maximum. With increasing L from the shortest tolerable cavity length required for lasing [8], $\omega_{-3\,\text{dB}}^{\max}$ increases from zero, approaches its highest value $\omega_{-3\,\text{dB}}^{\text{highest}}$ at a certain optimum cavity length L^{opt}, and then decreases. L^{opt} depends on σ_{int} – the larger is σ_{int}, the longer should be the optimum cavity.

From the condition

$$\left.\frac{\partial\omega_{-3\text{ dB}}^{\max}}{\partial L}\right|_{L=L^{\text{opt}}}=0, \tag{3.42}$$

where $\omega_{-3\,\text{dB}}^{\max}$ is given by (3.37), we obtain the following equation for finding L^{opt}:

$$f_{\text{n}0,\,1}(L^{\text{opt}})=\frac{3}{2}-\sqrt{\frac{3}{4}-\frac{\dfrac{1}{L^{\text{opt}}}\ln\dfrac{1}{R}+\alpha_0}{2g^{\max}}}, \tag{3.43}$$

where $f_{\text{n}0,\,1}(L^{\text{opt}})$ is given by (3.11) at $L = L^{\text{opt}}$. From (3.43), a cubic equation in L^{opt} is obtained.

When σ_{int} is small [so small that the second terms in the brackets in the right-hand sides of Eqs. (3.44) and (3.45) are much less compared to unity], the analysis of Eq. (3.37) for $\omega_{-3\,\text{dB}}^{\max}$ as a function of L yields the following expressions for L^{opt} and $\omega_{-3\,\text{dB}}^{\text{highest}}$:

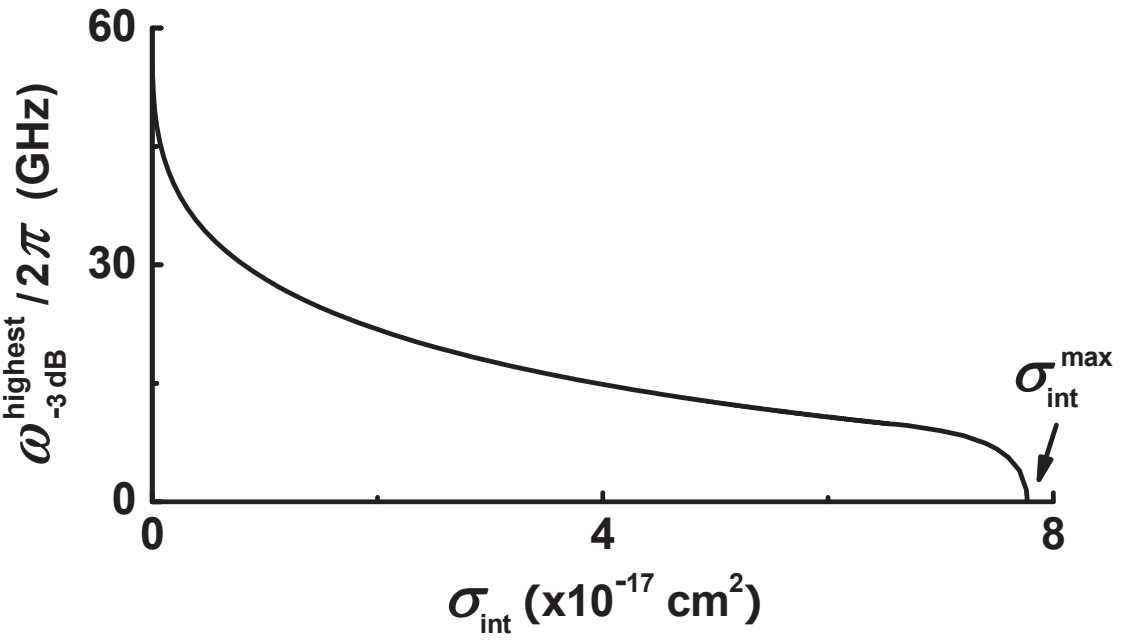

Fig. 3.7. Highest modulation bandwidth $\omega_{-3\,\mathrm{dB}}^{\mathrm{highest}}/2\pi$ vs. internal loss cross-section σ_{int}. α_0 = 3 cm^{-1}. $\sigma_{\mathrm{int}}^{\mathrm{max}}$ in the figure corresponds to $L = \infty$ and that is why it is larger than in Fig. 3.3 – see Appendix II. (Reprinted with permission from Fig. 5 of [A1]. Copyright (2012) by AIP.)

$$L^{\mathrm{opt}} \approx L_0^{\mathrm{min}}\left(1+\frac{g^{\mathrm{max}}}{g^{\mathrm{max}}-\alpha_0}\sqrt[3]{\frac{4\sigma_{\mathrm{int}}n_1}{g^{\mathrm{max}}}}\right)=\frac{\ln(1/R)}{g^{\mathrm{max}}-\alpha_0}\left(1+\frac{g^{\mathrm{max}}}{g^{\mathrm{max}}-\alpha_0}\sqrt[3]{\frac{4\sigma_{\mathrm{int}}n_1}{g^{\mathrm{max}}}}\right), \tag{3.44}$$

$$\omega_{-3\ \mathrm{dB}}^{\mathrm{highest}} \approx \omega_{-3\ \mathrm{dB}}^{\mathrm{highest}}\Big|_{\sigma_{\mathrm{int}}=0}\left(1-\frac{3}{2}\sqrt[3]{\frac{4\sigma_{\mathrm{int}}n_1}{g^{\mathrm{max}}}}\right)=\sqrt{2}\,\mathrm{v_g}g^{\mathrm{max}}\left(1-\frac{3}{2}\sqrt[3]{\frac{4\sigma_{\mathrm{int}}n_1}{g^{\mathrm{max}}}}\right), \tag{3.45}$$

where L_0^{min} is the shortest tolerable cavity length, and

$$\omega_{-3\,\mathrm{dB}}^{\mathrm{highest}}\Big|_{\sigma_{\mathrm{n}}=0}=\sqrt{2}\mathrm{v_g}g^{\mathrm{max}} \tag{3.46}$$

is the highest bandwidth when $\sigma_{\mathrm{int}} = 0$ [12].

The highest modulation bandwidth $\omega_{-3\,\mathrm{dB}}^{\mathrm{highest}}/2\pi$ is shown against σ_{int} in Fig. 3.7. As seen from the figure, in the ideal case of no free-carrier-density-dependent internal loss in the OCL

(and also no carrier capture delay from the OCL into QDs), $\omega_{-3\ \mathrm{dB}}^{\mathrm{highest}}\Big|_{\sigma_{\mathrm{int}}=0}/2\pi$ is about 60 GHz in a GaInAsP structure of Ref. [13] used for our calculations here. In the presence of such a loss, $\omega_{-3\ \mathrm{dB}}^{\mathrm{highest}}/2\pi$ is, however, considerably reduced and becomes vanishing as σ_{int} approaches its maximum tolerable value (Fig. 3.7) (the expression for this $\sigma_{\mathrm{int}}^{\mathrm{max}}$ at which $L^{\mathrm{opt}} = \infty$ is derived in Appendix II).

3.3. Conclusion

The free-carrier-density-dependent internal optical loss in the waveguide region has been shown to considerably reduce the modulation bandwidth $\omega_{-3\ \mathrm{dB}}$ of a QD laser. At a certain optimum value j_0^{opt} of the dc component of the injection current density, the maximum bandwidth $\omega_{-3\ \mathrm{dB}}^{\mathrm{max}}$ is attained and the response function becomes as flat as possible. While $\omega_{-3\ \mathrm{dB}}^{\mathrm{max}}$ depends strongly on the effective cross-section σ_{int} of internal absorption loss processes (decreases and becomes zero at the maximum tolerable value of σ_{int}), the flattest response function is universal in terms of the normalized modulation frequency $\omega/\omega_{-3\ \mathrm{dB}}^{\mathrm{max}}$. As with j_0^{opt}, there also exists the optimum cavity length, at which $\omega_{-3\ \mathrm{dB}}$ is highest; the larger is σ_{int}, the longer should be the optimum cavity.

Appendix I

Current density $j_0^{\text{opt-osc}}$ at which Ω_{osc} is maximum

The current density j_0^{opt} at which $\omega_{\text{peak}} = 0$ and the current density $j_0^{\text{opt-osc}}$ at which Ω_{osc} is maximum are very close to each other. The expression for j_0^{opt} is given by (3.38). The following expression for $j_0^{\text{opt-osc}}$ is obtained from

$$\left.\frac{\partial \Omega_{\text{osc}}}{\partial j_0}\right|_{j_0^{\text{opt-osc}}} = 0, \tag{A1}$$

$$j_0^{\text{opt-osc}} = j_{\text{th}} + \frac{eb}{v_g G^{\text{dif}} \tau_{\text{ph0, 1}}^2}\left\{2\left[1 - \frac{\sigma_{\text{int}} n_1}{2g^{\max}\left(1 - f_{\text{n0, 1}}\right)^2}\right] - \frac{\tau_{\text{ph0, 1}}}{\tau_{\text{non-stim}}^{\text{dif}}}\right\}. \tag{A2}$$

The maximum frequency of relaxation oscillations is

$$\Omega_{\text{osc}}^{\max} = \Omega_{\text{osc}}(j_0^{\text{opt-osc}}) = \frac{1}{\tau_{\text{ph0, 1}}}\sqrt{1 - \frac{\sigma_{\text{int}} n_1}{2g^{\max}(1 - f_{\text{n0, 1}})^2}}\sqrt{1 - \frac{\sigma_{\text{int}} n_1}{2g^{\max}(1 - f_{\text{n0, 1}})^2} - \frac{\tau_{\text{ph0, 1}}}{\tau_{\text{non-stim}}^{\text{dif}}}}. \tag{A3}$$

The modulation bandwidth at $j_0^{\text{opt-osc}}$ is

$$\begin{aligned}\omega_{-3\text{ dB}}\left(j_0^{\text{opt-osc}}\right) = {} & \sqrt[4]{r-1}\,\frac{\sqrt{2}}{\tau_{\text{ph0,1}}}\sqrt{1 - \frac{\sigma_{\text{int}} n_1}{2g^{\max}\left(1 - f_{\text{n0, 1}}\right)^2}} \times \\ & \times \sqrt{\sqrt{\left[1 - \frac{\sigma_{\text{int}} n_1}{2g^{\max}\left(1 - f_{\text{n0, 1}}\right)^2} - \frac{\tau_{\text{ph0, 1}}}{2\tau_{\text{non-stim}}^{\text{dif}}}\right]^2 + \frac{1}{r-1}\left(\frac{\tau_{\text{ph0, 1}}}{2\tau_{\text{non-stim}}^{\text{dif}}}\right)^2} - \frac{1}{\sqrt{r-1}}\,\frac{\tau_{\text{ph0, 1}}}{2\tau_{\text{non-stim}}^{\text{dif}}}}.\end{aligned} \tag{A4}$$

When σ_{int} is not very close to $\sigma_{\text{int}}^{\max}$, $\tau_{\text{ph0, 1}} \big/ \tau_{\text{non-stim}}^{\text{dif}} << 1$ and

$$j_0^{\text{opt}} \approx j_0^{\text{opt-osc}} \approx j_{\text{th}} + \frac{2eb}{v_g G^{\text{dif}} \tau_{\text{ph0, 1}}^2}\left[1 - \frac{\sigma_{\text{int}} n_1}{2g^{\max}\left(1 - f_{\text{n0, 1}}\right)^2}\right], \tag{A5}$$

$$\omega_{-3\text{ dB}}\left(j_0^{\text{opt-osc}}\right) \approx \omega_{-3\text{ dB}}\left(j_0^{\text{opt}}\right) \approx \omega_{-3\text{ dB}}^{\max} \approx \frac{\sqrt{2}}{\tau_{\text{ph0, 1}}}\left[1 - \frac{\sigma_{\text{int}} n_1}{2g^{\max}\left(1 - f_{\text{n0, 1}}\right)^2}\right]. \tag{A6}$$

Appendix II

Maximum σ_{int} at which $L^{opt} = \infty$

The optimum cavity length L^{opt} at which the modulation bandwidth is highest can be obtained from (3.43), which is a cubic equation in L^{opt}. The expression for L^{opt} when σ_{int} is small is given by (3.44). With increasing σ_{int}, L^{opt} increases and at a maximum σ_{int} [denoted as $(\sigma_{int}^{max})'$] L^{opt} becomes infinity.

Using $L^{opt} = \infty$ in (3.43) and (3.11), we obtain

$$(\sigma_{int}^{max})' = \frac{\left(\sqrt{3g^{max} - 2\alpha_0} - \sqrt{g^{max}}\right)^2}{2n_1} \frac{1}{\dfrac{2\sqrt{g^{max}}}{\sqrt{3g^{max} - 2\alpha_0} - \sqrt{g^{max}}} - 1}. \tag{A7}$$

The expression for the optimum cavity length when σ_{int} is close to $(\sigma_{int}^{max})'$ is

$$L^{opt}\Big|_{\sigma_{int} \to (\sigma_{int}^{max})'} = \left(\frac{\sqrt{3g^{max} - 2\alpha_0} - \sqrt{g^{max}}}{\sqrt{3g^{max} - 2\alpha_0} - 3\sqrt{g^{max}}}\right)^2 \left(4\sqrt{\frac{g^{max}}{3g^{max} - 2\alpha_0}} - 1\right) \frac{\ln\dfrac{1}{R}}{n_1\left[(\sigma_{int}^{max})' - \sigma_{int}\right]} \tag{A8}$$

$$\propto \frac{1}{(\sigma_{int}^{max})' - \sigma_{int}}.$$

The expression (3.13) for σ_{int}^{max} is obtained from the lasing condition. At $L = \infty$, it becomes

$$\sigma_{int}^{max}\Big|_{L=\infty} = \frac{\left(\sqrt{2g^{max}} - \sqrt{\alpha_0 + g^{max}}\right)^2}{n_1}. \tag{A9}$$

When $\alpha_0 = 0$, we obtain from (A9) and (A7),

$$\sigma_{int}^{max} = (3 - 2\sqrt{2})\frac{g^{max}}{n_1} \approx 0.17\frac{g^{max}}{n_1}, \tag{A10}$$

$$(\sigma_{\text{int}}^{\max})' = \left(2\frac{\sqrt{3}}{3} - 1\right)\frac{g^{\max}}{n_1} \approx 0.15\,\frac{g^{\max}}{n_1}. \tag{A11}$$

As seen from (A10) and (A11), the values of $(\sigma_{\text{int}}^{\max})'$ and $\sigma_{\text{int}}^{\max}$ are very close to each other. The difference between them is due to the fact that we used an approximate expression (3.37) for $\omega_{-3\text{ dB}}^{\max}$ ($\omega_{-3\text{ dB}}$ is maximum at approximately the current density at which $\omega_{\text{peak}} = 0$) to derive $(\sigma_{\text{int}}^{\max})'$. Hence the difference between the accurate and approximate expressions for $\sigma_{\text{int}}^{\max}$ at $L^{\text{opt}} = \infty$ [equations (A9) and (A7), respectively] is small at $\alpha_0 = 0$.

References [*)]

[A1] Y. Wu, R. A. Suris and L. V. Asryan, "Effect of internal optical loss on the modulation bandwidth of a quantum dot laser," *Appl. Phys. Lett.*, vol. 100, no. 13, Art. no. 131106, Mar. 2012.

[A2] L. V. Asryan, Y. Wu, and R. A. Suris, "Modulation bandwidth of a quantum dot laser: The upper limit and limiting factors," *Proc. 15th International Conf. "Laser Optics 2012"*, June 25-29, 2012, St. Petersburg, Russia. Paper no. WeR3-22.

[1] G. P. Agrawal and N. K. Dutta, Long-wavelength semiconductor lasers, Van Nostrand Reinhold, 1986, p. 474.

[2] D. Z. Garbuzov, A. V. Ovchinnikov, N. A. Pikhtin, Z. N. Sokolova, I. S. Tarasov and V. B. Khalfin, "Experimental and theoretical investigations of singularities of the threshold and power characteristics of InGaAsP/InP separate-confinement double-heterostructure lasers ($\lambda = 1.3$ μm)," *Sov. Phys. Semicond.*, vol. 25, no. 5, pp. 560-564, May 1991.

[3] C. H. Henry, R. A. Logan, F. R. Merritt and J. P. Luongo, "The effect of intervalence band absorption on the thermal behavior of InGaAsP lasers," *IEEE J. Quantum. Electron.*, vol. 19, no. 6, pp. 947-952, Jun. 1983.

[4] M. Asada, A. Kameyama and Y. Suematsu, "Gain and intervalence band absorption in quantum-well lasers," *IEEE J. Quantum. Electron.*, vol. 20, no. 7, pp. 745-753, July 1984.

[5] J. J. Lee, L. J. Mawst and D. Botez, "MOCVD growth of asymmetric 980 nm InGaAs/InGaAsP broad-waveguide diode lasers for high power applications," *J. Crystal Growth*, vol. 249, no. 1-2, pp. 100-105, Feb. 2003.

[6] D. A. Ackerman, G. E. Shtengel, M. S. Hybertsen, P. A. Morton, R. F. Kazarinov, T. Tanbunek and R. A. Logan, "Analysis of gain in determining T_0 in 1.3 μm semiconductor lasers," *IEEE J. Select. Topics Quantum Electron.*, vol. 1, no. 2, pp. 250-263, Jun. 1995.

[*)] "A" in the reference number indicates the publications of the author of this dissertation.

[7] L. V. Asryan and S. Luryi, "Two lasing thresholds in semiconductor lasers with a quantum-confined active region," *Appl. Phys. Lett.*, vol. 83, no. 26, pp. 5368-5370, Dec. 2003.

[8] L. V. Asryan and S. Luryi, "Effect of internal optical loss on threshold characteristics of semiconductor lasers with a quantum-confined active region," *IEEE J. Quantum. Electron.*, vol. 40, no. 7, pp. 833-843, Jul. 2004.

[9] L. V. Asryan, "Maximum power of quantum dot laser versus internal loss," *Appl. Phys. Lett.*, vol. 88, no. 7, Feb. 2006.

[10] L. Jiang and L. V. Asryan, "Internal-loss-limited maximum operating temperature and characteristic temperature of quantum dot laser," *Laser Phys. Lett.*, vol. 4, no. 4, pp. 265-269, Apr. 2007.

[11] L. V. Asryan, Y. Wu and R. A. Suris, "Capture delay and modulation bandwidth in a quantum dot laser," *Proc. SPIE*, vol. 7947, pp. 794708-1 -- 794708-8, Jan. 2011.

[12] L. V. Asryan and R. A. Suris, "Upper limit for the modulation bandwidth of a quantum dot laser," *Appl. Phys. Lett.*, vol. 96, no. 22, Art. no. 221112, May 2010.

[13] L. V. Asryan and R. A. Suris, "Inhomogeneous line broadening and the threshold current density of a semiconductor quantum dot laser," *Semicond. Sci. Technol.*, vol. 11, no. 4, pp. 554-567, Apr. 1996.

[14] T. Ikegami and Y. Suematsu, "Resonance-like characteristics of the direct modulation of a junction laser," *Proceedings of the IEEE*, vol. 55, no. 1, pp. 122-123, Jan. 1967.

[15] T. L. Paoli and J. E. Ripper, "Direct modulation of semiconductor lasers," *Proceedings of the IEEE*, vol. 58, no. 10, pp. 1457-1465, 1970.

[16] M. J. Adams, "Rate equations and transient phenomena in semiconductor lasers," *Opto-Electronics*, vol. 5, no. 2, pp. 201-215, 1973.

[17] R. F. Kazarinov and R. A. Suris, "Heterodyne reception of light by an injection laser," *Sov. Phys. JETP*, vol. 39, no. 3, pp. 522-527, Sept. 1974.

[18] C. B. Su and V. A. Lanzisera, "Ultra high-speed modulation of 1.3 μm InGaAsP diode lasers," *IEEE J. Quantum. Electron.*, vol. 22, no. 9, pp. 1568-1578, Sept. 1986.

[19] R. Olshansky, P. Hill, V. Lanzisera and W. Powazinik, "Frequency response of 1.3 μm InGaAsP high speed semiconductor lasers," *IEEE J. Quantum. Electron.*, vol. 23, no. 9, pp. 1410-1418, Sept. 1987.

[20] R. Nagarajan, M. Ishikawa, T. Fukushima, R. S. Geels and J. E. Bowers, "High speed quantum-well lasers and carrier transport effects," *IEEE J. Quantum. Electron.*, vol. 28, no. 10, pp. 1990-2008, Oct. 1992.

[21] L. V. Asryan, S. Luryi and R. A. Suris, "Internal efficiency of semiconductor lasers with a quantum-confined active region," *IEEE J. Quantum. Electron.*, vol. 39, no. 3, pp. 404-418, Mar. 2003.

Chapter 4

Effect of excited states on the modulation bandwidth in quantum dot lasers

Summary

We consider direct and indirect (excited-state-mediated) capture of carriers from the waveguide region into the lasing ground state in quantum dots (QDs) and calculate the modulation response of a QD laser [A1][*)]. We show that, when only indirect capture is involved, the excited-to-ground-state relaxation delay strongly limits the ground-state modulation bandwidth of the laser — at the longest tolerable relaxation time, the bandwidth becomes zero. When direct capture is also involved, the effect of excited-to-ground-state relaxation is less significant and the modulation bandwidth is considerably higher.

4.1. Introduction

In [1], the upper limit for the small-signal modulation bandwidth ideally attainable in QD lasers was estimated. The experimental modulation bandwidth in QD lasers [2, 3] is actually considerably lower. Several factors can affect the dynamic properties of QD lasers and limit the modulation bandwidth. Among such factors are the carrier capture delay from the higher-dimensionality reservoir regions (2-D wetting layer [4-7] and bulk optical confinement layer (OCL) [A2-A5]) into QDs, the internal optical loss, which increases with carrier density in the OCL [A5, A6], and the gain compression (see, e.g., [8]).

In this chapter, we study the effect of excited states, which are typically present in QDs [9, 10], on the ground-state modulation response of a QD laser. Recombination processes via excited states (Fig. 4.1) reduce the efficiency of carrier injection into the ground state in QDs (Fig. 4.1). In this regard, the role of recombination via excited states in QDs is similar to that of

---

[*)] "A" in the reference number indicates the publications of the author of this dissertation.

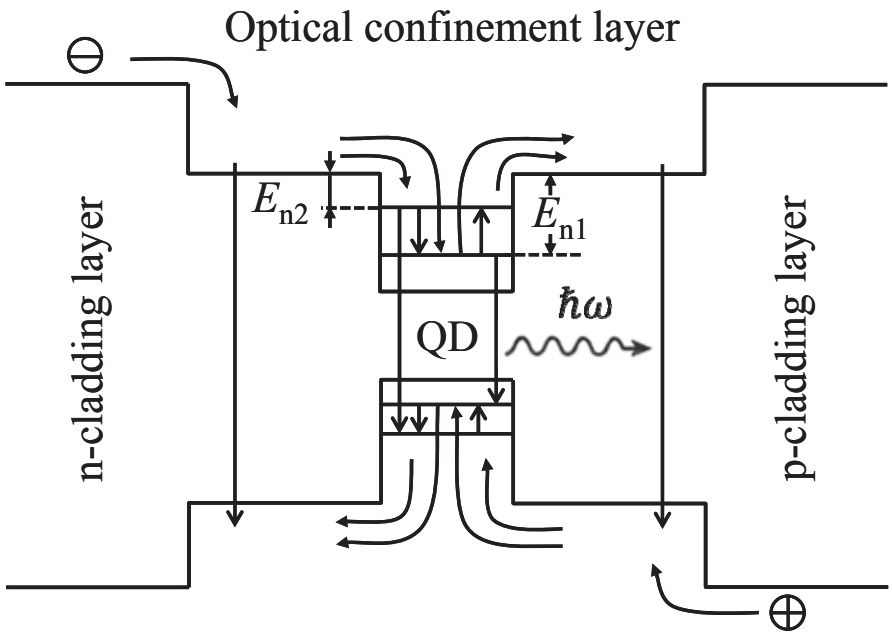

Fig. 4.1. Energy band diagram of a QD laser. One excited state is assumed for each type of carriers in QDs in addition to the ground state. Both direct and indirect (excited-state-mediated) capture processes into the lasing ground state are considered. (Reprinted with permission from Fig. 1 of ref. [A1], Copyright (2013) by AIP.)

parasitic recombination in the OCL [11] (Fig. 4.1). There is also relaxation delay from the excited- to ground-state in a QD [12-20]. Under the conditions of a two-step (excited-state-mediated) capture from the OCL into the QD ground-state, the excited-to-ground-state relaxation delay will be added to the OCL-to-excited-state capture delay.

In [A2-A5], [4, 5], the effect of carrier capture delay from the reservoir into single-level QDs (i.e., into the QD ground-state) on the modulation bandwidth was studied. In [6, 7], the effect of capture delay from the reservoir into the QD excited-state on the ground-state modulation response was discussed. While the capture delays from the reservoir into both the QD ground- and excited-states are inherently included in the model of the present work, the primary focus here is the effect of excited-to-ground-state relaxation delay inside QDs on the ground-state modulation bandwidth.

4.2. Rate equations model

Our theoretical model is illustrated in Fig. 4.1. The carriers injected in the OCL can be either directly captured into the QD ground-state, or first captured into the excited-states and then relax to the ground-states. The carriers localized in QDs can escape back to the OCL. For the carriers localized in the ground state, the escape process can be either direct or via the excited state. We used the detailed balance condition to derive the relationship between the time τ_{12} of upward transitions from the ground- to excited-state and the time τ_{21} of relaxation from the excited- to ground-state. The relation reads as

$$\tau_{12} = \tau_{21} \exp\left(\frac{E_{n1} - E_{n2}}{T}\right), \tag{4.1}$$

where E_{n1} and E_{n2} are the energies of carrier excitation from the QD ground- and excited-state to the OCL (see Fig. 4.1), and T is the temperature (in units of energy). The spontaneous radiative recombination occurs via the OCL states and both the ground- and excited-states in QDs. Since the focus of this work is the effect of carrier relaxation to the lasing state on the modulation bandwidth, we restrict our consideration to stimulated emission only via the QD ground-state. The case of lasing via the upper excited-state is not essentially different from the case of single-level QDs considered in [A2-A5].

With the above processes included in our model, we have the following set of four coupled rate equations for free carriers in the OCL, carriers confined in the QD excited-state, those confined in the QD ground-state, and photons:

$$\begin{aligned}\frac{\partial n_{OCL}}{\partial t} = {} & \frac{j}{eb} - \sigma_{n2} v_n \frac{N_S}{b}(1 - f_{n2}) n_{OCL} + \sigma_{n2} v_n n_2 \frac{N_S}{b} f_{n2} \\ & - \sigma_{n1} v_n \frac{N_S}{b}(1 - f_{n1}) n_{OCL} + \sigma_{n1} v_n n_1 \frac{N_S}{b} f_{n1} - B n_{OCL}^2,\end{aligned} \tag{4.2}$$

$$\begin{aligned}\frac{\partial}{\partial t}\left(2\frac{N_S}{b} f_{n2}\right) = {} & \sigma_{n2} v_n \frac{N_S}{b}(1 - f_{n2}) n_{OCL} - \sigma_{n2} v_n n_2 \frac{N_S}{b} f_{n2} \\ & + \frac{N_S}{b}\frac{f_{n1}(1 - f_{n2})}{\tau_{12}} - \frac{N_S}{b}\frac{f_{n2}(1 - f_{n1})}{\tau_{21}} - \frac{N_S}{b}\frac{f_{n2}^2}{\tau_{QD2}},\end{aligned} \tag{4.3}$$

$$\frac{\partial}{\partial t}\left(2\frac{N_{\mathrm{S}}}{b}f_{\mathrm{n1}}\right)=\sigma_{\mathrm{n1}}\mathrm{v}_{\mathrm{n}}\frac{N_{\mathrm{S}}}{b}(1-f_{\mathrm{n1}})n_{\mathrm{OCL}}-\sigma_{\mathrm{n1}}\mathrm{v}_{\mathrm{n}}n_1\frac{N_{\mathrm{S}}}{b}f_{\mathrm{n1}}+\frac{N_{\mathrm{S}}}{b}\frac{f_{\mathrm{n2}}(1-f_{\mathrm{n1}})}{\tau_{21}}$$
$$-\frac{N_{\mathrm{S}}}{b}\frac{f_{\mathrm{n1}}(1-f_{\mathrm{n2}})}{\tau_{12}}-\frac{N_{\mathrm{S}}}{b}\frac{f_{\mathrm{n1}}^2}{\tau_{\mathrm{QD1}}}-\mathrm{v}_{\mathrm{g}}g_1^{\max}(2f_{\mathrm{n1}}-1)n_{\mathrm{ph}}, \tag{4.4}$$

$$\frac{\partial n_{\mathrm{ph}}}{\partial t}=\mathrm{v}_{\mathrm{g}}g_1^{\max}(2f_{\mathrm{n1}}-1)n_{\mathrm{ph}}-\mathrm{v}_{\mathrm{g}}\beta n_{\mathrm{ph}}, \tag{4.5}$$

where n_{OCL} is the free carrier density in the OCL, f_{n1} and f_{n2} are the occupancies of the ground- and excited-state in a QD, and n_{ph} is the photon density (per unit volume of the OCL) in the lasing mode. The other parameters are as follows: j is the injection current density, b is the OCL thickness, σ_{n1} and σ_{n2} are the cross-sections of carrier capture from the OCL into the QD ground- and excited-state, v_{n} is the free carrier thermal velocity in the OCL, N_{S} is the surface density of QDs, B is the spontaneous radiative recombination constant for the OCL, τ_{QD1} and τ_{QD2} are the spontaneous radiative recombination lifetimes via the QD ground- and excited-state, $g_1^{\max}$ is the maximum modal gain for the ground-state transitions, $\beta = (1/L)\ln(1/R)$ is the mirror loss, L is the cavity length, and R is the facet reflectivity.

The quantities

$$n_1=N_{\mathrm{c}}^{3\mathrm{D}}\exp\left(-\frac{E_{\mathrm{n1}}}{T}\right) \tag{4.6}$$

and

$$n_2=N_{\mathrm{c}}^{3\mathrm{D}}\exp\left(-\frac{E_{\mathrm{n2}}}{T}\right) \tag{4.7}$$

characterize the intensities of thermal escapes from the QD ground- and excited-state to the OCL (Fig. 4.1), where $N_{\mathrm{c}}^{3\mathrm{D}}$ is the effective density of states in the OCL.

As in [A2-A5], [4, 5], our model does not include the fraction of spontaneous emission entering the lasing mode. This fraction is generally very small [21], and this is the more so in QD lasers, since the spontaneous emission rate in QDs is itself low [we discuss the ground-state lasing and, hence, we mean the ground-state emission rate $(N_{\mathrm{S}}/b)(f_{\mathrm{n1}}^2/\tau_{\mathrm{QD1}})$, although the excited-state emission rate $(N_{\mathrm{S}}/b)(f_{\mathrm{n2}}^2/\tau_{\mathrm{QD2}})$ is also low]. Even slightly above the lasing threshold, the fraction of spontaneous emission is negligible as compared to the stimulated

emission rate [the first term in the right-hand side of (4.5)]. Neglecting this fraction makes our analysis and derivations simpler while not considerably influencing the physical picture.

4.3. Results and discussions

4.3.1. Steady-state solutions of the rate equations

At the steady-state (i.e., when $\partial/\partial t = 0$; the steady-state quantities are denoted by "0" in the subscript), the rate equations (4.2) – (4.5) are

$$\begin{aligned} 0 = {} & \frac{j_0}{eb} - \sigma_{n2} v_n \frac{N_S}{b}(1 - f_{n2,0}) n_{OCL,0} + \sigma_{n2} v_n n_2 \frac{N_S}{b} f_{n2,0} \\ & - \sigma_{n1} v_n \frac{N_S}{b}(1 - f_{n1,0}) n_{OCL,0} + \sigma_{n1} v_n n_1 \frac{N_S}{b} f_{n1,0} - B n_{OCL,0}^2, \end{aligned} \tag{4.8}$$

$$\begin{aligned} 0 = {} & \sigma_{n2} v_n \frac{N_S}{b}(1 - f_{n2,0}) n_{OCL,0} - \sigma_{n2} v_n n_2 \frac{N_S}{b} f_{n2,0} \\ & + \frac{N_S}{b} \frac{f_{n1,0}(1 - f_{n2,0})}{\tau_{12}} - \frac{N_S}{b} \frac{f_{n2,0}(1 - f_{n1,0})}{\tau_{21}} - \frac{N_S}{b} \frac{f_{n2,0}^2}{\tau_{QD2}}, \end{aligned} \tag{4.9}$$

$$\begin{aligned} 0 = {} & \sigma_{n1} v_n \frac{N_S}{b}(1 - f_{n1,0}) n_{OCL,0} - \sigma_{n1} v_n n_1 \frac{N_S}{b} f_{n1,0} + \frac{N_S}{b} \frac{f_{n2,0}(1 - f_{n1,0})}{\tau_{21}} \\ & - \frac{N_S}{b} \frac{f_{n1,0}(1 - f_{n2,0})}{\tau_{12}} - \frac{N_S}{b} \frac{f_{n1,0}^2}{\tau_{QD1}} - v_g g_1^{max} (2 f_{n1,0} - 1) n_{ph,0}, \end{aligned} \tag{4.10}$$

$$0 = v_g g_1^{max} (2 f_{n1,0} - 1) n_{ph,0} - v_g \beta n_{ph,0}. \tag{4.11}$$

Above the lasing threshold ($n_{ph,0} \neq 0$), the QD ground-state level occupancy is obtained from (4.11),

$$f_{n1,0} = \frac{1}{2}\left(1 + \frac{\beta}{g_1^{max}}\right). \tag{4.12}$$

As seen from (4.12), $f_{n1,0}$ is pinned (i.e., does not depend on j_0) at its threshold value.

The photon lifetime in the cavity is expressed as

$$\tau_{ph} = \frac{1}{v_g g_1^{max} (2 f_{n1,0} - 1)} = \frac{1}{v_g \beta}. \tag{4.13}$$

From (4.9), we obtain the expression for the free carrier density in the OCL $n_{\mathrm{OCL},0}$ in terms of $f_{\mathrm{n1},0}$ and $f_{\mathrm{n2},0}$,

$$n_{\mathrm{OCL},0} = n_2 \frac{f_{\mathrm{n2},0}}{1-f_{\mathrm{n2},0}} + \frac{1}{\sigma_{\mathrm{n2}} \mathrm{v}_{\mathrm{n}}} \frac{1}{1-f_{\mathrm{n2},0}} \left[\frac{f_{\mathrm{n2},0}(1-f_{\mathrm{n1},0})}{\tau_{21}} - \frac{f_{\mathrm{n1},0}(1-f_{\mathrm{n2},0})}{\tau_{12}} + \frac{f_{\mathrm{n2},0}^2}{\tau_{\mathrm{QD2}}} \right]. \tag{4.14}$$

Eq. (4.14) can be rewritten as a quadratic equation in terms of $f_{\mathrm{n2},0}$. Solution of this equation gives $f_{\mathrm{n2},0}$ as a function of $n_{\mathrm{OCL},0}$.

From (4.10), we obtain the expression for the photon density $n_{\mathrm{ph},0}$ in terms of $f_{\mathrm{n1},0}$, $f_{\mathrm{n2},0}$, and $n_{\mathrm{OCL},0}$,

$$\begin{aligned} n_{\mathrm{ph},0} = \tau_{\mathrm{ph}} \frac{N_{\mathrm{S}}}{b} \Bigg[& \sigma_{\mathrm{n1}} \mathrm{v}_{\mathrm{n}} (1-f_{\mathrm{n1},0}) n_{\mathrm{OCL},0} - \sigma_{\mathrm{n1}} \mathrm{v}_{\mathrm{n}} n_1 f_{\mathrm{n1},0} + \frac{f_{\mathrm{n2},0}(1-f_{\mathrm{n1},0})}{\tau_{21}} \\ & - \frac{f_{\mathrm{n1},0}(1-f_{\mathrm{n2},0})}{\tau_{12}} - \frac{f_{\mathrm{n1},0}^2}{\tau_{\mathrm{QD1}}} \Bigg]. \end{aligned} \tag{4.15}$$

An expression for $n_{\mathrm{ph},0}$ equivalent to eq. (4.15) can also be obtained by adding equations (4.9) and (4.10),

$$\begin{aligned} n_{\mathrm{ph},0} = & \tau_{\mathrm{ph}} \frac{N_{\mathrm{S}}}{b} \left[\sigma_{\mathrm{n2}} \mathrm{v}_{\mathrm{n}} (1-f_{\mathrm{n2},0}) + \sigma_{\mathrm{n1}} \mathrm{v}_{\mathrm{n}} (1-f_{\mathrm{n1},0}) \right] n_{\mathrm{OCL},0} \\ & - \tau_{\mathrm{ph}} \frac{N_{\mathrm{S}}}{b} \left[\sigma_{\mathrm{n2}} \mathrm{v}_{\mathrm{n}} n_2 f_{\mathrm{n2},0} + \sigma_{\mathrm{n1}} \mathrm{v}_{\mathrm{n}} n_1 f_{\mathrm{n1},0} + \frac{f_{\mathrm{n2},0}^2}{\tau_{\mathrm{QD2}}} + \frac{f_{\mathrm{n1},0}^2}{\tau_{\mathrm{QD1}}} \right]. \end{aligned} \tag{4.16}$$

Adding equations (4.8), (4.9), and (4.10), we obtain the expression for the injection current density j_0,

$$j_0 = ebBn_{\mathrm{OCL},0}^2 + eN_{\mathrm{S}} \frac{f_{\mathrm{n2},0}^2}{\tau_{\mathrm{QD2}}} + eN_{\mathrm{S}} \frac{f_{\mathrm{n1},0}^2}{\tau_{\mathrm{QD1}}} + eb \frac{n_{\mathrm{ph},0}}{\tau_{\mathrm{ph}}}. \tag{4.17}$$

Using (4.14) and (4.15) in (4.17), we obtain a quartic equation in terms of $f_{\mathrm{n2},0}$. Solution of this equation will give us $f_{\mathrm{n2},0}$ as a function of j_0.

At the lasing threshold, $n_{\mathrm{ph},0} = 0$. The free carrier density in the OCL at lasing threshold can be obtained from (4.14), (4.15), or (4.16). We have the following three equivalent expressions for $n_{\mathrm{OCL},0}^{\mathrm{th}}$:

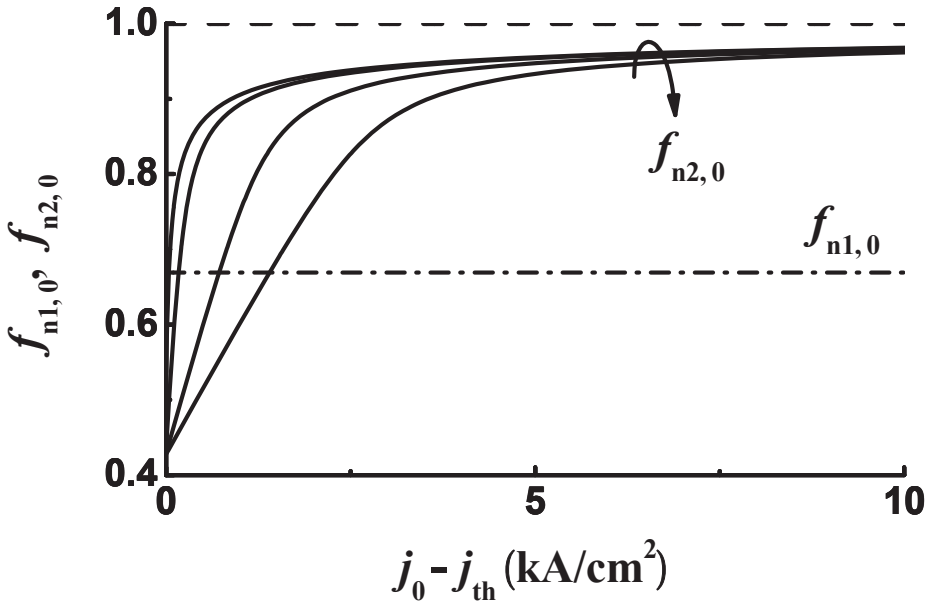

Fig. 4.2. Ground- (horizontal dash-dotted line) and excited-state (solid curves) occupancies in a QD against excess injection current density. GaInAsP/InP heterostructure lasing near 1.55 μm is considered here for illustration [22]. The values of τ_{21} for different curves (from the top down) are 100, 10, 2, and 1 ps. The corresponding threshold values of $f_{n2,0}^{th}$ are 0.537, 0.438, 0.429, and 0.428. In this figure, no direct capture into the QD ground-state was considered ($\sigma_{n1} = 0$) and $\sigma_{n2} = 10^{-11}$cm^2.

$$n_{OCL,0}^{th} = n_2 \frac{f_{n2,0}^{th}}{1-f_{n2,0}^{th}} + \frac{1}{\sigma_{n2} v_n} \frac{1}{1-f_{n2,0}^{th}} \left[\frac{f_{n2,0}^{th}(1-f_{n1,0})}{\tau_{21}} - \frac{f_{n1,0}(1-f_{n2,0}^{th})}{\tau_{12}} + \frac{(f_{n2,0}^{th})^2}{\tau_{QD2}} \right], \tag{4.18}$$

$$n_{OCL,0}^{th} = n_1 \frac{f_{n1,0}}{1-f_{n1,0}} + \frac{1}{\sigma_{n1} v_n (1-f_{n1,0})} \left[\frac{f_{n1,0}(1-f_{n2,0}^{th})}{\tau_{12}} - \frac{f_{n2,0}^{th}(1-f_{n1,0})}{\tau_{21}} + \frac{f_{n1,0}^2}{\tau_{QD1}} \right], \tag{4.19}$$

$$n_{OCL,0}^{th} = \frac{\sigma_{n1} v_n n_1 f_{n1,0} + \sigma_{n2} v_n n_2 f_{n2,0}^{th} + \frac{f_{n1,0}^2}{\tau_{QD1}} + \frac{(f_{n2,0}^{th})^2}{\tau_{QD2}}}{\sigma_{n1} v_n (1-f_{n1,0}) + \sigma_{n2} v_n (1-f_{n2,0}^{th})}. \tag{4.20}$$

When σ_{n1} (or σ_{n2}) is zero, the term in the square brackets in the right-hand side of (4.19) [or (4.18)] is also zero. For this case, it is more convenient to use eq. (4.20) for $n^{th}_{OCL,\,0}$.

By equalizing (4.18) and (4.19), we obtain the following quadratic equation in $f^{th}_{n2,\,0}$:

$$\begin{aligned}
&\left[\left(\frac{f_{n1,\,0}}{1-f_{n1,\,0}}\frac{1}{\tau_{12}}+\frac{1}{\tau_{21}}\right)\sigma_{n2}-\frac{1}{\tau_{QD2}}\sigma_{n1}\right](f^{th}_{n2,\,0})^2 \\
&-\left[\sigma_{n1}\sigma_{n2}V_n\left(\frac{n_1 f_{n1,0}}{1-f_{n1,0}}+n_2\right)+\left(\frac{f^2_{n1,0}}{1-f_{n1,0}}\frac{1}{\tau_{QD1}}+\frac{2f_{n1,0}}{1-f_{n1,0}}\frac{1}{\tau_{12}}+\frac{1}{\tau_{21}}\right)\sigma_{n2}\right. \\
&\qquad\left.+\left(\frac{f_{n1,0}}{\tau_{12}}+\frac{1-f_{n1,0}}{\tau_{21}}\right)\sigma_{n1}\right]f^{th}_{n2,0} \\
&+\left[\sigma_{n1}\sigma_{n2}V_n n_1\frac{f_{n1,\,0}}{1-f_{n1,\,0}}+\left(\frac{f^2_{n1,\,0}}{1-f_{n1,\,0}}\frac{1}{\tau_{QD1}}+\frac{f_{n1,\,0}}{1-f_{n1,\,0}}\frac{1}{\tau_{12}}\right)\sigma_{n2}+\frac{f_{n1,\,0}}{\tau_{12}}\sigma_{n1}\right]=0.
\end{aligned} \tag{4.21}$$

Only one of the roots of (4.21) is real and positive and smaller than unity. As seen from Fig. 4.2, $f_{n2,\,0}$ increases with injection current density j_0 and approaches unity as j_0 increases infinitely – see more discussions about this in Appendixes I and II.

From (4.17), the threshold current density can be written as

$$j_{th}=ebB(n^{th}_{OCL,\,0})^2+eN_S\frac{(f^{th}_{n2,\,0})^2}{\tau_{QD2}}+eN_S\frac{f^2_{n1,\,0}}{\tau_{QD1}}, \tag{4.22}$$

where $n^{th}_{OCL,\,0}$ is given by (4.18), (4.19), or (4.20), and $f^{th}_{n2,\,0}$ is given by the solution of (4.21).

The injection current density j_0 can be written in the form

$$j_0=j_{th}+ebB[n^2_{OCL,0}-(n^{th}_{OCL,0})^2]+eN_S\frac{1}{\tau_{QD2}}[f^2_{n2,0}-(f^{th}_{n2,0})^2]+j_{stim}, \tag{4.23}$$

where

$$j_{stim}=eb\frac{n_{ph,0}}{\tau_{ph}} \tag{4.24}$$

is the stimulated recombination current density.

The optical power is

$$P_0 = \hbar\omega_0 \frac{n_{\mathrm{ph},0}}{\tau_{\mathrm{ph}}} Sb, \tag{4.25}$$

where $\hbar\omega_0$ is the photon energy.

If the carrier capture/escape into/from a QD is excited-state-mediated only (i.e., $\sigma_{\mathrm{n1}} = 0$), the expression for the excited-state level occupancy at the lasing threshold considerably simplifies,

$$f_{\mathrm{n2},0}^{\mathrm{th}} = \frac{1}{(1-f_{\mathrm{n1},0})\dfrac{\tau_{12}}{\tau_{21}} + f_{\mathrm{n1},0}} \left(f_{\mathrm{n1},0} + \frac{\tau_{12}}{\tau_{\mathrm{QD1}}} f_{\mathrm{n1},0}^2 \right). \tag{4.26}$$

In this case, the free carrier density in the OCL at the lasing threshold is

$$n_{\mathrm{OCL},\,0}^{\mathrm{th}} = n_2 \frac{f_{\mathrm{n2},\,0}^{\mathrm{th}}}{1-f_{\mathrm{n2},\,0}^{\mathrm{th}}} + \frac{1}{\sigma_{\mathrm{n2}} \mathrm{v}_{\mathrm{n}}} \frac{1}{1-f_{\mathrm{n2},\,0}^{\mathrm{th}}} \left[\frac{f_{\mathrm{n1},\,0}^2}{\tau_{\mathrm{QD1}}} + \frac{(f_{\mathrm{n2},\,0}^{\mathrm{th}})^2}{\tau_{\mathrm{QD2}}} \right]. \tag{4.27}$$

Using (4.26) and (4.27) in (4.22), we can easily obtain the expression for j_{th} for the case of $\sigma_{\mathrm{n1}} = 0$.

4.3.2. Modulation response function and modulation bandwidth

We consider a direct modulation of the laser output by the small time-harmonic component δj of the pump current density j and, correspondingly, use the small-signal analysis [21, 23, 24] of rate equations (4.2)–(4.5). Our derivations are presented in Appendix III. Looking for the solutions of the rate equations in the form of the sum of the dc (steady-state) component and the small time-harmonic component, we arrive at the set of algebraic equations in the small frequency-dependent amplitudes $\delta n_{\mathrm{OCL-m}}$, $\delta f_{\mathrm{n1-m}}$, $\delta f_{\mathrm{n2-m}}$, and $\delta n_{\mathrm{ph-m}}$. From the solution of this set, we find the ratio

$$\frac{\delta n_{\mathrm{ph-m}}(\omega)}{\delta n_{\mathrm{ph-m}}(0)} = \frac{A_0}{(\omega^4 - A_2\omega^2 + A_0) - i\,(A_3\omega^3 - A_1\omega)}, \tag{4.28}$$

where ω is the angular frequency of modulation.

The modulation response function is

$$H(\omega)=\left|\frac{\delta n_{\text{ph-m}}(\omega)}{\delta n_{\text{ph-m}}(0)}\right|^2=\frac{A_0^2}{(\omega^4-A_2\omega^2+A_0)^2+(A_3\omega^3-A_1\omega)^2}. \tag{4.29}$$

The coefficients A_1, A_2, and A_3 are positive; A_0 is positive above the lasing threshold and zero at and below the lasing threshold. They are functions of the dc component j_0 of the injection current density and parameters of the laser structure. The expressions for these coefficients are cumbersome and are presented in Appendix III.

The modulation bandwidth $\omega_{-3\text{ dB}}$ is defined as the frequency, at which $H(\omega)$ has fallen to half its dc ($\omega = 0$) value,

$$10\log_{10} H(\omega_{-3\text{ dB}})=-3. \tag{4.30}$$

The following quartic equation for the square of the modulation bandwidth is obtained from (4.29) and (4.30):

$$\omega_{-3\text{ dB}}^8+(A_3^2-2A_2)\omega_{-3\text{ dB}}^6+(A_2^2+2A_0-2A_1A_3)\omega_{-3\text{ dB}}^4+(A_1^2-2A_0A_2)\omega_{-3\text{ dB}}^2-(r-1)A_0^2=0, \tag{4.31}$$

where the numerical parameter $r=10^{0.3}\approx 1.995$.

The analysis of (4.31) shows that, under the lasing condition, i.e., if the dc component of the pump current density is above the threshold current density ($j_0 > j_{\text{th}}$), only one out of four roots $\omega_{-3\text{ dB}}^2$ of (4.31) is positive and hence physically meaningful. At the lasing threshold ($j_0 = j_{\text{th}}$), this root $\omega_{-3\text{ dB}}^2$ becomes zero (Fig. 4.3). At a small excess of j_0 above j_{th},

$$\omega_{-3\text{dB}}\approx\sqrt{r-1}\,\frac{A_0}{A_1}\propto j_0-j_{\text{th}}. \tag{4.32}$$

For the case of $\sigma_{\text{n1}} = 0$,

$$\omega_{-3\text{dB}}\approx\frac{1}{eN_{\text{S}}}\text{v}_{\text{g}}g_1^{\max}\eta_{\text{int}}^{\text{th}}\frac{\sqrt{r-1}}{\dfrac{f_{\text{n1,0}}}{\tau_{\text{QD1}}}+\dfrac{\dfrac{1}{2}\left(\dfrac{f_{\text{n2,0}}^{\text{th}}}{\tau_{21}}+\dfrac{1-f_{\text{n2,0}}^{\text{th}}}{\tau_{12}}\right)}{1+\dfrac{\dfrac{1}{2}\left(\dfrac{f_{\text{n2,0}}^{\text{th}}}{\tau_{21}}+\dfrac{1-f_{\text{n2,0}}^{\text{th}}}{\tau_{12}}\right)}{\dfrac{f_{\text{n2,0}}^{\text{th}}}{\tau_{\text{QD2}}}+\dfrac{Bn_{\text{OCL,0}}^{\text{th}}(\sigma_{\text{n2}}\text{v}_{\text{n}}n_{\text{OCL,0}}^{\text{th}}+\sigma_{\text{n2}}\text{v}_{\text{n}}n_2)}{\sigma_{\text{n2}}\text{v}_{\text{n}}\dfrac{N_{\text{S}}}{b}(1-f_{\text{n2,0}}^{\text{th}})+2Bn_{\text{OCL,0}}^{\text{th}}}}}}(j_0-j_{\text{th}}), \tag{4.33}$$

(a)

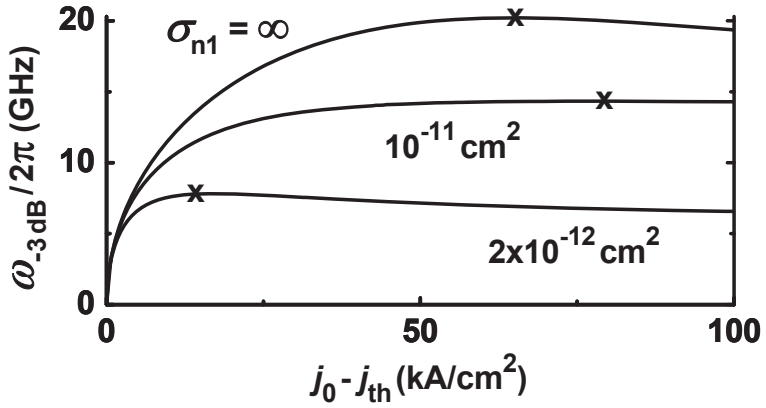

(b)

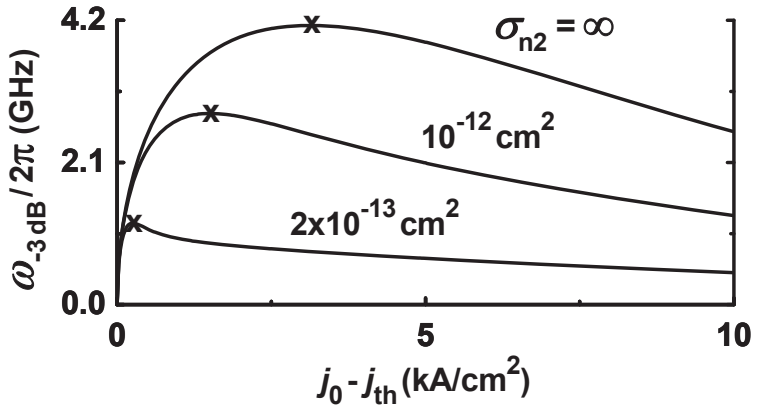

(c)

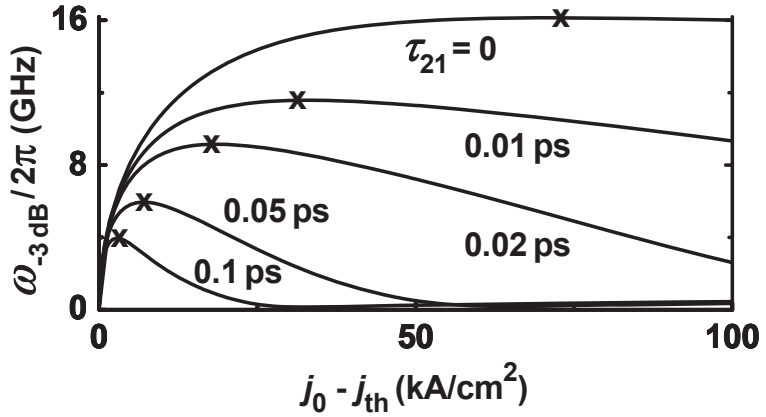

Fig. 4.3. Modulation bandwidth $\omega_{-3\,dB}/2\pi$ vs. excess of the dc component of the injection current density over the threshold current density. In (a), $\sigma_{n2} = 10^{-11}$ cm^2, $\tau_{21} = 0.1$ ps, and σ_{n1} is different for different curves; $\sigma_{n1} = \infty$ corresponds to instantaneous carrier exchange between the OCL and the QD ground-state. In (b), $\sigma_{n1} = 0$ (no direct capture into the QD ground-state), $\tau_{21} = 0.1$ ps, and σ_{n2} is different for different curves; $\sigma_{n2} = \infty$ corresponds to instantaneous exchange between

the OCL and the QD excited-state. In (c), $\sigma_{n1} = 0$ (no direct capture into the QD ground-state), $\sigma_{n2} = 10^{-11}\,\mathrm{cm}^2$, and τ_{21} is different for different curves; $\tau_{21} = 0$ corresponds to instantaneous exchange between the QD excited- and ground-state. Throughout the paper, the cavity length L = 1.139 mm is assumed (the mirror loss $\beta = 10\,\mathrm{cm}^{-1}$). The symbol "×" marks the maximum modulation bandwidth $\omega_{-3\,\mathrm{dB}}^{\max}/2\pi$ on each curve. (Reprinted with permission from Fig. 2 of ref. [A1], Copyright (2013) by AIP.)

where $\eta_{\mathrm{int}}^{\mathrm{th}}$ is the threshold value of the steady-state internal differential quantum efficiency.

For the case of $\sigma_{n1} = 0$, the following expression is derived for η_{int}:

$$\eta_{\mathrm{int}} = \frac{j_{\mathrm{stim}}}{j_0 - j_{\mathrm{stim}}} = \frac{1}{1 + \dfrac{\tau_{12}}{\tau_{\mathrm{QD2}}} \dfrac{1}{(1 - f_{\mathrm{n1},0})\dfrac{\tau_{12}}{\tau_{21}} + f_{\mathrm{n1},0}} (f_{\mathrm{n2},0} + f_{\mathrm{n2},0}^{\mathrm{th}}) + \dfrac{B\left[n_{\mathrm{OCL},0}^2 - (n_{\mathrm{OCL},0}^{\mathrm{th}})^2\right]}{n_{\mathrm{ph},0}/\tau_{\mathrm{ph}}}}. \tag{4.34}$$

For $j_0 < j_{\mathrm{th}}$ (below the lasing threshold), eq. (4.31) does not have any positive root $\omega_{-3\,\mathrm{dB}}^2$. Below, we discuss the dependences of the modulation bandwidth $\omega_{-3\,\mathrm{dB}}$ on j_0 and parameters of the structure. We consider a GaInAsP heterostructure lasing near 1.55 μm at room-temperature [22, 25]. The maximum gain for the ground-state transitions in the structure with a single layer of QDs $g_1^{\max} = 29.52\,\mathrm{cm}^{-1}$, which corresponds to 10% QD-size fluctuations, the surface density of QDs $N_S = 6.11\times10^{10}\,\mathrm{cm}^{-2}$, and an ideal overlap between the electron and hole ground-state wave functions [26]. The mirror loss $\beta = 10\,\mathrm{cm}^{-1}$ (at the as-cleaved facet reflectivity R = 0.32, this corresponds to the cavity length L = 1.139 mm) and the OCL thickness b = 0.28 μm.

Figure 4.3 shows the modulation bandwidth against excess of j_0 over j_{th}. As seen from the figure, with increasing j_0 increasing from j_{th}, $\omega_{-3\,\mathrm{dB}}$ increases from zero, approaches its maximum value $\omega_{-3\,\mathrm{dB}}^{\max}$ (marked by the symbol "×") at a certain optimum value of j_0, and then decreases.

In the presence of fast direct capture into the ground state (when σ_{n1} is large), $\omega_{-3\,\mathrm{dB}}$ is mainly controlled by σ_{n1} and only slightly affected by σ_{n2} and τ_{21}. In Fig. 4.3(a), the cross-

(a)

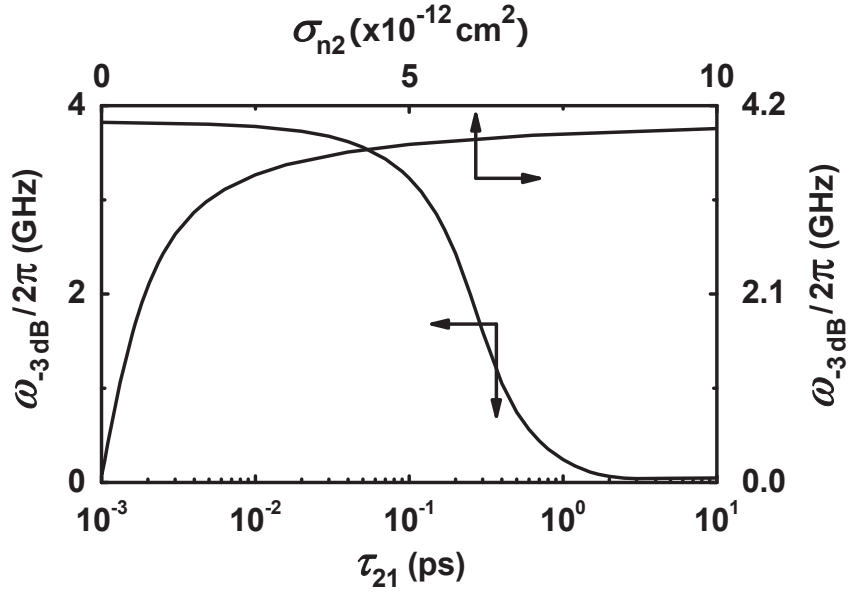

(b)

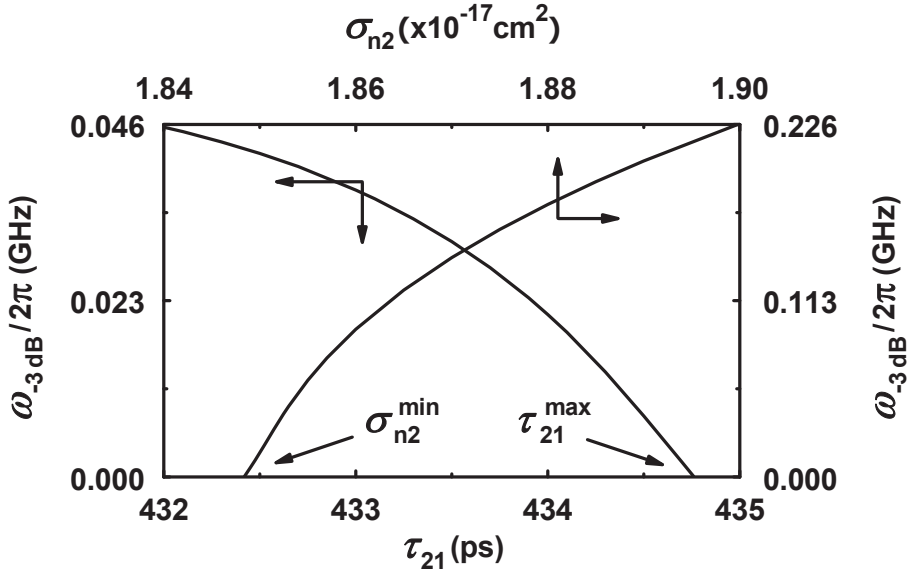

Fig. 4.4. Modulation bandwidth $\omega_{-3\,dB}/2\pi$ vs. capture cross-section into the QD excited-state (at j_0 = 3 kA/cm^2 and τ_{21} = 0.1 ps) and excited-to-ground-state relaxation time (at j_0 = 1 kA/cm^2 and $\sigma_{n2} = 10^{-11}$ cm^2) for the case of no direct capture into the QD ground-state (σ_{n1} = 0). In (b), the portions of the curves near the minimum tolerable value σ_{n2}^{min} of σ_{n2} and the maximum tolerable value τ_{21}^{max} of τ_{21} are shown. (Reprinted with permission from Fig. 3 of ref. [A1], Copyright (2013) by AIP.)

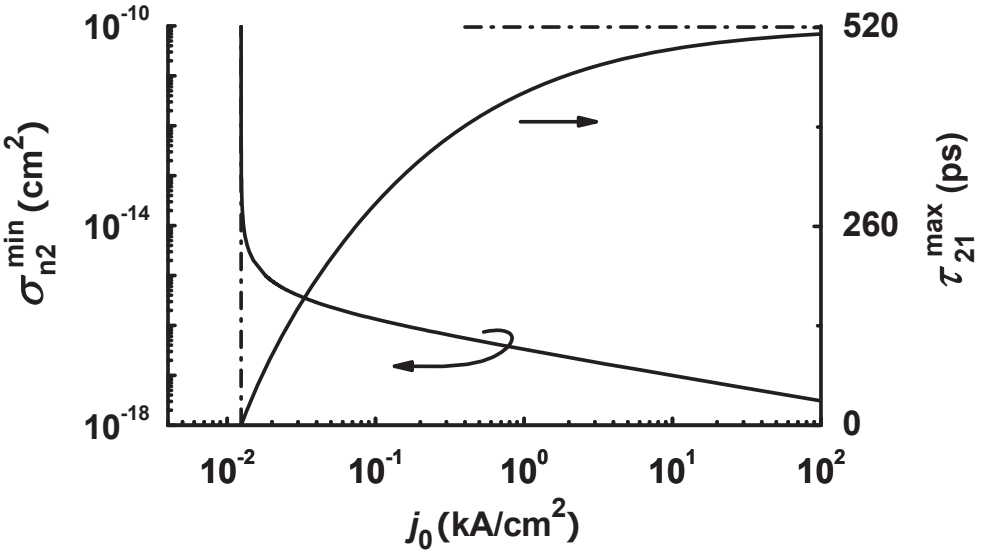

Fig. 4.5. Minimum tolerable value σ_{n2}^{min} of the capture cross-section into the QD excited-state (at τ_{21} = 0.1 ps) and maximum tolerable value τ_{21}^{max} of the excited-to-ground-state relaxation time (at $\sigma_{n2} = 10^{-11}$ cm^2) vs. dc component of the injection current density. No direct capture into the QD ground-state is involved (σ_{n1} = 0). The vertical dash-dotted line marks the value $j_0 = j_{th,\sigma_{n2}=\infty}$. The horizontal dash-dotted line marks the saturation value of τ_{21}^{max} at $j_0 \to \infty$ given by eq. (4.38). (Reprinted with permission from Fig. 4 of ref. [A1], Copyright (2013) by AIP.)

section σ_{n2} of capture from the OCL into the QD excited-state and the excited-to-ground-state relaxation time τ_{21} are fixed while the capture cross-section σ_{n1} into the ground state is different for different curves. As seen from the figure, with reducing σ_{n1} (i.e., making slower the capture to the ground state), $\omega_{-3\,dB}$ decreases.

Making slower the excited-state-mediated capture into the lasing ground-state (i.e., decreasing σ_{n2} and/or increasing τ_{21}) also reduces the modulation bandwidth. However, only when σ_{n1} is small, the effect of σ_{n2} and τ_{21} on $\omega_{-3\,dB}$ becomes stronger. The modulation bandwidth is particularly strongly affected by σ_{n2} and τ_{21} when there is no direct capture from the OCL into the QD ground-state, i.e., σ_{n1} = 0 [Fig. 4.3(b, c) and Figs. 4.4–4.6]. In Fig. 3(b), τ_{21}

is fixed while σ_{n2} is different for different curves. In Fig. 4.3(c), σ_{n2} is fixed while τ_{21} is different for different curves.

As seen from Fig. 4.3(b, c) and Fig. 4.4, in such a case of no direct capture, the modulation bandwidth drops rapidly with decreasing capture cross-section σ_{n2} or increasing relaxation time τ_{21}. Even at a short relaxation time of 0.1 ps, the maximum modulation bandwidth (4 GHz) is four times lower than that at instantaneous relaxation (16 GHz at $\tau_{21} = 0$) – see Fig. 4.3(c) and Fig. 4.6.

It is seen from Fig. 4.4(b) that there exist the minimum tolerable value $\sigma_{n2}^{\min}$ of σ_{n2} and the maximum tolerable value $\tau_{21}^{\max}$ of τ_{21} at which $\omega_{-3\,\mathrm{dB}}$ becomes zero. The point is that, for lasing to occur and for direct modulation of laser output, the dc component j_0 of the pump current density should be higher than the threshold current density j_{th}. With decreasing σ_{n2} or increasing τ_{21}, the threshold current density increases. It is at $\sigma_{n2} = \sigma_{n2}^{\min}$ or $\tau_{21} = \tau_{21}^{\max}$ when j_{th} becomes equal to j_0. The following expression is obtained for $\sigma_{n2}^{\min}$ from the condition $j_{th} = j_0$:

$$\sigma_{n2}^{\min} = \frac{1}{v_n} \frac{1}{1 - f_{n2,\,0}^{th}} \frac{j_{th}^{QD}}{eN_S} \sqrt{ebB}\, \frac{\sqrt{j_0 - j_{th}^{QD}} + \sqrt{j_{th,\,\sigma_{n2}=\infty} - j_{th}^{QD}}}{j_0 - j_{th,\,\sigma_{n2}=\infty}}, \tag{4.35}$$

where $f_{n2,\,0}^{th}$ is the excited-state level occupancy at the lasing threshold [given by (4.26)]. j_{th}^{QD} is the component of j_{th} associated with the spontaneous recombination in QDs, and $j_{th,\,\sigma_{n2}=\infty}$ is the threshold current density for the case of instantaneous capture into the excited state ($\sigma_{n2} = \infty$). The expressions for them are

$$j_{th}^{QD} = eN_S \frac{f_{n1,\,0}^2}{\tau_{QD1}} + eN_S \frac{(f_{n2,\,0}^{th})^2}{\tau_{QD2}}, \tag{4.36}$$

$$j_{th,\,\sigma_{n2}=\infty} = ebB\left(n_2 \frac{f_{n2,\,0}^{th}}{1 - f_{n2,\,0}^{th}}\right)^2 + eN_S \frac{(f_{n2,\,0}^{th})^2}{\tau_{QD2}} + eN_S \frac{f_{n1,\,0}^2}{\tau_{QD1}}. \tag{4.37}$$

The same condition $j_{th} = j_0$ should be used to calculate $\tau_{21}^{\max}$ but no closed-form expression can be derived for $\tau_{21}^{\max}$.

As seen from (4.35) and Fig. 4.5, $\sigma_{n2}^{\min}$ depends strongly on j_0. At $j_0 \to j_{th,\,\sigma_{n2}=\infty}$ (the vertical dash-dotted line in the figure), $\sigma_{n2}^{\min} \to \infty$. The higher is j_0, the smaller is $\sigma_{n2}^{\min}$.

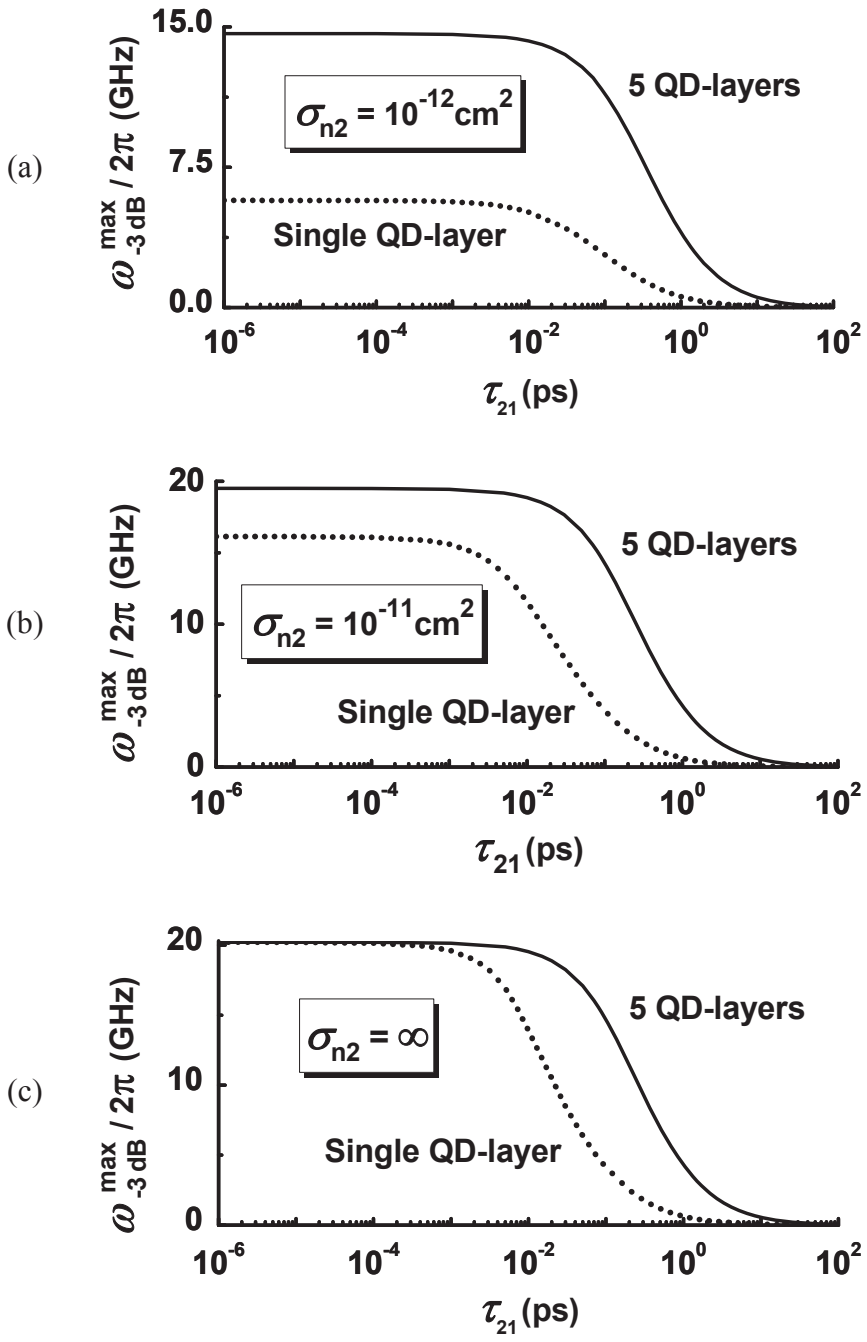

Fig. 4.6. Maximum modulation bandwidth $\omega_{-3\,dB}^{max} / 2\pi$ (maximum of the dependence of $\omega_{-3\,dB}/2\pi$ on j_0 – see Fig. 4.3) vs. excited-to-ground-state relaxation time for a single- and a 5-QD-layer structures at different values of the capture cross-section σ_{n2} into the QD excited-state: (a) $\sigma_{n2} = 10^{-12}cm^2$, (b) $\sigma_{n2} = 10^{-11}cm^2$, and (c) $\sigma_{n2} = \infty$. For both structures, $L = 0.1139$ cm and no direct capture into the QD ground-state is involved ($\sigma_{n1} = 0$). (Reprinted with permission from Fig. 5 of ref. [A1], Copyright (2013) by AIP.)

The longest relaxation time $\tau_{21}^{\max}$ also depends strongly on j_0 (Fig. 4.5). $\tau_{21}^{\max}$ is zero at $j_0 = j_{\text{th},\,\tau_{21}=0}$ (the difference between $j_{\text{th},\,\tau_{21}=0}$ and $j_{\text{th},\,\sigma_{\text{n2}}=\infty}$ is very small and cannot be seen in Fig. 4.5). The expression for $j_{\text{th},\,\tau_{21}=0}$ can be obtained using $\tau_{21} = 0$ in (4.22). $\tau_{21}^{\max}$ increases with j_0 and saturates at the value (the horizontal dash-dotted line)

$$\tau_{21}^{\max}\Big|_{j_0\to\infty} = \frac{1-f_{\text{n1,0}}}{f_{\text{n1,0}}^2}\,\tau_{\text{QD1}}. \tag{4.38}$$

Eq. (4.38) is obtained from (A3) using $f_{\text{n2,0}}^{\text{th}} = 1$ there.

It is clear from the above discussion, that, if the abscissa and the ordinate are interchanged in Fig. 4.5, we will obtain the threshold current density j_{th} against σ_{n2} and τ_{21}.

For the case of no direct capture into the QD ground-state, Fig. 4.6 shows the dependence of the maximum modulation bandwidth $\omega_{-3\text{ dB}}^{\max}$ on τ_{21}. To obtain this dependence, we calculated the modulation bandwidth $\omega_{-3\text{ dB}}$ as a function of the dc component j_0 of the injection current density at different values of τ_{21} [Fig. 4.3(c)]; we then determined for each τ_{21} the corresponding maximum value $\omega_{-3\text{ dB}}^{\max}$ [marked by the symbol "x" in Fig. 4.3(c)] of the function $\omega_{-3\text{ dB}}(j_0)$. For comparison, single- and 5-QD-layer structures are considered and three different values of σ_{n2} are used in the figure. As seen from the figure, with reducing τ_{21}, $\omega_{-3\text{ dB}}^{\max}$ increases and saturates. The saturation value of $\omega_{-3\text{ dB}}^{\max}$ corresponds to the case of instantaneous excited-to-ground-state relaxation in QDs (τ_{21} = 0). At a finite value of σ_{n2} [10^{-12} and $10^{-11}\,\text{cm}^2$ in (a) and (b), respectively], i.e., at noninstantaneous capture from the OCL into the QD excited-state, the saturation value in a 5-layer structure is higher than that in a single-layer structure [14.6 vs. 5.7 GHz in (a), and 19.5 vs. 16.1 GHz in (b)]. The difference in $\omega_{-3\text{ dB}}^{\max}$ between a 5- and a single-layer-structure becomes larger at noninstantaneous relaxation – it is considerable [9.4 vs. 1.9 GHz in (a), 11.2 vs. 2.4 GHz in (b), and 11.4 vs. 2.5 GHz in (c)] already at a short relaxation time τ_{21} = 0.2 ps. The physical mechanism behind the enhancement of $\omega_{-3\text{ dB}}^{\max}$ in a multi-layer structure is similar to the case of single-level QDs [A2-A5] – with increasing N_{s} (i.e., number of QD layers and/or surface density of QDs in a single-layer), the carrier exchange [either direct or

excited-state-mediated – see the second through fifth terms in the right-hand side of (4.2)] between the OCL and the lasing ground state in QDs becomes faster.

In going from (a) to (b) and then to (c) in Fig. 4.6, i.e., with increasing σ_{n2}, the saturation values of $\omega_{-3\,dB}^{max}$ in 5- and single-layer structures increase and become closer to each other. At $\sigma_{n2} = \infty$ [Fig. 4.6(c)], i.e., at instantaneous capture from the OCL into the QD excited-state, the saturation values in 5- and single-layer structures become the same (20.2 GHz).

4.4. Conclusion

We have considered direct and excited-state-mediated capture of carriers from the OCL into the lasing ground state in QDs and calculated the modulation response of a QD laser. We have shown that, when only indirect capture is involved, the delays in the carrier capture from the OCL into the QD excited-state and in excited-to-ground-state relaxation strongly limit the modulation bandwidth $\omega_{-3\,dB}$ of the laser — at the minimum tolerable capture cross-section or longest relaxation time, $\omega_{-3\,dB}$ becomes zero. When a fast direct capture is also involved, the modulation bandwidth is considerably higher and only slightly affected by the presence of excited states. The effect of excited states is also less significant and $\omega_{-3\,dB}$ is higher in multi-QD-layer structures as compared to a single-layer structure.

Appendix I

Excited-state level occupancy in a QD at the lasing threshold

Only one root of the quadratic equation (4.21) is real, positive, and smaller than unity. Let us analyze the solution of equation (4.21).

i) $\sigma_{n1} = 0$, i.e., there is no direct carrier-capture into the QD ground-state

Eq. (4.21) becomes

$$\left(\frac{f_{n1,\,0}}{1-f_{n1,\,0}}\frac{1}{\tau_{12}}+\frac{1}{\tau_{21}}\right)(f_{n2,\,0}^{th})^2-\left(\frac{f_{n1,\,0}^2}{1-f_{n1,0}}\frac{1}{\tau_{QD1}}+\frac{2f_{n1,\,0}}{1-f_{n1,0}}\frac{1}{\tau_{12}}+\frac{1}{\tau_{21}}\right)f_{n2,0}^{th}$$
$$+\left(\frac{f_{n1,\,0}^2}{1-f_{n1,\,0}}\frac{1}{\tau_{QD1}}+\frac{f_{n1,\,0}}{1-f_{n1,\,0}}\frac{1}{\tau_{12}}\right)=0. \tag{A1}$$

The roots are

$$f_{n2,\,0}^{th}=1, \tag{A2}$$

and

$$f_{n2,\,0}^{th}=\frac{f_{n1,\,0}^2\dfrac{\tau_{12}}{\tau_{QD1}}+f_{n1,\,0}}{\left(1-f_{n1,\,0}\right)\dfrac{\tau_{12}}{\tau_{21}}+f_{n1,\,0}}. \tag{A3}$$

The physically meaningful root is given by (A3) since it is less than unity. Using $f_{n2,0}^{th}=1$ in (A3), eq. (4.38) is obtained. Depending on the value of τ_{12} [i.e., the energy difference between the excited- and ground-state – see eq. (4.1)], $f_{n2,\,0}^{th}$ could be larger, smaller than, or equal to $f_{n1,\,0}$ [given by (4.12)]. Let us denote τ_{12}^{equal} as the transition time at which

$$f_{n2,\,0}^{th}\left(\tau_{12}^{equal}\right)=f_{n1,\,0}. \tag{A4}$$

Using (A3) for $f_{n2,\,0}^{th}$ and (4.12) for $f_{n1,\,0}$, the following expression is obtained for τ_{12}^{equal}:

$$\tau_{12}^{\text{equal}} = \frac{\tau_{21}}{1 - \dfrac{\tau_{21}}{\tau_{\text{QD1}}} \dfrac{f_{\text{n1, 0}}}{1 - f_{\text{n1, 0}}}} \,. \tag{A5}$$

Since typically τ_{21} is in the range of ps while τ_{QD1} is in the range of ns, then $\tau_{21} / \tau_{\text{QD1}} << 1$ in (A5) and hence, $\tau_{12}^{\text{equal}} \approx \tau_{21}$ (assuming that $f_{\text{n1, 0}}$ is not close to unity).

If we use the detailed balance condition at the equilibrium,

$$\frac{f_{\text{n2, 0}}^{\text{eq}} \left(1 - f_{\text{n1, 0}}^{\text{eq}}\right)}{\tau_{21}} = \frac{f_{\text{n1, 0}}^{\text{eq}} \left(1 - f_{\text{n2, 0}}^{\text{eq}}\right)}{\tau_{12}}, \tag{A6}$$

where $f_{\text{n1, 0}}^{\text{eq}}$ and $f_{\text{n2, 0}}^{\text{eq}}$ are given by the Fermi-Dirac distribution function, we will obtain the relationship (4.1) between τ_{21} and τ_{12}.

The energy difference between the excited- and ground-state is

$$\Delta = E_{\text{n1}} - E_{\text{n2}} = T \ln\left(\frac{\tau_{12}}{\tau_{21}}\right), \tag{A7}$$

where E_{n1} and E_{n2} are the energies of carrier excitation from the QD ground- and excited-state to the OCL (see Fig. 4.1), and T is the temperature (in units of energy). In order to have $f_{\text{n2, 0}}^{\text{th}} = f_{\text{n1, 0}}$ [see (A4) and (A5)], this energy difference should be

$$\Delta^{\text{equal}} = T \ln\left(\frac{1}{1 - \dfrac{\tau_{21}}{\tau_{\text{QD1}}} \dfrac{f_{\text{n1, 0}}}{1 - f_{\text{n1, 0}}}}\right). \tag{A8}$$

When $\tau_{12} > \tau_{12}^{\text{equal}}$, i.e., $\Delta > \Delta^{\text{equal}}$, then $f_{\text{n2, 0}}^{\text{th}} < f_{\text{n1, 0}}$. At very large τ_{12}, eq. (A3) simplifies as follows:

$$f_{\text{n2, 0}}^{\text{th}} \approx \frac{\tau_{21}}{\tau_{\text{QD1}}} \frac{f_{\text{n1, 0}}^2}{1 - f_{\text{n1, 0}}} \,. \tag{A9}$$

When $\tau_{12} < \tau_{12}^{\text{equal}}$, i.e., $\Delta < \Delta^{\text{equal}}$, then $f_{\text{n2, 0}}^{\text{th}} > f_{\text{n1, 0}}$. However, τ_{12} cannot be smaller than τ_{21} (since Δ is positive) – the smallest value of τ_{12} is τ_{21}, which corresponds to the case of $\Delta = 0$. In this case,

$$f_{\mathrm{n2,\,0}}^{\mathrm{th}}\Big|_{\tau_{12}=\tau_{21}} = f_{\mathrm{n1,\,0}} + \frac{\tau_{12}}{\tau_{\mathrm{QD1}}} f_{\mathrm{n1,\,0}}^{2}. \tag{A10}$$

This expression is exactly the same as that in [20].

ii) The coefficient at the quadratic term in (4.21) is zero, i.e.,

$$\left(\frac{f_{\mathrm{n1,\,0}}}{1-f_{\mathrm{n1,\,0}}}\frac{1}{\tau_{12}} + \frac{1}{\tau_{21}}\right)\sigma_{\mathrm{n2}} = \frac{1}{\tau_{\mathrm{QD2}}}\sigma_{\mathrm{n1}}. \tag{A11}$$

In such a case, the quadratic equation (4.21) reduces to a linear equation and the solution for $f_{\mathrm{n2,\,0}}^{\mathrm{th}}$ is

$$f_{\mathrm{n2,0}}^{\mathrm{th}} = \frac{1}{1 + \dfrac{\sigma_{\mathrm{n1}}\sigma_{\mathrm{n2}}\mathrm{v_n}n_2 + \sigma_{\mathrm{n1}}\left(\dfrac{1}{\tau_{\mathrm{QD2}}} + \dfrac{1-f_{\mathrm{n1,0}}}{\tau_{21}}\right)}{\sigma_{\mathrm{n1}}\sigma_{\mathrm{n2}}\mathrm{v_n}n_1\dfrac{f_{\mathrm{n1,0}}}{1-f_{\mathrm{n1,0}}} + \sigma_{\mathrm{n1}}\dfrac{f_{\mathrm{n1,0}}}{\tau_{12}} + \sigma_{\mathrm{n2}}\dfrac{f_{\mathrm{n1,0}}}{1-f_{\mathrm{n1,0}}}\left(\dfrac{f_{\mathrm{n1,0}}}{\tau_{\mathrm{QD1}}} + \dfrac{1}{\tau_{12}}\right)}}. \tag{A12}$$

Appendix II

Steady-state characteristics at high injection current density j_0

As seen from Fig. 4.2, $f_{n2,0}$ increases with j_0 and approaches unity as j_0 goes to infinity. At very high j_0,

$$f_{n2,0} \approx 1 - \frac{n_2 + \frac{1}{\sigma_{n2} v_n}\left(\frac{1-f_{n1,0}}{\tau_{21}} + \frac{1}{\tau_{QD2}}\right)}{\sqrt{\frac{j_0}{ebB}}}. \tag{A13}$$

Using (A13) in (4.18), we obtain the following expression for $n_{OCL,0}$ at high j_0:

$$n_{OCL,0} \approx \sqrt{\frac{j_0}{ebB}}. \tag{A14}$$

Using (A13) in (4.15), we obtain for $n_{ph1,0}$

$$n_{ph,0} \approx \tau_{ph} \sigma_{n1} v_n \frac{N_S}{b}(1 - f_{n1,0})\sqrt{\frac{j_0}{ebB}}. \tag{A15}$$

As seen from (A15), at very high j_0, the emitted photon density is controlled by the process of carrier capture to the QD ground-state.

With (4.24) and (A15), the stimulated recombination current density becomes

$$j_{stim} \approx \sigma_{n1} v_n N_S (1 - f_{n1,0})\sqrt{e\frac{j_0}{bB}}. \tag{A16}$$

Finally, the output optical power [see (4.25)] is

$$P_0 \approx \hbar\omega_0 \, S N_S \sigma_{n1} v_n (1 - f_{n1,0})\sqrt{\frac{j_0}{ebB}}. \tag{A17}$$

Appendix III

Relaxation oscillations and modulation response in a QD laser in the presence of excited states in QDs: Small-signal analysis

The rate equations for free carriers in the OCL, carriers confined in the QD excited-state, those confined in the QD ground-state, and photons are given by (4.2)–(4.5).

Similarly to the case of three rate equations (Appendix I in Chapter 2), we linearize eqs. (4.2)–(4.5), i.e., consider the injection current density in the form

$$j = j_0 + j_{\mathrm{m}}(t), \tag{A18}$$

and, correspondingly, the solutions of (4.2)–(4.5) in the form

$$n_{\mathrm{OCL}} = n_{\mathrm{OCL},0} + \nu(t), \tag{A19}$$

$$f_{\mathrm{n2}} = f_{\mathrm{n2},0} + \varphi_2(t), \tag{A20}$$

$$f_{\mathrm{n1}} = f_{\mathrm{n1},0} + \varphi_1(t), \tag{A21}$$

$$n_{\mathrm{ph}} = n_{\mathrm{ph},0} + s(t), \tag{A22}$$

where $j_{\mathrm{m}}(t)$, $\nu(t)$, $\varphi_2(t)$, $\varphi_1(t)$, and $s(t)$ are small quantities compared to j_0, $n_{\mathrm{OCL},0}$, $f_{\mathrm{n2},0}$, $f_{\mathrm{n1},0}$, and $n_{\mathrm{ph},0}$, respectively, i.e.,

$$j_{\mathrm{m}}(t) << j_0, \tag{A23}$$

$$\nu(t) << n_{\mathrm{OCL},0}, \tag{A24}$$

$$\varphi_2(t) << f_{\mathrm{n2},0}, \tag{A25}$$

$$\varphi_1(t) << f_{\mathrm{n1},0}, \tag{A26}$$

$$s(t) << n_{\mathrm{ph},0}, \tag{A27}$$

where j_0 is the dc component of the injection current density, and $n_{\mathrm{OCL},0}$, $f_{\mathrm{n2},0}$, $f_{\mathrm{n1},0}$, and $n_{\mathrm{ph},0}$ are the solutions of the rate equations at the steady-state, i.e., at $j = j_0$. $n_{\mathrm{OCL},0}$, $f_{\mathrm{n1},0}$, and $n_{\mathrm{ph},0}$ are given by (4.14), (4.12), and (4.15), respectively. The expression for $f_{\mathrm{n2},0}$ is obtained using (4.14) and (4.15) in (4.17), and it presents a quartic equation in $f_{\mathrm{n2},0}$. To ensure lasing, the following condition should hold for $j_{\mathrm{m}}(t)$:

$$j_{\mathrm{m}}(t) << j_0 - j_{\mathrm{th}}\,, \tag{A28}$$

where j_{th} is the threshold current density given by (4.22).

Using (A18)–(A22) in (4.2)–(4.5) and dropping the quadratic terms in the small quantities $\nu(t)$, $\varphi_2(t)$, $\varphi_1(t)$, and $s(t)$, we obtain the following set of linearized differential equations:

$$\begin{aligned}\frac{\partial \nu(t)}{\partial t} = \frac{j_{\mathrm{m}}(t)}{eb} - \left[\sigma_{\mathrm{n}2}\mathrm{v}_{\mathrm{n}}\frac{N_{\mathrm{S}}}{b}(1-f_{\mathrm{n}2,0}) + \sigma_{\mathrm{n}1}\mathrm{v}_{\mathrm{n}}\frac{N_{\mathrm{S}}}{b}(1-f_{\mathrm{n}1,0}) + 2Bn_{\mathrm{OCL},0}\right]\nu(t) \\ + \sigma_{\mathrm{n}2}\mathrm{v}_{\mathrm{n}}\frac{N_{\mathrm{S}}}{b}(n_{\mathrm{OCL},0}+n_2)\varphi_2(t) + \sigma_{\mathrm{n}1}\mathrm{v}_{\mathrm{n}}\frac{N_{\mathrm{S}}}{b}(n_{\mathrm{OCL},0}+n_1)\varphi_1(t),\end{aligned} \tag{A29}$$

$$\begin{aligned}2\frac{N_{\mathrm{S}}}{b}\frac{\partial \varphi_2(t)}{\partial t} = \sigma_{\mathrm{n}2}\mathrm{v}_{\mathrm{n}}\frac{N_{\mathrm{S}}}{b}(1-f_{\mathrm{n}2,0})\nu(t) \\ - \left[\sigma_{\mathrm{n}2}\mathrm{v}_{\mathrm{n}}\frac{N_{\mathrm{S}}}{b}(n_{\mathrm{OCL},0}+n_2) + \frac{N_{\mathrm{S}}}{b}\frac{f_{\mathrm{n}1,0}}{\tau_{12}}\right. \\ \left. + \frac{N_{\mathrm{S}}}{b}\frac{1-f_{\mathrm{n}1,0}}{\tau_{21}} + 2\frac{N_{\mathrm{S}}}{b}\frac{f_{\mathrm{n}2,0}}{\tau_{\mathrm{QD2}}}\right]\varphi_2(t) \\ + \left(\frac{N_{\mathrm{S}}}{b}\frac{1-f_{\mathrm{n}2,0}}{\tau_{12}} + \frac{N_{\mathrm{S}}}{b}\frac{f_{\mathrm{n}2,0}}{\tau_{21}}\right)\varphi_1(t),\end{aligned} \tag{A30}$$

$$\begin{aligned}2\frac{N_{\mathrm{S}}}{b}\frac{\partial \varphi_1(t)}{\partial t} = \sigma_{\mathrm{n}1}\mathrm{v}_{\mathrm{n}}\frac{N_{\mathrm{S}}}{b}(1-f_{\mathrm{n}1,0})\nu(t) + \left(\frac{N_{\mathrm{S}}}{b}\frac{1-f_{\mathrm{n}1,0}}{\tau_{21}} + \frac{N_{\mathrm{S}}}{b}\frac{f_{\mathrm{n}1,0}}{\tau_{12}}\right)\varphi_2(t) \\ - \left[\sigma_{\mathrm{n}1}\mathrm{v}_{\mathrm{n}}\frac{N_{\mathrm{S}}}{b}(n_{\mathrm{OCL},0}+n_1) + \frac{N_{\mathrm{S}}}{b}\frac{f_{\mathrm{n}2,0}}{\tau_{21}}\right. \\ \left. + \frac{N_{\mathrm{S}}}{b}\frac{1-f_{\mathrm{n}2,0}}{\tau_{12}} + 2\frac{N_{\mathrm{S}}}{b}\frac{f_{\mathrm{n}1,0}}{\tau_{\mathrm{QD1}}} + 2\mathrm{v}_{\mathrm{g}}g_1^{\max}n_{\mathrm{ph},0}\right]\varphi_1(t) \\ - \frac{1}{\tau_{\mathrm{ph}}}s(t),\end{aligned} \tag{A31}$$

$$\frac{\partial s(t)}{\partial t} = 2\mathrm{v}_{\mathrm{g}}g_1^{\max}n_{\mathrm{ph},0}\,\varphi_1(t)\,, \tag{A32}$$

where the photon lifetime in the cavity τ_{ph} is given by (4.13).

For relaxation oscillations, we put

$$j_{\mathrm{m}} = 0 \tag{A33}$$

and look for the solutions of the set of linear first-order differential equations (A29)–(A32) in the form

$$\nu(t) = (\delta n_{\mathrm{OCL-m}})e^{-ht}, \tag{A34}$$

$$\varphi_2(t) = (\delta f_{\mathrm{n2-m}})e^{-ht}, \tag{A35}$$

$$\varphi_1(t) = (\delta f_{\mathrm{n1-m}})e^{-ht}, \tag{A36}$$

$$s(t) = (\delta n_{\mathrm{ph-m}})e^{-ht}. \tag{A37}$$

Using (A34)–(A37) in (A29)–(A32), we obtain

$$\begin{bmatrix} A_{11}(h) & A_{12} & A_{13} & 0 \\ A_{21} & A_{22}(h) & A_{23} & 0 \\ A_{31} & A_{32} & A_{33}(h) & A_{34} \\ 0 & 0 & A_{43} & A_{44}(h) \end{bmatrix} \begin{pmatrix} \delta n_{\mathrm{OCL-m}} \\ \delta f_{\mathrm{n2-m}} \\ \delta f_{\mathrm{n1-m}} \\ \delta n_{\mathrm{ph-m}} \end{pmatrix} = 0, \tag{A38}$$

where

$$A_{11}(h) = -h + \sigma_{\mathrm{n2}}\mathrm{v}_{\mathrm{n}}\frac{N_{\mathrm{S}}}{b}(1-f_{\mathrm{n2},0}) + \sigma_{\mathrm{n1}}\mathrm{v}_{\mathrm{n}}\frac{N_{\mathrm{S}}}{b}(1-f_{\mathrm{n1},0}) + 2Bn_{\mathrm{OCL},0}, \tag{A39}$$

$$A_{12} = -\sigma_{\mathrm{n2}}\mathrm{v}_{\mathrm{n}}\frac{N_{\mathrm{S}}}{b}(n_{\mathrm{OCL},0} + n_2), \tag{A40}$$

$$A_{13} = -\sigma_{\mathrm{n1}}\mathrm{v}_{\mathrm{n}}\frac{N_{\mathrm{S}}}{b}(n_{\mathrm{OCL},0} + n_1), \tag{A41}$$

$$A_{21} = -\sigma_{\mathrm{n2}}\mathrm{v}_{\mathrm{n}}\frac{N_{\mathrm{S}}}{b}(1-f_{\mathrm{n2},0}), \tag{A42}$$

$$A_{22}(h) = -2\frac{N_{\mathrm{S}}}{b}h + \frac{N_{\mathrm{S}}}{b}\left[\sigma_{\mathrm{n2}}\mathrm{v}_{\mathrm{n}}(n_{\mathrm{OCL},0} + n_2) + \frac{f_{\mathrm{n1},0}}{\tau_{12}} + \frac{1-f_{\mathrm{n1},0}}{\tau_{21}} + 2\frac{f_{\mathrm{n2},0}}{\tau_{\mathrm{QD2}}}\right], \tag{A43}$$

$$A_{23} = -\frac{N_{\mathrm{S}}}{b}\frac{1-f_{\mathrm{n2},0}}{\tau_{12}} - \frac{N_{\mathrm{S}}}{b}\frac{f_{\mathrm{n2},0}}{\tau_{21}}, \tag{A44}$$

$$A_{31} = -\sigma_{\mathrm{n1}}\mathrm{v}_{\mathrm{n}}\frac{N_{\mathrm{S}}}{b}(1-f_{\mathrm{n1},0}), \tag{A45}$$

$$A_{32} = -\frac{N_{\mathrm{S}}}{b}\frac{1-f_{\mathrm{n1},0}}{\tau_{21}} - \frac{N_{\mathrm{S}}}{b}\frac{f_{\mathrm{n1},0}}{\tau_{12}}, \tag{A46}$$

$$A_{33}(h) = -2\frac{N_S}{b}h + \frac{N_S}{b}\left[\sigma_{n1}v_n(n_{OCL,0}+n_1) + \frac{f_{n2,0}}{\tau_{21}} + \frac{1-f_{n2,0}}{\tau_{12}} + 2\frac{f_{n1,0}}{\tau_{QD1}} + 2\frac{b}{N_S}v_g g_1^{max} n_{ph,0}\right], \tag{A47}$$

$$A_{34} = \frac{1}{\tau_{ph}}, \tag{A48}$$

$$A_{43} = -2v_g g_1^{max} n_{ph,0}, \tag{A49}$$

$$A_{44}(h) = -h. \tag{A50}$$

A set (A38) of linear equations is homogeneous. The condition for the existence of non-zero solutions of (A38) is

$$\begin{vmatrix} A_{11} & A_{12} & A_{13} & 0 \\ A_{21} & A_{22} & A_{23} & 0 \\ A_{31} & A_{32} & A_{33} & A_{34} \\ 0 & 0 & A_{43} & A_{44} \end{vmatrix} = A_{12}A_{21}A_{34}A_{43} - A_{11}A_{22}A_{34}A_{43} + A_{11}A_{22}A_{33}A_{44} - A_{11}A_{23}A_{32}A_{44} - A_{12}A_{21}A_{33}A_{44} + A_{12}A_{23}A_{31}A_{44} + A_{13}A_{21}A_{32}A_{44} - A_{13}A_{22}A_{31}A_{44} = 0 \tag{A51}$$

Eq. (A51) is a quartic equation in h,

$$\left(2\frac{N_S}{b}\right)^2\left(h^4 - A_3h^3 + A_2h^2 - A_1h + A_0\right) = 0, \tag{A52}$$

where the coefficients A_0, A_1, A_2, and A_3 are given as follows:

$$A_0 = \frac{b}{N_S}v_g g_1^{max}\frac{n_{ph,0}}{\tau_{ph}}\left\{\sigma_{n2}v_n\frac{N_S}{b}(1-f_{n2,0})\left(\frac{1}{2}\frac{f_{n1,0}}{\tau_{12}} + \frac{1}{2}\frac{1-f_{n1,0}}{\tau_{21}} + \frac{f_{n2,0}}{\tau_{QD2}}\right) + \frac{1}{2}\left[\sigma_{n1}v_n\frac{N_S}{b}(1-f_{n1,0}) + 2Bn_{OCL,0}\right] \times \left[\sigma_{n2}v_n(n_{OCL,0}+n_2) + \frac{f_{n1,0}}{\tau_{12}} + \frac{1-f_{n1,0}}{\tau_{21}} + 2\frac{f_{n2,0}}{\tau_{QD2}}\right]\right\}, \tag{A53}$$

$$
\begin{aligned}
A_1 = {} & \frac{1}{2}\sigma_{n2}\mathrm{v}_n\frac{N_S}{b}(1-f_{n2,0})\left(\frac{f_{n1,0}}{\tau_{12}}+\frac{1-f_{n1,0}}{\tau_{21}}\right)\left(\frac{f_{n1,0}}{\tau_{QD1}}+\frac{b}{N_S}\mathrm{v}_g g_1^{\max} n_{ph,0}\right) \\
& +\frac{1}{2}\sigma_{n1}\mathrm{v}_n\frac{N_S}{b}(1-f_{n1,0})\left(\frac{f_{n1,0}}{\tau_{12}}+\frac{1-f_{n1,0}}{\tau_{21}}\right)\left(\frac{f_{n1,0}}{\tau_{QD1}}+\frac{b}{N_S}\mathrm{v}_g g_1^{\max} n_{ph,0}\right) \\
& +Bn_{OCL,0}\left(\frac{f_{n1,0}}{\tau_{12}}+\frac{1-f_{n1,0}}{\tau_{21}}\right)\left[\frac{1}{2}\sigma_{n1}\mathrm{v}_n(n_{OCL,0}+n_1)+\frac{f_{n1,0}}{\tau_{QD1}}+\frac{b}{N_S}\mathrm{v}_g g_1^{\max} n_{ph,0}\right] \\
& +\frac{1}{2}\sigma_{n1}\mathrm{v}_n\frac{N_S}{b}(1-f_{n1,0})[\sigma_{n2}\mathrm{v}_n(n_{OCL,0}+n_2)]\left(\frac{f_{n1,0}}{\tau_{QD1}}+\frac{b}{N_S}\mathrm{v}_g g_1^{\max} n_{ph,0}\right) \\
& +\sigma_{n1}\mathrm{v}_n\frac{N_S}{b}(1-f_{n1,0})\frac{f_{n2,0}}{\tau_{QD2}}\left(\frac{1}{2}\frac{f_{n2,0}}{\tau_{21}}+\frac{1}{2}\frac{1-f_{n2,0}}{\tau_{12}}+\frac{f_{n1,0}}{\tau_{QD1}}+\frac{b}{N_S}\mathrm{v}_g g_1^{\max} n_{ph,0}\right) \\
& +\frac{1}{2}\sigma_{n2}\mathrm{v}_n\frac{N_S}{b}(1-f_{n2,0})\frac{f_{n2,0}}{\tau_{QD2}} \\
& \quad\times\left[\sigma_{n1}\mathrm{v}_n(n_{OCL,0}+n_1)+\frac{f_{n2,0}}{\tau_{21}}+\frac{1-f_{n2,0}}{\tau_{12}}+\frac{2f_{n1,0}}{\tau_{QD1}}+2\frac{b}{N_S}\mathrm{v}_g g_1^{\max} n_{ph,0}\right] \\
& +\frac{1}{2}Bn_{OCL,0}\left[\sigma_{n2}\mathrm{v}_n(n_{OCL,0}+n_2)+2\frac{f_{n2,0}}{\tau_{QD2}}\right] \\
& \quad\times\left[\sigma_{n1}\mathrm{v}_n(n_{OCL,0}+n_1)+\frac{f_{n2,0}}{\tau_{21}}+\frac{1-f_{n2,0}}{\tau_{12}}+\frac{2f_{n1,0}}{\tau_{QD1}}+2\frac{b}{N_S}\mathrm{v}_g g_1^{\max} n_{ph,0}\right] \\
& +\frac{b}{N_S}\mathrm{v}_g g_1^{\max}\frac{n_{ph,0}}{\tau_{ph}}\left[\sigma_{n2}\mathrm{v}_n\frac{N_S}{b}(1-f_{n2,0})+\sigma_{n1}\mathrm{v}_n\frac{N_S}{b}(1-f_{n1,0})+2Bn_{OCL,0}\right] \\
& +\frac{1}{2}\frac{b}{N_S}\mathrm{v}_g g_1^{\max}\frac{n_{ph,0}}{\tau_{ph}}\left[\sigma_{n2}\mathrm{v}_n(n_{OCL,0}+n_2)+\frac{f_{n1,0}}{\tau_{12}}+\frac{1-f_{n1,0}}{\tau_{21}}+2\frac{f_{n2,0}}{\tau_{QD2}}\right],
\end{aligned}
\tag{A54}
$$

$$
\begin{aligned}
A_2 = {} & \frac{b}{N_\mathrm{S}} \mathrm{v_g} g_1^{\max} \frac{n_{\mathrm{ph},0}}{\tau_\mathrm{ph}} + \frac{1}{2}\sigma_{\mathrm{n}2}\mathrm{v_n}\frac{N_\mathrm{S}}{b}(1-f_{\mathrm{n}2,0})\left(\frac{f_{\mathrm{n}1,0}}{\tau_{12}} + \frac{1-f_{\mathrm{n}1,0}}{\tau_{21}} + 2\frac{f_{\mathrm{n}2,0}}{\tau_{\mathrm{QD}2}}\right) \\
& + \frac{1}{2}\left[\sigma_{\mathrm{n}1}\mathrm{v_n}\frac{N_\mathrm{S}}{b}(1-f_{\mathrm{n}1,0}) + 2Bn_{\mathrm{OCL},0}\right] \\
& \times\left[\sigma_{\mathrm{n}2}\mathrm{v_n}(n_{\mathrm{OCL},0}+n_2) + \frac{f_{\mathrm{n}1,0}}{\tau_{12}} + \frac{1-f_{\mathrm{n}1,0}}{\tau_{21}} + 2\frac{f_{\mathrm{n}2,0}}{\tau_{\mathrm{QD}2}}\right] \\
& + \frac{1}{2}\sigma_{\mathrm{n}1}\mathrm{v_n}\frac{N_\mathrm{S}}{b}(1-f_{\mathrm{n}1,0})\left(\frac{f_{\mathrm{n}2,0}}{\tau_{21}} + \frac{1-f_{\mathrm{n}2,0}}{\tau_{12}} + 2\frac{f_{\mathrm{n}1,0}}{\tau_{\mathrm{QD}1}} + 2\frac{b}{N_\mathrm{S}}\mathrm{v_g} g_1^{\max} n_{\mathrm{ph},0}\right) \\
& + \frac{1}{4}\left(\frac{f_{\mathrm{n}1,0}}{\tau_{12}} + \frac{1-f_{\mathrm{n}1,0}}{\tau_{21}}\right)\left[\sigma_{\mathrm{n}1}\mathrm{v_n}(n_{\mathrm{OCL},0}+n_1) + 2\frac{f_{\mathrm{n}1,0}}{\tau_{\mathrm{QD}1}} + 2\frac{b}{N_\mathrm{S}}\mathrm{v_g} g_1^{\max} n_{\mathrm{ph},0}\right] \\
& + \frac{1}{2}\left[\sigma_{\mathrm{n}2}\mathrm{v_n}\frac{N_\mathrm{S}}{b}(1-f_{\mathrm{n}2,0}) + 2Bn_{\mathrm{OCL},0} + \frac{1}{2}\sigma_{\mathrm{n}2}\mathrm{v_n}(n_{\mathrm{OCL},0}+n_2) + \frac{f_{\mathrm{n}2,0}}{\tau_{\mathrm{QD}2}}\right] \\
& \times\left[\sigma_{\mathrm{n}1}\mathrm{v_n}(n_{\mathrm{OCL},0}+n_1) + \frac{f_{\mathrm{n}2,0}}{\tau_{21}} + \frac{1-f_{\mathrm{n}2,0}}{\tau_{12}} + 2\frac{f_{\mathrm{n}1,0}}{\tau_{\mathrm{QD}1}} + 2\frac{b}{N_\mathrm{S}}\mathrm{v_g} g_1^{\max} n_{\mathrm{ph},0}\right],
\end{aligned}
\tag{A55}
$$

$$
\begin{aligned}
A_3 = {} & \sigma_{\mathrm{n}2}\mathrm{v_n}\frac{N_\mathrm{S}}{b}(1-f_{\mathrm{n}2,0}) + \sigma_{\mathrm{n}1}\mathrm{v_n}\frac{N_\mathrm{S}}{b}(1-f_{\mathrm{n}1,0}) + 2Bn_{\mathrm{OCL},0} \\
& + \frac{1}{2}\sigma_{\mathrm{n}2}\mathrm{v_n}(n_{\mathrm{OCL},0}+n_2) + \frac{1}{2}\frac{f_{\mathrm{n}1,0}}{\tau_{12}} + \frac{1}{2}\frac{1-f_{\mathrm{n}1,0}}{\tau_{21}} + \frac{f_{\mathrm{n}2,0}}{\tau_{\mathrm{QD}2}} \\
& + \frac{1}{2}\sigma_{\mathrm{n}1}\mathrm{v_n}(n_{\mathrm{OCL},0}+n_1) + \frac{1}{2}\frac{f_{\mathrm{n}2,0}}{\tau_{21}} + \frac{1}{2}\frac{1-f_{\mathrm{n}2,0}}{\tau_{12}} + \frac{f_{\mathrm{n}1,0}}{\tau_{\mathrm{QD}1}} + \frac{b}{N_\mathrm{S}}\mathrm{v_g} g_1^{\max} n_{\mathrm{ph},0}.
\end{aligned}
\tag{A56}
$$

For the modulation response, the ac component j_m of the injection current density is not zero. We consider a time-harmonic j_m,

$$
j_\mathrm{m} = (\delta j_\mathrm{m}) e^{i\omega t}. \tag{A57}
$$

We correspondingly look for the solutions of the set of linearized differential equations (A29)–(A32) in the form

$$
\nu(\omega) = (\delta n_{\mathrm{OCL-m}}) e^{i\omega t}, \tag{A58}
$$

$$
\varphi_2(\omega) = (\delta f_{\mathrm{n2-m}}) e^{i\omega t}, \tag{A59}
$$

$$
\varphi_1(\omega) = (\delta f_{\mathrm{n1-m}}) e^{i\omega t}, \tag{A60}
$$

$$s(\omega) = (\delta n_{\mathrm{ph-m}})e^{i\omega t}. \tag{A61}$$

Using (A57)–(A61) in (A29)–(A32), we obtain

$$\begin{pmatrix} C_{11} & C_{12} & C_{13} & 0 \\ C_{21} & C_{22} & C_{23} & 0 \\ C_{31} & C_{32} & C_{33} & C_{34} \\ 0 & 0 & C_{43} & C_{44} \end{pmatrix} \begin{pmatrix} \delta n_{\mathrm{OCL-m}} \\ \delta f_{\mathrm{n2-m}} \\ \delta f_{\mathrm{n1-m}} \\ \delta n_{\mathrm{ph-m}} \end{pmatrix} = \begin{pmatrix} \delta j_{\mathrm{m}}/eb \\ 0 \\ 0 \\ 0 \end{pmatrix}. \tag{A62}$$

The coefficients C_{nm} in (A62) are related to the coefficients A_{nm} in (A38) as follows:

$$C_{\mathrm{nm}} = A_{\mathrm{nm}}\big|_{h=-i\omega}, \tag{A63}$$

where A_{nm} are given by (A39)–(A50).

The solutions of the set (A62) are

$$\delta n_{\mathrm{OCL-m}}(\omega) = \frac{\begin{vmatrix} \delta j_{\mathrm{m}}/eb & C_{12} & C_{13} & 0 \\ 0 & C_{22} & C_{23} & 0 \\ 0 & C_{32} & C_{33} & C_{34} \\ 0 & 0 & C_{43} & C_{44} \end{vmatrix}}{\Delta}, \tag{A64}$$

$$\delta f_{\mathrm{n2-m}}(\omega) = \frac{\begin{vmatrix} C_{11} & \delta j_{\mathrm{m}}/eb & C_{13} & 0 \\ C_{21} & 0 & C_{23} & 0 \\ C_{31} & 0 & C_{33} & C_{34} \\ 0 & 0 & C_{43} & C_{44} \end{vmatrix}}{\Delta}, \tag{A65}$$

$$\delta f_{\mathrm{n1-m}}(\omega) = \frac{\begin{vmatrix} C_{11} & C_{12} & \delta j_{\mathrm{m}}/eb & 0 \\ C_{21} & C_{22} & 0 & 0 \\ C_{31} & C_{32} & 0 & C_{34} \\ 0 & 0 & 0 & C_{44} \end{vmatrix}}{\Delta}, \tag{A66}$$

$$\delta n_{\mathrm{ph-m}}(\omega) = \frac{\begin{vmatrix} C_{11} & C_{12} & C_{13} & \delta j_{\mathrm{m}}/eb \\ C_{21} & C_{22} & C_{23} & 0 \\ C_{31} & C_{32} & C_{33} & 0 \\ 0 & 0 & C_{43} & 0 \end{vmatrix}}{\Delta}, \tag{A67}$$

where

$$\Delta = \begin{vmatrix} C_{11} & C_{12} & C_{13} & 0 \\ C_{21} & C_{22} & C_{23} & 0 \\ C_{31} & C_{32} & C_{33} & C_{34} \\ 0 & 0 & C_{43} & C_{44} \end{vmatrix} = \begin{vmatrix} A_{11} & A_{12} & A_{13} & 0 \\ A_{21} & A_{22} & A_{23} & 0 \\ A_{31} & A_{32} & A_{33} & A_{34} \\ 0 & 0 & A_{43} & A_{44} \end{vmatrix}_{h=-i\omega} \tag{A68}$$

$$= \left(2\frac{N_S}{b}\right)^2 \left(\omega^4 - i\,A_3\omega^3 - A_2\omega^2 + i\,A_1\omega + A_0\right).$$

With eq. (A67) for $\delta n_{\text{ph-m}}(\omega)$, we obtain eq. (4.29) for the modulation response function.

References [*)]

[A1] Y. Wu, R. A. Suris, and L. V. Asryan, "Effect of excited states on the ground-state modulation bandwidth in quantum dot lasers," *Appl. Phys. Lett.*, vol. 102, no. 19, Art. no. 191102, May 2013.

[A2] L. V. Asryan, Y. Wu, and R. A. Suris, "Carrier capture delay and modulation bandwidth in an edge-emitting quantum dot laser," *Appl. Phys. Lett.*, vol. 98, no. 13, Art. no. 131108, Mar. 2011.

[A3] L. V. Asryan, Y. Wu, and R. A. Suris, "Capture delay and modulation bandwidth in a quantum dot laser," *Proc. SPIE*, vol. 7947, pp. 794708-1--794708-8, Jan. 2011.

[A4] L. V. Asryan, Y. Wu, and R. A. Suris, "Carrier capture delay and modulation bandwidth in an edge-emitting quantum dot laser," *Proc. "Nanostructures: Physics and Technology"*, pp. 19-20, June 2011.

[A5] L. V. Asryan, Y. Wu, and R. A. Suris, "Modulation bandwidth of a quantum dot laser: The upper limit and limiting factors," *Proc. 15th International Conf. "Laser Optics 2012*", June 25-29, 2012, St. Petersburg, Russia. Paper no. WeR3-22.

[A6] Y. Wu, R. A. Suris and L. V. Asryan, "Effect of internal optical loss on the modulation bandwidth of a quantum dot laser," *Appl. Phys. Lett.*, vol. 100, no. 13, Art. no. 131106, Mar. 2012.

[1] L. V. Asryan and R. A. Suris, "Upper limit for the modulation bandwidth of a quantum dot laser," *Appl. Phys. Lett.*, vol. 96, no. 22, Art. no. 221112, May 2010.

[2] K. Kamath, J. Phillips, H. Jiang, J. Singh and P. Bhattacharya, "Small-signal modulation and differential gain of single-mode self-organized $In_{0.4}Ga_{0.6}As$/GaAs quantum dot lasers," *Appl. Phys. Lett.*, vol. 70, no. 22, pp. 2952-2953, Jun. 1997.

[*)] "A" in the reference number indicates the publications of the author of this dissertation.

[3] S. Fathpour, Z. Mi and P. Bhattacharya, "High-speed quantum dot lasers," *J. Phys. D. Appl. Phys.*, vol. 38, no. 13, pp. 2103-2111, Jul. 2005.

[4] M. Ishida, N. Hatori, T. Akiyama, K. Otsubo, Y. Nakata, H. Ebe, M. Sugawara and Y. Arakawa, "Photon lifetime dependence of modulation efficiency and *K* factor in 1.3 μm self-assembled InAs/GaAs quantum-dot lasers: impact of capture time and maximum modal gain on modulation bandwidth," *Appl. Phys. Lett.*, vol. 85, no. 18, pp. 4145-4147, Nov. 2004.

[5] M. Ishida, M. Sugawara, T. Yamamoto, N. Hatori, H. Ebe, Y. Nakata and Y. Arakawa, "Theoretical study on high-speed modulation of Fabry-Pérot and distributed-feedback quantum-dot lasers: *K*-factor-limited bandwidth and 10 Gbit/s eye diagrams," *J. Appl. Phys.*, vol. 101, no. 1, Jan. 2007.

[6] D. G. Deppe and H. Huang, "Fermi's golden rule, nonequilibrium electron capture from the wetting layer, and the modulation response in p-doped quantum-dot lasers," *IEEE J. Quantum. Electron.*, vol. 42, no. 3, pp. 324-330, Mar. 2006.

[7] D. G. Deppe and D. L. Huffaker, "Quantum dimensionality, entropy, and the modulation response of quantum dot lasers," *Appl. Phys. Lett.*, vol. 77, no. 21, pp. 3325-3327, Nov. 2000.

[8] A. E. Zhukov, M. V. Maksimov and A. R. Kovsh, "Device characteristics of long-wavelength lasers based on self-organized quantum dots," *Semicond.*, vol. 46, no. 10, pp. 1225-1250, Oct. 2012.

[9] L. W. Wang, J. N. Kim and A. Zunger, "Electronic structures of [110]-faceted self-assembled pyramidal InAs/GaAs quantum dots," *Phys. Rev. B*, vol. 59, no. 8, pp. 5678-5687, Feb. 1999.

[10] O. Stier, M. Grundmann and D. Bimberg, "Electronic and optical properties of strained quantum dots modeled by 8-band k·p theory," *Phys. Rev. B*, vol. 59, no. 8, pp. 5688-5701, Feb. 1999.

[11] L. V. Asryan, S. Luryi and R. A. Suris, "Intrinsic nonlinearity of the light-current characteristic of semiconductor lasers with a quantum-confined active region," *Appl. Phys. Lett.*, vol. 81, no. 12, pp. 2154-2156, Sept. 2002.

[12] Y. Arakawa, "Progress in self-assembled quantum dots for optoelectronic device application," *IEICE Trans. Electron.*, vol. E85C, no. 1, pp. 37-44, Jan. 2002.

[13] S. Grosse, J. H. H. Sandmann, G. vonPlessen, J. Feldmann, H. Lipsanen, M. Sopanen, J. Tulkki and J. Ahopelto, "Carrier relaxation dynamics in quantum dots: scattering mechanisms and state-filling effects," *Phys. Rev. B*, vol. 55, no. 7, pp. 4473-4476, Feb. 1997.

[14] I. V. Ignatiev, I. E. Kozin, S. V. Nair, H. W. Ren, S. Sugou and Y. Masumoto, "Carrier relaxation dynamics in InP quantum dots studied by artificial control of nonradiative losses," *Phys. Rev. B*, vol. 61, no. 23, pp. 15633-15636, Jun. 2000.

[15] P. Boucaud, K. S. Gill, J. B. Williams, M. S. Sherwin, W. V. Schoenfeld and P. M. I. P.-O. Petroff, "Saturation of THz-frequency intraband absorption in InAs/GaAs quantum dot molecules," *Appl. Phys. Lett.*, vol. 77, no. 4, pp. 510-512, Jul. 2000.

[16] U. Bockelmann and T. Egeler, "Electron relaxation in quantum dots by means of Auger processes," *Phys. Rev. B*, vol. 46, no. 23, pp. 15574-15577, Dec. 1992.

[17] U. Bockelmann, "Exciton relaxation and radiative recombination in semiconductor quantum dots," *Phys. Rev. B*, vol. 48, no. 23, pp. 17637-17640, Dec. 1993.

[18] J. Urayama, T. B. Norris, J. Singh and P. Bhattacharya, "Observation of phonon bottleneck in quantum dot electronic relaxation," *Phys. Rev. Lett.*, vol. 86, no. 21, pp. 4930-4933, May 2001.

[19] T. Kitamura, R. Ohtsubo, M. Murayama, T. Kuroda, K. Yamaguchi and A. Tackeuchi, "Direct observation of phonon relaxation bottleneck in InAs quantum dots of high-uniformity," *Phys. Stat. Sol. C*, vol. 0, no. 4, pp. 1165-1168, Jun. 2003.

[20] L. Jiang and L. V. Asryan, "Excited-state-mediated capture of carriers into the ground state and the saturation of optical power in quantum-dot lasers," *IEEE Photon. Technol. Lett.*, vol. 18, no. 24, pp. 2611-2613, Dec. 2006.

[21] S. L. Chuang, Physics of Photonic Devices, John Wiley & Sons, 2009, p. 821.

[22] L. V. Asryan and R. A. Suris, "Inhomogeneous line broadening and the threshold current density of a semiconductor quantum dot laser," *Semicond. Sci. Technol.*, vol. 11, no. 4, pp. 554-567, Apr. 1996.

[23] P. S. Zory, Quantum well lasers, Academic Press, 1993, p. 504.

[24] L. A. Coldren and S. W. Corzine, Diode lasers and photonic integrated circuits, Wiley, 1995, p. 594.

[25] L. V. Asryan and R. A. Suris, "Spatial hole burning and multimode generation threshold in quantum-dot lasers," *Appl. Phys. Lett.*, vol. 74, no. 9, pp. 1215-1217, Mar. 1999.

[26] L. V. Asryan, M. Grundmann, N. N. Ledentsov, O. Stier, R. A. Suris and D. Bimberg, "Maximum modal gain of a self-assembled InAs/GaAs quantum-dot laser," *J. Appl. Phys.*, vol. 90, no. 3, pp. 1666-1668, Aug. 2001.